UNIVERSITAT DE BARCELONA

Regulation of skeletal muscle atrophy by the ZEB1 transcription factor

Chiara Ninfali

ADVERTIMENT. La consulta d'aquesta tesi queda condicionada a l'acceptació de les següents condicions d'ús: La difusió d'aquesta tesi per mitjà del servei TDX (**www.tdx.cat**) i a través del Dipòsit Digital de la UB (**diposit.ub.edu**) ha estat autoritzada pels titulars dels drets de propietat intel·lectual únicament per a usos privats emmarcats en activitats d'investigació i docència. No s'autoritza la seva reproducció amb finalitats de lucre ni la seva difusió i posada a disposició des d'un lloc aliè al servei TDX ni al Dipòsit Digital de la UB. No s'autoritza la presentació del seu contingut en una finestra o marc aliè a TDX o al Dipòsit Digital de la UB (framing). Aquesta reserva de drets afecta tant al resum de presentació de la tesi com als seus continguts. En la utilització o cita de parts de la tesi és obligat indicar el nom de la persona autora.

ADVERTENCIA. La consulta de esta tesis queda condicionada a la aceptación de las siguientes condiciones de uso: La difusión de esta tesis por medio del servicio TDR (**www.tdx.cat**) y a través del Repositorio Digital de la UB (**diposit.ub.edu**) ha sido autorizada por los titulares de los derechos de propiedad intelectual únicamente para usos privados enmarcados en actividades de investigación y docencia. No se autoriza su reproducción con finalidades de lucro ni su difusión y puesta a disposición desde un sitio ajeno al servicio TDR o al Repositorio Digital de la UB. No se autoriza la presentación de su contenido en una ventana o marco ajeno a TDR o al Repositorio Digital de la UB (framing). Esta reserva de derechos afecta tanto al resumen de presentación de la tesis como a sus contenidos. En la utilización o cita de partes de la tesis es obligado indicar el nombre de la persona autora.

WARNING. On having consulted this thesis you're accepting the following use conditions: Spreading this thesis by the TDX (**www.tdx.cat**) service and by the UB Digital Repository (**diposit.ub.edu**) has been authorized by the titular of the intellectual property rights only for private uses placed in investigation and teaching activities. Reproduction with lucrative aims is not authorized nor its spreading and availability from a site foreign to the TDX service or to the UB Digital Repository. Introducing its content in a window or frame foreign to the TDX service or to the UB Digital Repository is not authorized (framing). Those rights affect to the presentation summary of the thesis as well as to its contents. In the using or citation of parts of the thesis it's obliged to indicate the name of the author.

Regulation of skeletal muscle atrophy by the ZEB1 transcription factor

TESIS DOCTORAL
UNIVERSITAT DE BARCELONA
Programa de Doctorado en Biomedicina
December 2019

Memoria presentada por Chiara Ninfali para optar al grado de
Doctor en Biomedicina por la Universidad de Barcelona

Doctorando	**Director**	**Tutor**
Chiara Ninfali	Antonio Postigo	Carles Enrich Bastùs

Group of Transcriptional Regulation of Gene Expression
Instituto de Investigaciones Biomédicas August Pi i Sunyer (IDIBAPS)
Barcelona

Logic will get you from A to B.
Imagination will take you everywhere.

(Albert Einstein)

Act as if what you do makes a difference.
It does.

(William James)

PREFACE

The experimental study presented in this doctoral thesis was performed at the Instituto de Investigaciones Biomédicas August Pi i Sunyer (IDIBAPS) in Barcelona, in the laboratory of “Transcriptional Regulation of Gene Expression”, under the supervision of Dr. Antonio Postigo. The work was supported by a scholarship from the Catalan Agency for Management of University and Research Grants (AGAUR) and from funding from the Ministry of Economy and Competitiveness.

ABSTRACT

Muscle atrophy, which is characterized by excessive protein catabolism, is one of the major adaptive processes that occur in several physiopathological and clinical conditions, to counteract stressing stimuli. Skeletal muscle atrophy is triggered by the induction of a group of proteins (atrogenes) that includes components of the ubiquitin–proteasome and autophagy-lysosomal systems. Atrogenes are induced by FOXO transcription factors, but their regulation had not been fully dissected. In this dissertation, it has been studied the role of the transcription factor ZEB1, best known for promoting tumor progression, in muscle atrophy induced by disuse and fasting. It was found that, in both conditions, ZEB1 inhibited muscle atrophy, but through different mechanisms. In disuse-induced atrophy, ZEB1 antagonized FOXO3-mediated induction of atrogenes, while during fasting ZEB1 promoted the expression of NRF1 and NRF2, two important mitochondrial and oxidative stress regulatory genes.

During hindlimb immobilization, global *Zeb1* heterozygous deletion results in enhanced muscle atrophy and higher expression of a number of atrogenes, including Atrogin-1/*Fbxo32* and MuRF1/*Trim63.* Mechanistically, ZEB1 directly represses *in vitro* and *in vivo Fbxo32* and *Trim63* promoter transcription in a stage-dependent manner and in a reverse pattern with MYOD1. ZEB1 binds to the *Fbxo32* promoter in undifferentiated myoblasts and atrophic myotubes, but not in non-atrophic myotubes, where it is displaced by MYOD1. ZEB1 represses both promoters through CtBP-mediated inhibition of FOXO3 transcriptional activity.

Using a conditional muscle-specific *Zeb1* knockout mouse model, it was found that ZEB1 promoted the formation of oxidative slow-type I fibers, through the induction of MEF2C and PGC1ß. During fasting-induced muscle atrophy, the specific knock out of *Zeb1* in myofibers induced higher muscle atrophy (*Zeb1* KO muscles have an increased number of fibers with lower CSA), lower mitochondrial respiration, due to mitochondrial complex III dysfunction, and higher ROS production. ZEB1 directly binds to *Nrf1* and *Nrf2* promoters, two key regulatory genes of mitochondrial biogenesis and oxidative stress.

Altogether, these results set ZEB1 as a key driver of muscle atrophy, highlighting its importance as a possible new target in therapeutic approaches to clinical conditions causing muscle mass loss.

TABLE OF CONTENTS

ABBREVIATIONS

ARE: antioxidant response element

ATPase: adenosine triphosphatase

CI, CII, CIII, CIV: Complexes I, II, III and IV of the respiratory chain, respectively

CID: CtBP interaction domain

CSA: cross sectional area

DM: differentiation medium

EMT: epithelial-to-mesenchymal transition

GM: growth medium

H&E: hematoxylin and eosin

IMM: inner mitochondrial membrane

IMTG: Intramyocellular triacylglycerols

LD: lipid droplets

MHC: Myosin heavy chain

MRF: muscle regulatory factors

mtDNA: mitochondrial DNA

nDNA: nuclear DNA

OMM: outer mitochondrial membrane

Oxphos: oxidative phosphorylation

ROS: reactive oxygen species

SDH: succinate dehydrogenase

TAG: triacylglycerols

UPS: ubiquitin-proteasome system

INTRODUCTION

INTRODUCTION

The muscular system is one of the most abundant tissues of the body, accounting for almost half of the total body mass in vertebrates (Janssen et al., 2000). Depending on its architecture, it is possible to distinguish two main categories of muscles: striated and smooth muscle. In the striated muscles, the contractile fibrils are aligned in parallel bundles, forming functional units called sarcomeres. Sarcomeres consist of several repeated units of myofibrils of thick filaments, formed primarily by myosin, which can move over actin thin filaments. There are two types of striated muscle: the cardiac and the skeletal muscle. The former is found in the heart and is not voluntary, while the latter is attached to the skeleton through the tendons and is under the voluntary control of the central nervous system. As the skeletal muscle is the subject of this doctoral dissertation, only it would be reviewed in the Introduction

1. SKELETAL MUSCLE

In vertebrates, the skeletal muscle represents the most common type of muscle in the body and it is formed by a strict arrangement of muscle fibers that sustain and coordinate a variety of functional activities. Besides myofibrils, the skeletal muscle contains other tissues such as blood vessels, nerve fibers and connective tissue and it can vary considerably in size, shape and fiber composition (Figure 1).

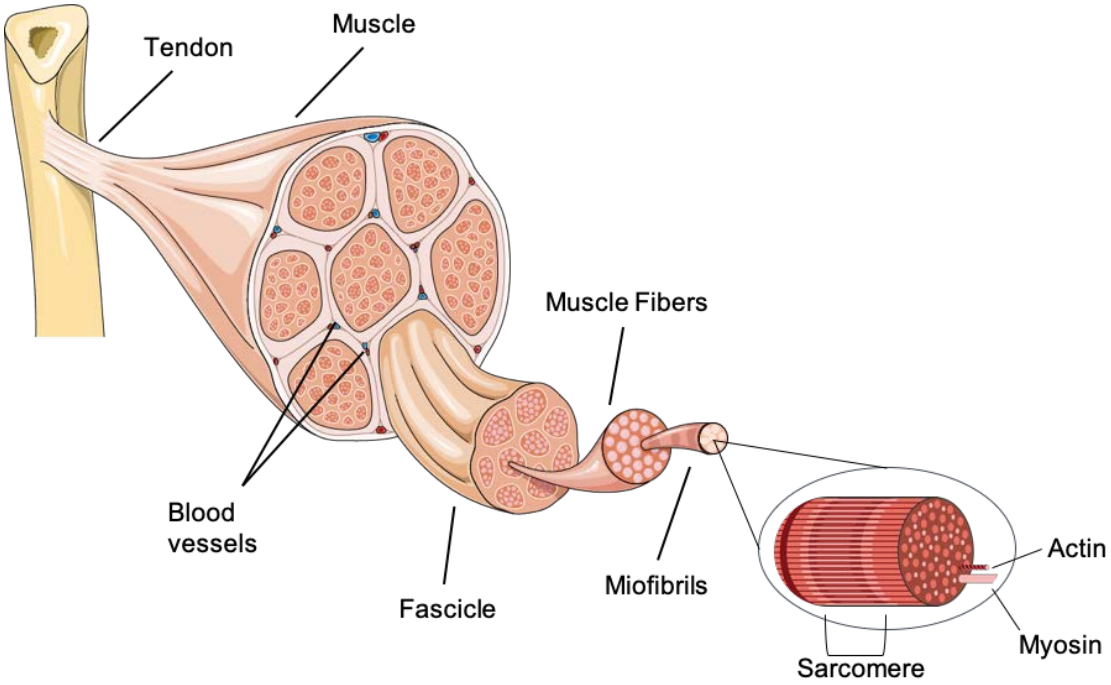

Figure 1 Skeletal muscle structure. Skeletal muscle is formed by several fibers organized in sarcomeres. Sarcomeres are formed by strictly arranged myosin-actin based motor units. *Picture adapted with permission from Servier Medical Art.*

1.1 Myogenesis and Muscle Differentiation

Embryonic myogenesis and muscle differentiation are orchestrated by a network of four myogenic transcriptional factors (MRFs): myogenic factor 5 (MYF5), myoblast determination protein (MYOD1), myogenin and muscle-specific regulatory factor 4 (MRF4 or MYF6) (Braun & Gautel, 2011; Lluís et al., 2006). They are transcriptional activators that are expressed in a well-defined spatial and temporal manner during embryogenesis, and they undergo several epigenetic modifications to induce muscle cell commitment and differentiation (Braun & Gautel, 2011; Carrió & Suelves, 2015; Carrió et al., 2016). MYF5 and MYOD1 are required for the initial commitment to the myogenic lineage, while myogenin is essential for the terminal differentiation of myoblasts. MRF4 seems to have a dual role, being expressed both in proliferating undifferentiated cells as in post-mitotic differentiated ones (Berkes & Tapscott, 2005).

MRFs belong to the basic helix-loop-helix (bHLH) DNA-binding family. They form homo- or heterodimers with E proteins to bind and activate their target genes, by recognizing the consensus CANNTG sites (E-boxes) in the regulatory regions of their target genes (Sabourin & Rudnicki, 2000, Bentzinger et al., 2012). Overexpression of MRFs in non-muscle cells, like fibroblasts, is sufficient to induce muscle gene expression and drive a myogenic differentiation (Davis et al., 1987; Weintraub et al., 1989).

1.2 Skeletal muscle fiber type composition and oxidative capacity

The skeletal muscle contains different types of myofibrils that vary in their structural and functional properties. Myofibers are broadly categorized in three types, depending on their contractile capacity, mitochondrial content and metabolic properties (Scott et al., 2001; Spangenburg & Booth, 2003): the oxidative slow, or type I, the glycolytic fast-fatigue resistant, or type IIa and the glycolytic fast fatigable, or type IIb. Their relative abundance within each muscle varies, determining the phenotypic and contractile characteristics of the muscle.

Slow-type I fibers produce a modest force when they are stimulated and they contract and relax slower in comparison to the fast fibers. Slow fibers can withstand prolonged stimuli and maintain contraction and force over long periods. These fibers are enriched in mitochondrial content and sustain their activity mainly by producing ATP by oxidative metabolism. Type IIa fast-fatigue resistant fibers can produce a larger amount of force for an overall quite long period. Despite their high mitochondrial content, their metabolism is preferentially glycolytic. The third type, type IIb fast-fatigable fibers, can produce a more intense force than the other fibers when stimulated, but they exhaust after a short period. Type IIb fibers present a very low mitochondrial content and they use almost exclusively glycolysis as a fuel of energy (Scott et al., 2001; Spangenburg & Booth, 2003).

The contractile properties of each type of fiber are closely related to the expression of specific myofibrillar profiles, especially to the myosin heavy chain (MHC) protein isoforms expression (Schiaffino et al., 2015). The skeletal muscle contains four main MHC isoforms: MHC-Iβ expressed in slow-type I fibers, MHC-IIa

expressed in fast-fatigue resistant and MHC-IIb expressed in fast-fatigable fibers. A fourth type of MHC isoform, the MHC-IIx/d, has been identified in a small subset of fibers (Gorza et al., 1990; Schiaffino et al., 2015). The various fiber types correspond to different gene expression, among them the isoforms of the Myosin Heavy Chain (MHC) gene superfamily. Especially, *Myh7* encodes for slow MHC-I, *Myh4* for MHC-IIb, *Myh2* for MHC-IIa and *Myh1* for MHC-IIx/d (Schiaffino et al., 2015). Single fiber analysis has revealed that myofibrillar adenosine triphosphatase (mATPase) activity, which is associated with the globular head region of the myosin heavy chain, correlates with specific MHC profiles (Pette & Staron, 1997). Thus, histochemical staining based on mATPase activity is a useful method to determine muscle fiber type composition (Figure 2).

Fibers can also be distinguished by their relative oxidative capacity, which is assessed by histochemical staining for succinate dehydrogenase (SDH) activity (Schiaffino, 2010; Bloemberg & Quadrilatero, 2012). The SDH mitochondrial respiratory chain enzyme, that converts succinate into fumarate, localizes in the inner mitochondrial membrane and it is completely codified by nuclear DNA (nDNA), thus, it does not depend on mitochondrial DNA variations. Hence, SDH staining intensity serves as a proxy of the mitochondrial content and the SDH enzyme activity within each fiber (Nemeth & Pette, 1981) (Figure 2). Fibers that need more energy to sustain contraction, like slow-type I, produce energy by the oxidative phosphorylation (Oxphos) in mitochondria, thus are more oxidative and display greater staining for SDH than glycolytic ones.

Lastly, fibers can be distinguished by their differential expression of MHC isoforms, usually assessed by immunofluorescence. This method is especially useful to evaluate those fiber types that express more than one MHC isoforms (Bloemberg & Quadrilatero, 2012) (Figure 2).

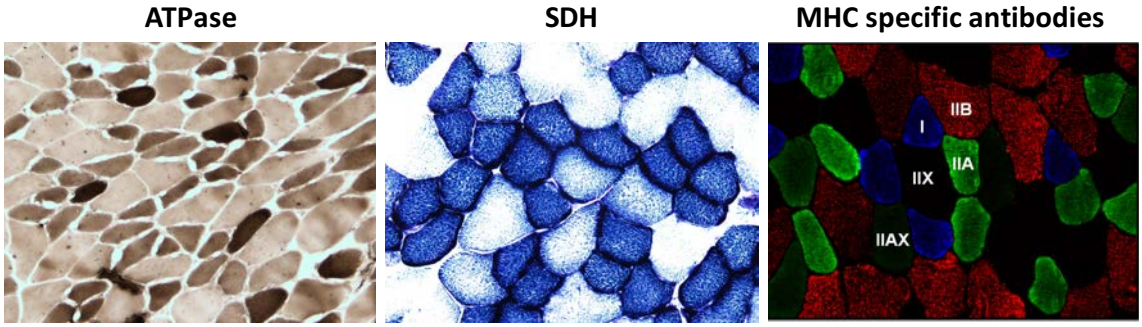

Figure 2: Histological analysis of fiber type composition in mouse skeletal muscle. **A)** mATPase staining of the mouse gastrocnemius muscle which shows the three principal fiber types: the darkest represent type I, the lightest type IIa, and the intermediate type IIb. **B)** SDH staining which distinguishes fiber types basing on their oxidative capacity. The more intense blue corresponds to higher mitochondrial content and Oxphos activity. **C)** Fiber types are evaluated using specific antibodies against MHC isoforms. Source: *Pictures in A) and B) originated from own results whereas picture in C) was adapted from Bloemberg et al., 2012, with permission.*

The relative abundance of each fiber type within the muscle is not static but rather can change depending on muscle physiological requirements and pathological conditions (Schiaffino, 2010). In basal conditions or during endurance training, fiber conversion between IIb and IIa is more common, while during the pathological atrophying conditions, like muscle disuse or overall nutrient starvation and cachexia, the switch from type I to II is the prevalent mechanism adopted to adapt to atrophic stimuli (Scott et al., 2001). Hence, the analysis of the individual muscle fiber type relative abundance is a useful strategy to detect early pathological changes.

1.3 Skeletal muscle lipid storage

Skeletal muscle represents an important site of glucose and lipid storage. Lipids are stored in myofibers as intramyocellular triacylglycerols (IMTG), which are triacylglycerols (TAG), compacted in lipid droplets (LD). Although they account for only 1% of total-body lipid content, they represent an important source of fuel during energy demanding conditions, like fasting or exercise (Badin et al., 2013). Immunohistochemical stainings have determined that IMTG content appears to be two-to-three fold higher in type I oxidative myofibers, compared to glycolytic type II, suggesting that they represent an important source of energy for oxidative metabolism (Badin et al., 2013).

In the resting muscle, IMTG pools turn over at a high rate (Sacchetti et al., 2004). The enzymes responsible for the catabolism of TAG from LD are the lipases, particularly the adipose triglyceride lipase (ATGL) and the hormone-sensitive lipase (HSL), which are mainly expressed in type I oxidative fibers (Jocken et al., 2008), suggesting a role for oxidative metabolism. Moreover, ATGL mutations in humans lead to neutral lipid storage diseases, with consequent myopathy, indicating a role for ATGL in muscle function (Fischer et al., 2007).

1.4 Mitochondria and energy regulation

Mitochondria are the controllers of cellular metabolism and the main subcellular structures that supply energy production in the muscle (Garesse & Vallejo, 2001). They form a reticular network within mammalian skeletal muscle and are responsible to convert oxygen and nutrients into ATP, that powers cells' metabolic activities.

Mitochondria contain an inner (IMM) and an outer (OMM) membrane, which are separated by an intermembrane space (Figure 3). The IMM is where most ATP is created, through the mitochondrial respiratory chain (detailed below). Within the IMM is situated a mitochondrial matrix, that contains mitochondrial DNA (mtDNA) as well as hundreds of enzymes, and it is important in the production of ATP.

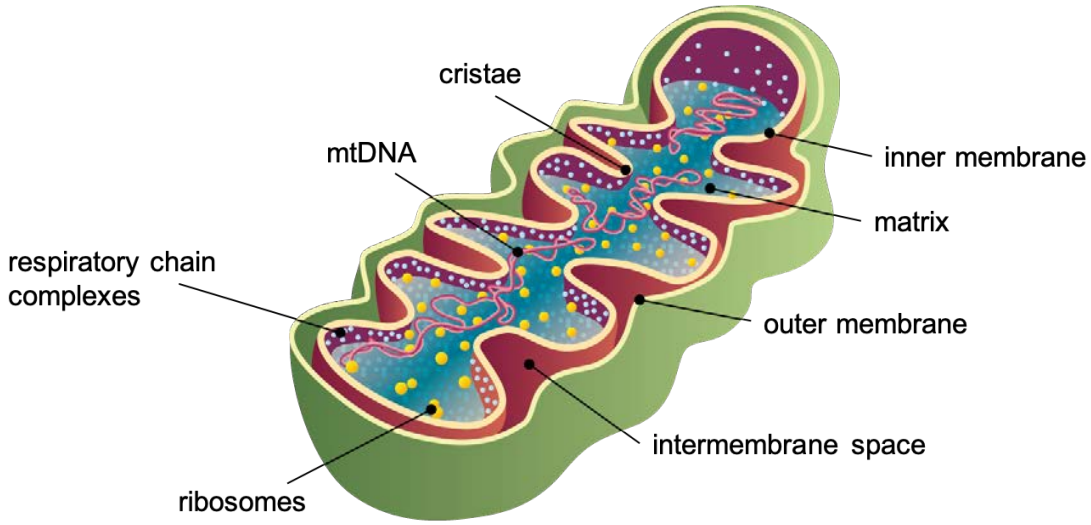

Figure 3: Mitochondria structure. Mitochondria are formed by an outer and an inner membrane, separated from an intermembrane space. Within the inner membrane, there is the matrix, which contains several proteins and the mitochondrial DNA. *Picture drew by Sara Ninfali.*

Mitochondria convert chemical energy into ATP through oxidative phosphorylation (Oxphos), a process that involves five multiprotein enzymes complexes, located in the IMM, and two electron carriers (coenzyme Q and cytochrome c) (Figure 4). The main function of the respiratory chain system is to coordinate the transport of electrons and protons, generating a charge and a proton gradient across the IMM, which finally leads to ATP synthesis. The electron passage, in fact, releases energy, which is stored in the form of a proton gradient and is used by the last Oxphos complex, the ATP synthase enzyme or complex V, to generate ATP, starting from ADP and inorganic phosphate (Schultz & Chan, 2001). The other four main complexes of the respiratory chain are the complex I (CI, NADH-CoQ oxidoreductase), the complex II (CII, succinate-CoQ oxidoreductase), the complex III (CIII, $CoQH_2$-cytochrome c oxidoreductase) and the complex CIV (CIV, cytochrome c-O_2 oxidoreductase) (Figure 4).

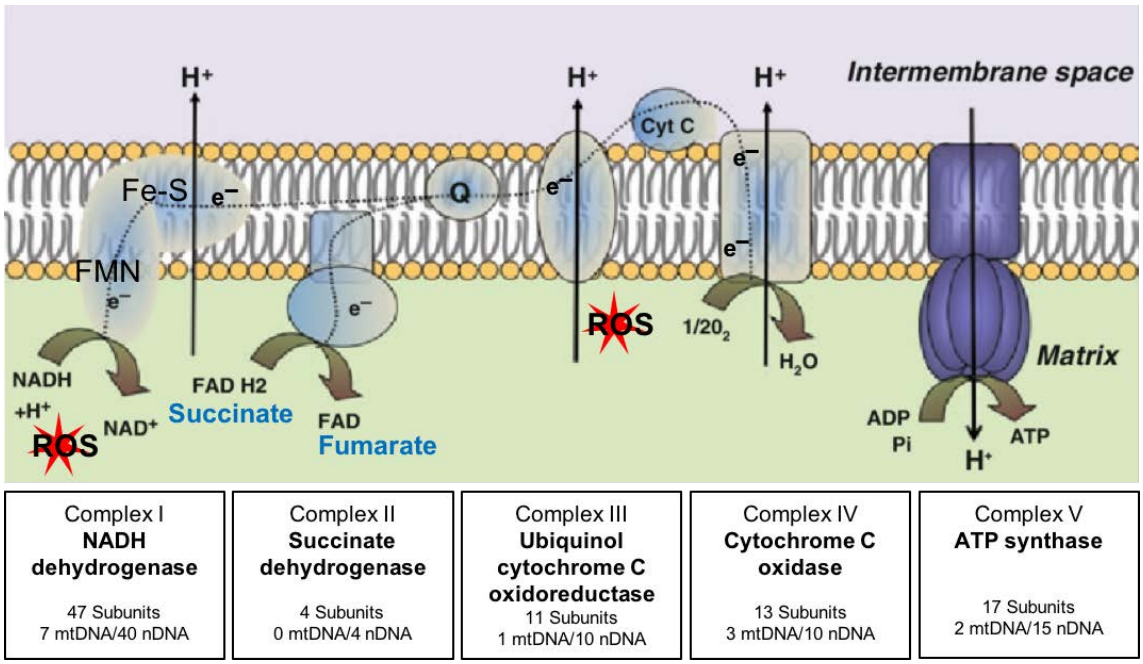

Figure 4: Mitochondrial respiratory chain complexes. ATP is produced by oxidative phosphorylation in the mitochondrial respiratory chain. Electrons pass through the four main respiratory complexes, creating an energy charge that is used from the final ATP synthase complex to produce ATP. See the main text for more details. *Picture adapted with permission from Bénard G et al., 2011 © Springer Science+Business Media.*

OxPhos begins with the entry of electrons into complexes I or II. The CI transfers the electrons from NADH to ubiquinone (Q), the first electron acceptor, through two electrons transfers (FMN and Fe-S cluster), while the CII transfers electrons to ubiquinone from succinate substrate (Mimaki et al., 2009). Electrons accepted from CI or CII are then transferred to CIII, and then to cytochrome c, the second mobile electron transfer. Finally, electrons are transferred to the final electron acceptor, the terminal respiratory chain complex (CIV), which is responsible to reduce oxygen to water by using the delivered electrons (Crofts, 2004).

The mitochondrial respiratory chain is the major site of reactive oxygen species (ROS) production inside the cells, due to the “leak” of a small number of electrons to oxygen prematurely (Muller et al., 2000). Especially, mitochondrial complex I and III of the respiratory chain are considered the main sites of superoxide production (Barja et al., 1999; Muller et al., 2004) (Figure 4). Under normal conditions, the balance between ROS generation and detoxification is controlled by a set of detoxifying enzymes, including superoxide dismutase (SOD), catalase, and glutathione peroxidase (Diebold & Chandel, 2016). However, during cellular stress,

ROS production increases leading to oxidative damage of different cellular components (Rubattu et al., 2014).

1.5 Mitochondria regulatory pathways

Although mitochondria possess their own mitochondrial DNA (mtDNA), this has a limited coding ability, as nuclear genes are the main contributors for mitochondrial architecture and metabolic capacity (Garesse & Vallejo, 2001). The mitochondrial genome, for instance, encodes for only thirteen of the approximately 100 subunits that constitute the respiratory apparatus. The other vast majority of respiratory subunits, as wells as the factors that regulate mitochondrial gene expression and enzymes of oxidative phosphorylation, are nuclear-encoded (Clayton, 1991).

The expression of mitochondrial genes is coordinated by several transcription factors. Among them, the NF-E2-related nuclear factors 1 and 2 (NRF1 and NRF2) and the estrogen-related receptor α (ERRα) are considered the main nuclear transcription factors involved in mitochondrial biogenesis and regulation (Schreiber et al., 2004; Gleyzer et al., 2005). ERRα promotes the cellular energy metabolic genes in cooperation with many transcription factors and acts by binding to the ERR response elements in the promoter regions of its target genes (Schreiber et al., 2004; Gleyzer et al., 2005). NRF1 and NRF2 present partially overlapping function and act by binding to the nuclear antioxidant response element (ARE) of target genes in response to a variety of stimuli. They promote the expression of genes required for mitochondrial biogenesis and encoding the majority of mitochondrial components and they coordinate the oxidative stress response during stressing conditions (Kelly & Scarpulla, 2004). Moreover, NRF1 and NRF2 modulate the expression of mitochondrial transcription factor A (TFAM), a mitochondrial matrix protein, which is involved in mitochondrial biogenesis and is responsible to induce transcription and replication of mtDNA (M. J. Evans & Scarpulla, 1990; Virbasius & Scarpulla, 1994) (Figure 5). NRFs and EERα promote mitochondrial gene transcription by interacting with the transcriptional co-activators, members of the PPARγ coactivator-1 (PGC-1) family of transcriptional co-factors, PGC1α and PGC1β (Schreiber et al., 2004; Gleyzer et al., 2005). Both co-factors are preferentially expressed in active metabolic

tissues, like brown adipose tissue, heart and skeletal muscle, where they regulate metabolic functions and energy metabolism (Handschin & Spiegelman, 2006). PGC1α and PGC1β share extensive sequence identity (Lin et al., 2002) and exert partially overlapping functions, but they are not fully reductant. In fact, in skeletal muscle, PGC1α is preferentially expressed in slow-twitch type I fibers, where it drives their formation (Lin et al., 2002), while mice with skeletal muscle specific *Pgc1β* ablation do not change their myofiber composition (Ramamoorthy et al., 2015). PGC1α is a powerful coactivator of both NRF1 and NRF2, that upregulate the expression of TFAM, mitofusins (proteins involved in mitochondria remodeling) and nuclear genes encoding mitochondrial proteins. PGC1β is also capable to stimulate mitochondrial respiration and *Pgc1β* deficient myofibers present mitochondrial structural and functional abnormalities that lead to decreased muscle oxidative capacity and reduced antioxidant defense (Ramamoorthy et al., 2015).

Myogenesis is associated with a switch from glycolytic to oxidative metabolism, with the consequent increase in mitochondrial biogenesis (Kraft et al., 2006). Interestingly, MYOD1, one of the major transcriptional regulators of skeletal muscle myogenesis, as described above, activates several skeletal muscle metabolic genes, including PGC1β (but not PGC1α), by directly binding to their promoter regions (Shintaku et al., 2016). Hence, in skeletal muscle, MYOD1 functions as a regulator of mitochondrial biogenesis and oxidative metabolism and is required to maintain its normal oxidative capacity.

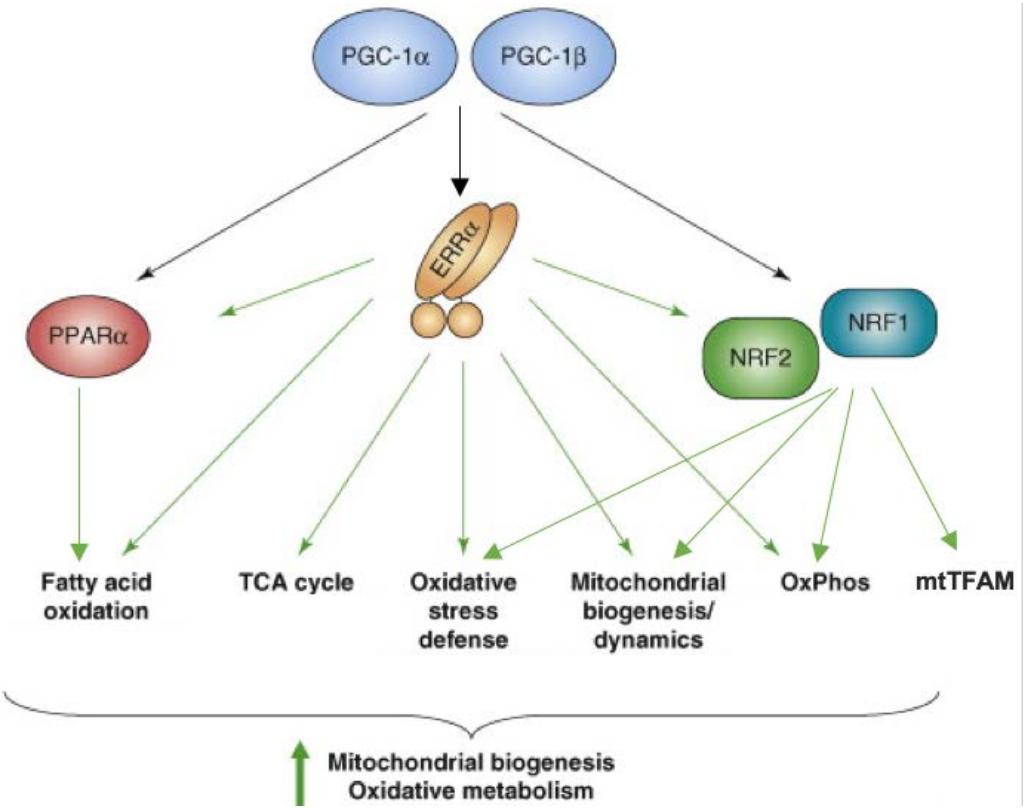

Figure 5: Mitochondrial biogenesis and Oxphos regulation. PGC1α and PGC1β interact with several transcriptional factors, including NRF1, NRF2 and ERRα, to induce mitochondrial biogenesis and oxidative metabolism. *Picture adapted with permission from Villena J et al., 2008.*

1.6 Mitochondrial dynamics and distribution in skeletal muscle

Skeletal muscle cells need to maintain high bioenergetic efficiency to support contraction. Mitochondrial morphology varies extremely depending on the tissue and according to its physiological or pathological status. Mitochondrial shape continuously changes by ongoing events of fusion and fission of outer and inner membranes, thus the fusion and fission machinery play a pivotal role in the mitochondrial dynamics (Twig et al., 2008; Rambold & Pearce, 2018) (Figure 6). This brief transition between connected and divided mitochondria is essential to share mitochondrial components, enabling the reorganization of their proteins and complexes and the elimination of damaged material. The fusion of isolated mitochondria induces the formation of an extended network that permits to prevent the local accumulation of defective or abnormal mitochondria and allows the

redistribution of metabolites, proteins and mtDNA. On the other hand, mitochondrial fission machinery permits to segregate not functional components of the mitochondrial network and to remove them by autophagy. These two opposite processes enable to maintain a healthy mitochondria population inside the tissue (Raben et al., 2008).

The three most important proteins involved in the fusion machinery are *Mitofusins* (MFN1 and MFN2) and optic atrophy protein 1 (OPA1). All three are GTPases that orchestrate the fusion of OMM and IMM and are required for the maintenance of a reticular mitochondrial network in cells (Mishra & Chan, 2014). MFN1 and MFN*2* are situated in the OMM and form homo- or hetero-oligomers that promote the fusion of the OMMs from two different mitochondria. In turn, OPA1 is anchored to the IMM and requires MFN1 to regulate mitochondrial fusion (Cipolat et al., 2004). Mitochondrial fission depends on the GTPase DRP1, which, if not recruited, shows a cytosolic localization. After specific cellular signals, it translocates from the cytosol to the OMM, mediating its fission. Several DRP1 receptors have been identified, including FIS1, MFF, MiD49 and MiD51, which exert partially overlapping functions (Civiletto et al., 2015) (Figure 6).

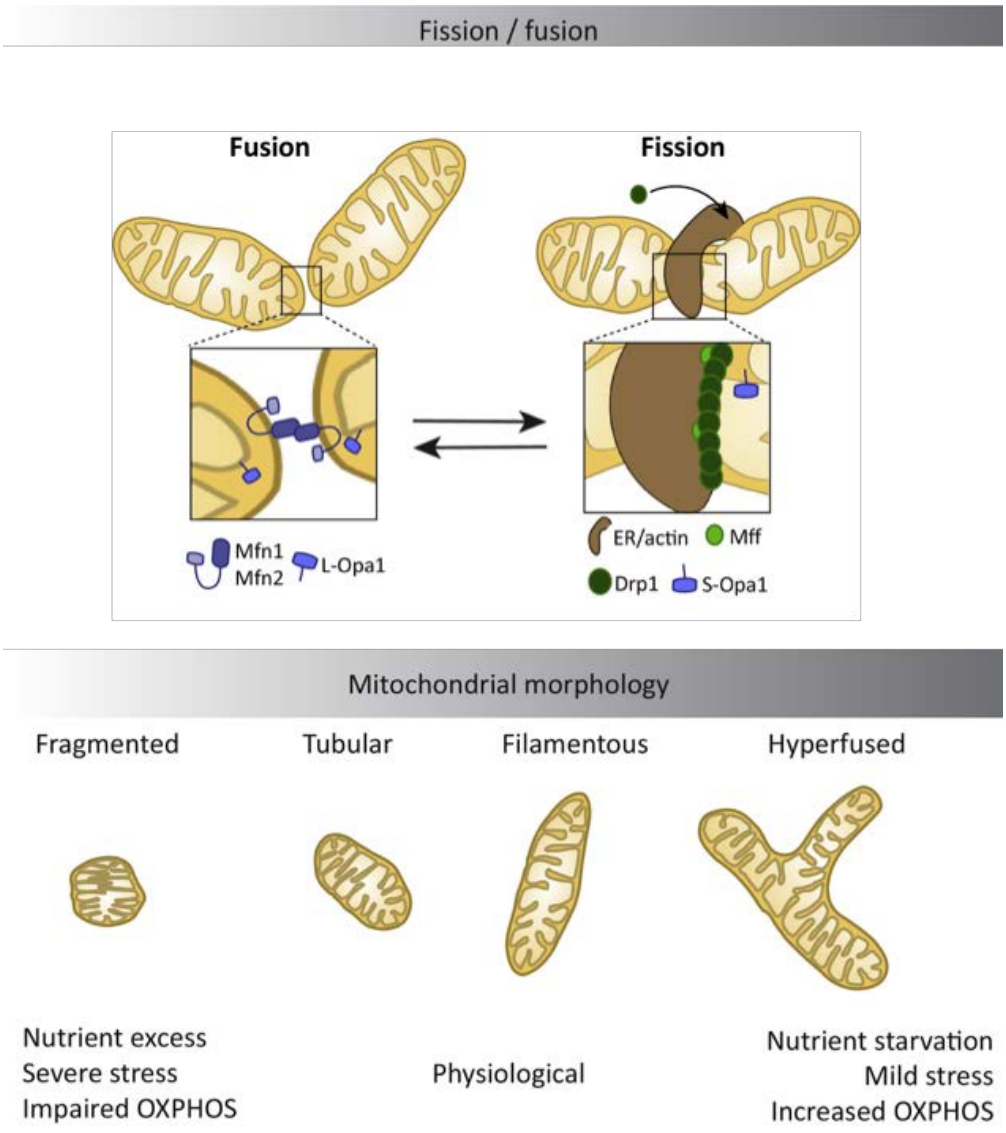

Figure 6: Mitochondrial dynamics. Mitochondrial architecture is modulated by fusion and fission events depending on physiological or pathological events. During fusion events, two separated mitochondria fuse generating a network in which components of the two mitochondria are mixed and reorganized. Fission splits fused mitochondria into two daughter organelles with different membrane potential. *Picture adapted with permission from Rambold and Pierce, 2018.*

The fission mechanism is essential to remove mitochondrial damaged components. In fact, when the mitochondrion divides, it generates two organelles with different membrane potential. The fragment with lower membrane potential is removed by autophagic processes, called mitophagy, while the other one enters again in the mitochondrial fusion-fission cycle (Twig et al., 2008). Hence, a balanced mitochondrial turnover is essential for mitochondrial function.

Autophagy represents a key process in eukaryotes for the removal of damaged or dysfunctional organelles. The autophagy pathway degrades macromolecules and organelles to rejuvenate their function and represents an important mechanism to preserve muscle mass and to maintain myofiber integrity. Inhibition or alteration of the autophagy pathway can contribute to muscle degeneration, exacerbated by the accumulation of abnormal mitochondria and toxic products (Masiero et al., 2009).

2. MUSCLE ATROPHY

Skeletal muscle is a highly adaptable tissue that can change its morphology and composition depending on physiological and pathological conditions. Under homeostatic conditions, skeletal muscle maintains a balance between protein synthesis and proteolysis by finely tuning signaling pathways (Bonaldo & Sandri, 2013; Schiaffino et al., 2013; Cohen et al., 2015). When protein synthesis rate increases versus proteolysis, myofibers augment their mass and size, in a process defined as hypertrophy. Hypertrophy occurs during development, after anabolic hormonal stimuli or in response to mechanical overload. The reverse process is referred as atrophy. During muscle atrophy, the rate of protein breakdown increases over the protein synthesis, resulting in a reduction of muscle mass and myofiber cross sectional area (CSA). Multiple physiopathological and clinical conditions (e.g. immobilization, aging, denervation, starvation) result in skeletal muscle consumption.

Muscle atrophy is an active and finely controlled process, which requires a specific transcriptional program. In eukaryotic cells, protein turnover and degradation are achieved mainly via two proteolytic systems: the ubiquitin-proteasome and the autophagy-lysosomal pathways. In skeletal muscle, these two systems are coordinately regulated to breakdown proteins and remove damaged organelles in atrophying fibers (Mammucari et al., 2007; Sandri, 2010). Microarray analyses have identified a subset of genes that are commonly up- or down-regulated in a variety of atrophic stimuli. These genes are collectively referred as atrophy-related genes or “atrogenes” and encode enzymes that catalyze important steps in autophagy-lysosome, ubiquitin-proteasome, ROS detoxification, mitochondrial function and

energy balance pathways (Bodine et al., 2001; Gomes et al., 2001; Jagoe et al., 2002; Lecker et al., 2004).

2.1 The ubiquitin-proteasome system (UPS)

Most sarcomeric proteins are degraded by the ubiquitin–proteasome pathway. Ubiquitination marks proteins for their subsequent recognition and degradation by the 26S proteasome complex. The ubiquitination of target proteins is a finely regulated process, which involves the sequential action of three types of enzymes. The E1 enzymes bind and activate a molecule of ubiquitin, which is then moved to E2 enzymes. The final ubiquitination of target proteins is catalyzed by the E3 ubiquitin-ligases enzymes, which are responsible to transfer the ubiquitin from E2 to substrates, to induce their degradation by the 26S proteasome (Bonaldo & Sandri, 2013; Bodine & Baehr, 2014; Collins & Goldberg, 2017) (Figure 7).

The two archetypal muscle-specific atrogene proteins, whose expression increases the strongest during muscle atrophy, are the E3 ubiquitin ligases Atrogin-1 (also known as MAFbx and encoded by the gene *Fbxo32*) and MuRF1 (encoded by *Trim63*) (Bodine et al., 2001; Gomes et al., 2001).

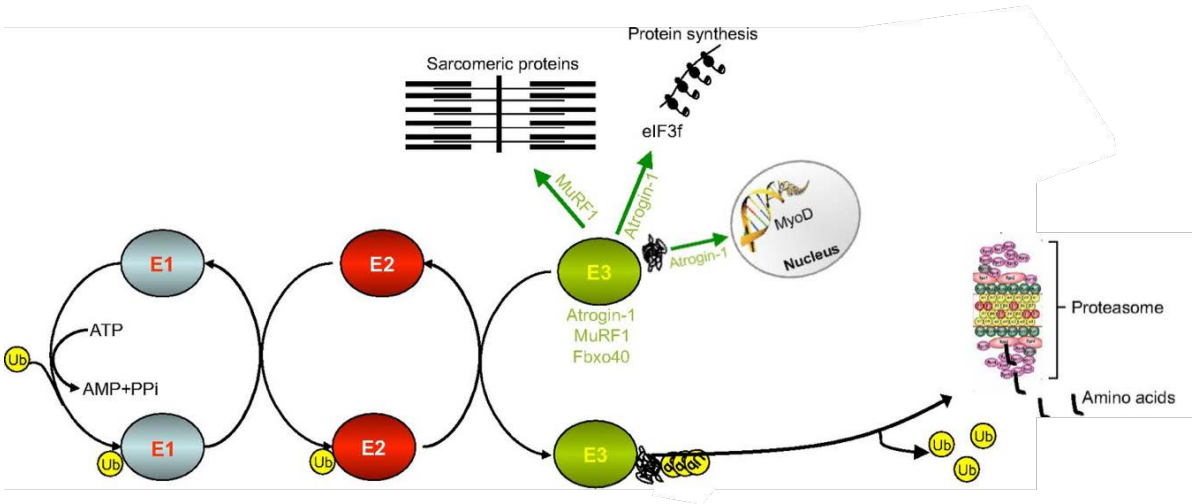

Figure 7: The ubiquitin proteasome system. The E1 enzymes activate ubiquitin proteins after the cleavage of ATP. The ubiquitin is then moved from E1 to members of the E2 enzyme class. Members of the E3 enzyme class catalyze the final protein ubiquitylation reaction. Atrogin-1 and Murf-1 are muscle-specific ubiquitin ligases involved in almost all forms of muscle atrophy. See the main text for more detailed informations. *Picture adapted with permission from Bonaldo and Sandri, 2013.*

During muscle atrophy, Atrogin-1 catalyzes the degradation of proteins involved in protein synthesis and survival pathways, while Murf-1 promotes the ubiquitination of important structural proteins of the myofibrillar apparatus and cytoskeleton, including myosin heavy and light chain and troponin (Cohen et al., 2009). Moreover, Atrogin-1 promotes the degradation of MYOD1, thereby impairing myoblasts fusion and differentiation (Tintignac et al., 2005). *Fbxo32* (-/-) and *Trim63* (-/-) mice exhibit reduced muscle sparing in response to atrophy-inducing experimental protocols (Bodine et al., 2001), highlighting their important role in this process.

Atrogin-1 and MuRF-1 expression are directly activated by O-type forkhead transcription factors (FOXO), chiefly by FOXO3. The FOXO family of transcription factors in skeletal muscle is comprised of three isoforms: FOXO1, FOXO3 and FOXO4 and it seems that they cover redundant, instead of synergistic, functions. Among the three factors, FOXO3 is the most critical for the activation of atrophic program, in fact, activation of FOXO3 alone is sufficient to trigger proteolysis via UPS and the autophagy system causing severe atrophy (Mammucari et al., 2007; Bonaldo & Sandri, 2013; Milan et al., 2015; Cheng, 2019).

In homeostatic conditions, FOXO proteins are phosphorylated by the phosphoinositide 3 kinase (PI3K)-Akt-mammalian target of rapamycin (mTOR) signaling pathway and remain sequestered in the cytoplasm (Brunet et al., 1999). During energy demand, the PI3K-Akt pathway is inhibited, producing the consequent FOXO3 dephosphorylation. Dephosphorylated FOXOs enter into the nucleus of the atrophying myotubes, promoting the atrogene's transcription and proteolytic genes activation (Sandri et al., 2004). Of note, induction of atrogenes by FOXO and the subsequent signaling network that controls the atrophic program are specific for each catabolic condition (Brocca et al., 2017). Interestingly, PGC1α and PGC1β, which in basal condition reduce protein breakdown by inhibiting the transcriptional activity of FOXO3, are downregulated during different models of muscle wasting (Sandri et al., 2006).

2.2 The autophagy-lysosome system

Autophagy plays a crucial role in the turnover of cell components, both in basal condition and in response to various stressing stimuli (Sandri, 2010; García-Prat et al., 2016). Three different autophagic mechanisms have been described in mammals: the macro-autophagy, the chaperone-mediated autophagy and the micro-autophagy. In muscle atrophy, macro-autophagy, hereafter referred as autophagy, is considered the predominant pathway responsible for intracellular protein degradation (Mortimore & Poso, 1987).

During autophagy, cytoplasmic contents and organelles, particularly mitochondria, are delivered to the lysosome for degradation (Mammucari et al., 2007; Zhao et al., 2007). Autophagy activation results in the sequestration of the target material by an autophagosome, which then fuses to a lysosome. The autophagosome formation starts with nucleation of the membrane, initiated by Beclin1 complex, followed by its maturation and elongation, induced by LC3 peptide recruitment to its membrane (Figure 8).

The specific removal of mitochondria is named mitophagy and requires the PINK1-Parkin complex and Bnip3 factors (Bonaldo & Sandri, 2013). Bnip3 and Bnip3L are BH3-only proteins that localize at the OMM after cellular stresses and bind directly to LC3, thereby recruiting the autophagosome to damaged mitochondria (Hanna et al., 2012). An efficient mitophagy is critical to preserve a healthy muscle at several levels, including in satellite cells (SCs), the muscle stem cells responsible for muscle regeneration, where impaired mitophagy induces higher ROS production and provokes their entry in the senescent state (García-Prat et al., 2017).

During nutrient deprivation, the autophagy-lysosome machinery is the major proteolytic pathway activated.

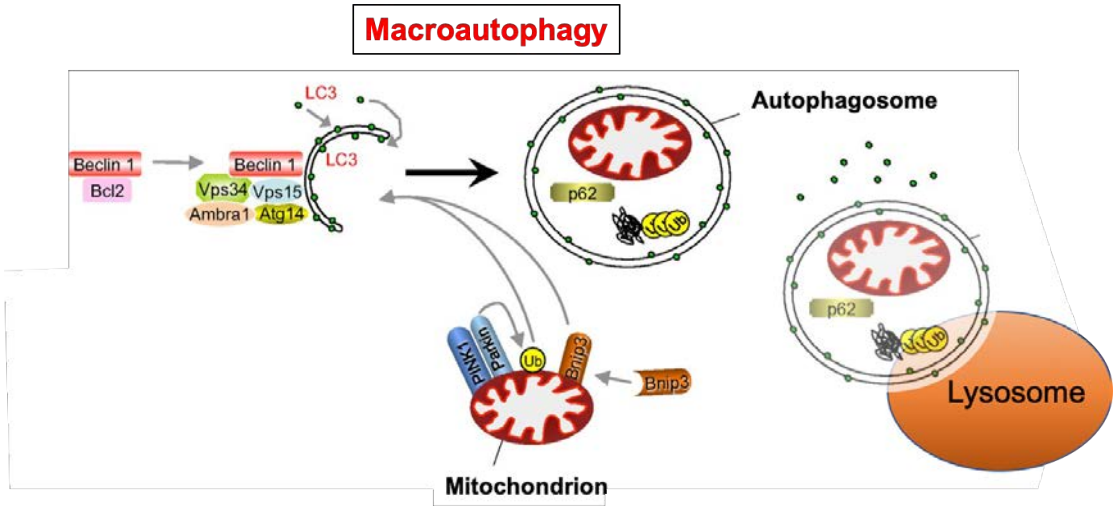

Figure 8: The autophagy-lysosomal pathway. Macroautophagy is triggered by the activation of a regulatory complex, containing several proteins, including Beclin1. This complex induces LC3 recruitment to the nascent autophagosome. Mitophagy, the selective removal of mitochondria, requires the PINK1-Parkin complex and Bnip3 factors. Proteins that are committed for lysosomal degradation are labeled by polyubiquitin chains and delivered to the autophagosome by the p62 scaffold protein. *Picture adapted with permission from Bonaldo and Sandri, 2013.*

Interestingly, not all fiber types undergo atrophy to the same extent. Slow type-I oxidative fibers tend to be more resistant to muscle atrophy compared to the more glycolytic ones (Sandri et al., 2008). Moreover, fast fibers display a higher content of autophagosomes than slow fibers (Mizushima et al., 2004).

Another adaptive response to muscle atrophy is the shift in muscle fiber type composition. The nature of the fiber shift can change depending on the atrophic stimulus. During fasting, for example, there is a suppression of oxidative program, inducing a slow-to-fast fiber conversion (Potthoff et al., 2007; Schiaffino et al., 2007).

2.3 Oxidative stress and atrophy

Several models of muscle atrophy, including immobilization, starvation or bed rest, are associated with increased ROS production (Pellegrino et al., 2011; Powers et al., 2016). While low levels of ROS are associated with beneficial effects in muscle physiology, excessive ROS production accelerates muscle proteolysis (Barbieri & Sestili, 2012; Powers et al., 2012). Accordingly, in vitro exposure of myotubes to oxidants results in muscle atrophy (Gilliam et al., 2012). Free radicals promote

atrophy through several mechanisms, including the regulation of FOXO factors, with the consequent activation of the ubiquitin-proteasome and autophagy-lysosome systems, the activation of the cell apoptotic pathways and the oxidation of several proteins, making them more susceptible to degradation (Dobrowolny et al., 2008; Dodd et al., 2010; Smuder et al., 2010; Romanello & Sandri, 2016), Mitochondrial ROS production, hence, is a necessary step in mitochondrial dysfunction and muscle atrophy (Powers et al., 2012; Talbert et al., 2013). ROS production and atrophic process induce the upregulation of NRF1 and NRF2 transcription factors, which in turn activate important pathways for the antioxidant response (Biswas & Chan, 2010; Bellezza et al., 2018).

The AMP-activated protein kinase (AMPK) acts as a cellular metabolic sensor being activated when the AMP:ATP cellular ratio increases. Under condition of energy demand, it initiates several biological processes aimed at restoring energy balance, including the activation of FOXO3 proteolytic program, the stimulation of NRF1-PGC1α dependent remodeling of mitochondrial content and the induction of fatty acid oxidation enzymes, as an alternative source of energy (Hardie, 2007). Recently, it has been proposed a novel non-canonical regulation of AMPK by mitochondrial reactive oxygen species, showing that mitochondrial ROS are physiological activators of AMPK, and that AMPK triggers PGC1α-dependent antioxidant response to limit mitochondrial ROS production (Rabinovitch et al., 2017).

2.4 Mitochondrial dynamic during muscle atrophy

Alterations in mitochondrial number, morphology and function are common features in atrophying muscles. During fasting, the mitochondrial network is dramatically remodeled and autophagy, in association with the fission machinery, contributes to mitochondria remodeling (Romanello & Sandri, 2013).

As noted above, mitochondrial morphology is highly dynamic and sensitive to metabolic alterations and, vice versa, mitochondrial dynamics affect metabolism (Rambold & Pearce, 2018). For instance, fasting causes acute inhibition of mitochondrial fission, by inhibiting DRP1 recruitment to mitochondria, and a

consequent mitochondria elongation, due to unopposed mitochondrial fusion and Mfn1/2 overexpression (Gomes et al., 2011; Rambold et al., 2011). This elongation prevents the starvation-induced mitophagy in order to increase ATP synthesis, to sustain energy demand during periods of limited nutrient availability. Perturbations in fusion and fission machinery could induce mitochondria dysfunction. In that line overexpression of DRP1, *per se*, causes muscle atrophy, perturbing mitochondrial structure and impairing skeletal muscle metabolism (Touvier et al., 2015).

3. THE ZEB1 TRANSCRIPTION FACTOR

The ZEB family of transcription factors comprises two highly homologous proteins in vertebrates: ZEB1 (also known as ZEB, TCF8 or δEF1 among others) and ZEB2 (SIP1). They are zinc finger/homeodomains proteins that act as transcriptional factors by binding G/C centered E-boxes sequences in the regulatory regions of their target genes (Dongre & Weinberg, 2019).

ZEB1 is best known for promoting tumor progression by triggering an epithelial-to-mesenchymal transition (EMT) in cancer cells (Sánchez-Tilló et al., 2012; Dongre & Weinberg, 2019). EMT is a complex transcriptional program, indispensable for normal embryogenesis and tissue development. During physiological embryogenesis, the EMT factors induce the transformation of polarized epithelial cells into highly motile mesenchymal ones, allowing cells migration into newly formed tissues. If EMT is aberrantly activated in adult tissues, it drives malignant tumor progression and metastasis formation, enabling cells to acquire stem cells properties and dissociate to the primary tumor and invade the neighboring tissues (Gheldof et al., 2012; Nieto et al., 2016; Dongre & Weinberg, 2019).

The ZEB factors orchestrate the EMT process together with other two main families of transcription factors, Snail and Twist. The upregulation of these transcription factors promotes cancer initiation and progression through multiple mechanisms (Nieto et al., 2016; Cortés et al., 2017; de Barrios et al., 2017; Dongre & Weinberg, 2019; Stemmler et al., 2019; de Barrios et al., 2019).

ZEB1 also plays an important role during cell differentiation, which it inhibits in several tissues, including cartilage, bone and hematopoietic compartment (Vandewalle et al., 2009; Dongre & Weinberg, 2019).

3.1 ZEB1 structure and mechanism of action

ZEB1 (named as δEF1 in mouse) and *ZEB2* genes encode for two highly similar proteins of 1124 and 1214 aminoacids in humans respectively. They contain two zinc finger clusters at their N- and C- terminal ends that serve as DNA binding domains and that are highly conserved between ZEB1 and ZEB2 (Postigo et al., 2000) (Figure 9).

The zinc-finger domains are the most common DNA binding motifs in eukaryotes and they independently mediate the ZEB's DNA-binding capacity to their target genes. They recognize E-box and E-box like sequences (CANNT) in the regulatory regions of their target genes, with the highest affinity for the CACCT motif (Sekido et al., 1994). ZEB proteins, moreover, contain multiple independent domains to interact with other transcriptional factors as well as non-DNA transcriptional regulators.

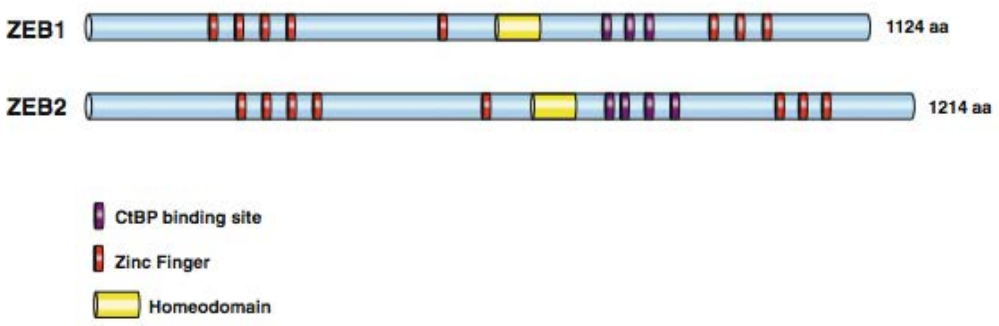

Figure 9: Schematic representation of the ZEB1 and ZEB2 structure. ZEB1 and ZEB2 proteins present two zinc finger clusters in their N- and C- terminal regions, separated from a homeodomain and a CtBP binding domain (CID). *Adapted with permission from Sanchez-Tilló et al., 2012.*

ZEB1 is best known as a transcriptional repressor. It represses the activity of a wide range of transcriptional activators with mechanisms that vary depending on

the promoter, the co-repressors it recruits and the activation/differentiation stage of the cells (Postigo & Dean, 1997; Postigo et al, 1997; Postigo, 2003; Sánchez-Tilló et al., 2011; Siles et al., 2013). ZEB1 presents a CtBP interacting domain (CID) to bind two homologous C-terminal binding protein of adenovirus E1A (CtBP1/2) co-repressors, that in turn recruit other transcriptional co-factors, like histone deacetylases and methyltransferases, polycomb and coREST (Postigo & Dean, 1999; Postigo et al., 2000). CtBP1/2 interact with ZEB1, enhancing its transcriptional repression activity, through the PLDLSL sequence in *Drosophila* homolog Zfh-1 and two additional CtBP like binding sites (variations of PLDLS sequence) in vertebrates. Modification of all these three sites leads to loss of CtBP1/2 co-repression activity, abolishing the CtBP1/2 binding to CID (Furusawa et al., 1999; Postigo & Dean, 1999). The CID alone can repress transcription in a CtBP dependent manner.

However, ZEB1 can often also function as a transcriptional activator; binding of ZEB1 to the histone acetyltransferase p300 acetylates the CID region of ZEB1, thus displacing CtBP (Postigo et al., 2003). In that line, in B lymphocytes, ZEB1 synergizes with FOXO3, rather than repressing it, in the activation of cell cycle genes cyclin G2 (*Ccng2)* and p130 (*Rbl2*) (Chen et al., 2006), highlighting the promoter and cell-type specificity of the link between ZEB1 and FOXO3

Another mechanism of action of ZEB proteins is through the competition and displacement of other transcription factors to their promoter sites. For example, during muscle differentiation, ectopic expression of ZEB1 counteracts MyoD/Myf5- or MyoD/Myf6- transcriptional activation on the p73 gene and it controls α7 integrin expression in myoblasts by competing with MyoD1 for binding to its promoter (Genetta et al., 1994; Fontemaggi et al., 2005, Jethanandani & Kramer, 2005).

3.2 Role of the ZEB family in development and muscle

In the developing mouse embryo, ZEB1 is expressed in the primary myotome, where the first muscle progenitors arise (Takagi et al., 1998). ZEB1 imposes a stage-dependent inhibition of muscle differentiation, by binding and repressing, in a CtBP dependent manner, multiples key muscle promoter genes. ZEB1 and MYOD1 partially overlap in their DNA sequence recognition with ZEB1 repressing key muscle

differentiation genes in a reverse temporal pattern vis-à-vis MYOD1 (Siles et al., 2013). Thus, during the myoblast stage, ZEB1 binds to E-boxes in the promoters of differentiation genes and represses their transcription but, as differentiation proceeds, MYOD1 accumulates and displaces ZEB1 from these E-boxes. *Zeb1* (-/-) and *Zeb1* (+/-) embryos display premature expression of adult muscle differentiation genes (Postigo & Dean, 1997; Siles et al., 2013) and both mutation and overexpression of ZEB1's ortholog in Drosophila (zfh-1) disrupt somatic musculature (Postigo et al., 1999; Siles et al., 2013). Despite its important role during embryogenesis, ZEB1 expression is down-regulated after birth and its expression is restricted to some human adult tissues. Interestingly, skeletal muscle is one of the tissues with the highest expression levels of ZEB1 (Human Atlas Database, *www.proteinatlas.org*).

Notably, ZEB1 has been involved in muscle pathologies. Thus, in the context of acute and chronic (muscular dystrophies) muscle injury, ZEB1 protects adult skeletal muscle from damage and is required for its regeneration (Siles et al., 2019).

Homozygous ZEB1 deficient mice die before birth, due to multiple musculoskeletal defects, respiratory failure and severe T cell deficiency of the thymus (Takagi et al., 1998), converting the ZEB1 heterozygous mice in the only viable model used for *in vivo* assays. *Zeb1 +/-* mice used in the first part of this dissertation, express almost half levels of ZEB1 in all tissues and this downregulation is sufficient to confer different phenotypic response to several pathological conditions, like cancer progression or muscle regeneration upon injury (Cortés et al., 2017; de Barrios et al., 2017; de Barrios et al., 2019; Siles et al., 2019). Despite this, the heterozygous *Zeb1 +/-* model does not permit to distinguish the specific contribution of each cell type in the pathological process. For this reason, the generation of conditional floxed mouse models is important in the study of the cell-type specific contribution during physiological and pathological conditions, as we have done in the second chapter of this dissertation.

Despite its important role in myogenesis, muscle differentiation and regeneration, the ZEB1 expression and role during muscle atrophy have not been explored.

OBJECTIVES

OBJECTIVES

This dissertation aimed to study the potential role and the mechanisms of action of ZEB1 during muscle atrophy induced by hindlimb immobilization and fasting.

The objectives of this dissertation are:

I. Investigate the role of ZEB1 in hindlimb immobilization-induced muscle atrophy

II. Determine the molecular mechanism by which ZEB1 regulates *atrogene* expression

III. Investigate the role of ZEB1 in homeostatic muscle structure in a muscle specific KO system

IV. Investigate the role of ZEB1 in fasting-induced muscle atrophy

MATERIALS AND METHODS

MATERIALS AND METHODS

Zeb1 +/- mouse models and hindlimb immobilization-induced atrophy protocol

The use of mouse models in this study was approved by Animal Experimentation Ethics Committee of the University of Barcelona under protocol number CEEA 234/15 and CEEA 521/16 for the immobilization and fasting protocols, respectively. The following models were used: C57BL/6 [referred throughout as either wild-type or *Zeb1* (+/+)] (Jackson Laboratories) and *Zeb1* (+/-) (Takagi et al., 1998). Unilateral hindlimb immobilization was performed as described in (Madaro, Smeriglio, Molinaro, & Bouché, 2008). Briefly, one of the hindlimbs of two-to-three months old wild type or *Zeb1* +/- mice was immobilized by covering it with a plastic cast for 3, 5 or 17 days. The other hindlimb was not immobilized allowing the mouse to move and eat freely. At the end of the protocol, mice were euthanized and the gastrocnemius muscle extracted for further analyses.

Generation of transgenic *Zeb1*$^{f/f}$ and *Zeb1*$^{skm-/-}$ mouse model and fasting-induced atrophy protocol

The conditional *Zeb1* flox (*Zeb1*$^{f/f}$) mouse model (B6.B6CBA-Zeb1$^{em1/cnbbm}$) was generated in collaboration with the CNB-CBMSO Transgenesis Service at CSIC's *Centro Nacional de Biotecnologia*, in Madrid. Two sgRNAs were designed to elicit double strand breaks (DSBs) flanking exon 6 in the *Zeb1* gene (sgRNA 5'-TTACAGACACCTCTAACACA**AGG;** sgRNA 3'-AGTACCAGCAAACCCTTTCT**TGG)**. In addition, two ssDNA oligos, that contain the corresponding LoxP site and a restriction enzyme flanked by two 40 bp homology arms, which correspond to the sequence surrounding each Cas9 cut site, were designed. (**ssDNA 5'-**agctaagtcccttcaagtgcctggtcactgaggaaagctggggttacagacacctctaacGCTAGCataacttcgtatagcatacattatacgaagttatacaaggcttcctccccaaaagggagccgtacagacatgaaaatatttatcaatcaaaggc; **ssDNA 3'-**

aaccaaaggttaacctaactcctaacaaaggagttggcacacgaagtaccagcaaaccctgaattcataacttcgta taatgtatgctatacgaagttatttcttggctttatggtgaatgggaacatggttgtttaatagtgatcataagcaaagaag a). A mixture of *in vitro* transcribed RNA (Cas9 and sgRNAs) and ssDNAs (ssDNA 5' + ssDNA 3'; 100ng/µl) was injected into the cytoplasm of B6CBAF2 zygotes, using standard procedures (Behringer et al., 2014). The concentrations of RNAs injected were as follows: 100 ng/µl for *Cas9*, 50 ng/µl for sgRNA 5'- and sgRNA 3'-, and 100 ng/µl for each ssDNAs. Zygotes that survived the injections were transferred into the oviducts of pseudopregnant foster mothers for development to term. The progeny was then crossed 3 times with wild type C57BL6/Jcrl mice to generate the *Zeb1*$^{f/+}$ mice (mice expressing one floxed allele and one wild type allele). The presence of LoxP sequences was analyzed by DNA sequencing, Mice bearing floxed *Zeb1* alleles, were then crossed with mice carrying the tamoxifen-inducible Cre-ER^{T2} recombinase selectively in myofibers under the human skeletal actin promoter (HSA)-Cre-ER$^{T2\ (tg/0)}$) (official name: Tg(ACTA1-cre/ERT2)97.16Mtz), (Schuler et al., 2005), to create the experimental control (*Zeb1*$^{f/f}$ (HSA)-Cre-ER$^{T2(0/0)}$, called here *Zeb1*$^{f/f}$) and the myofiber conditional *Zeb1* KO (*Zeb1*$^{f/f}$ (HSA)-Cre-ER$^{T2\ (tg/0)}$, called here *Zeb1*$^{skm-/-}$) mice, respectively. The floxed and Cre sequences in experimental mice were genotyped by PCR amplification of genomic DNA extracted from tail samples. Two-to-three months old *Zeb1*$^{f/f}$ control and *Zeb1*$^{skm-/-}$ mutant mice were treated daily with intraperitoneal injections of Tamoxifen (Sigma-Aldrich, T5648) (2 mg/day/mouse in 10% EtOH and 90% corn oil), for five consecutive days. After five days from the last tamoxifen injection, mice were sacrificed and their gastrocnemius muscles were collected for further analysis. In the fasting protocol, four days after the last tamoxifen injection, mice were deprived of food for 36-38 hours but with readily access to water. Then, mice were euthanized and gastrocnemius muscles were collected for further analysis.

Cell lines, cell culture, and C2C12 myotube differentiation and starvation

C2C12 and 293T cells were obtained from the American Type Culture Collection (ATCC)-LGC Standards (Middlesex, England, UK). C2C12 cells were plated on 12-

well plates and cultured in Dulbecco's modified Eagle Medium (DMEM) (Lonza, Basel, Switzerland) supplemented with 15% Fetal Bovine Serum (Sigma-Aldrich. St. Louis, MO), and 1% penicillin-streptomycin (Pen/Strep) (Lonza). This media is referred hereafter to Growth Medium. When cells reached confluence, the medium was replaced with DMEM supplemented with 2% of Horse serum (Sigma-Aldrich) and 1% Penicillin/Streptomycin (referred hereafter as Differentiation Medium) for an additional 4 days. For starvation, C2C12 myotubes were placed in DMEM without glucose (Lonza) (referred as Atrophic Medium) for different periods. 293T cells were grown in Growth Medium but containing only 10% FBS. In selected experiments, C2C12 myoblasts were treated for 24 hours with 2-keto-4-methylthiobutyrate acid (MTOB) (Sigma Aldrich), dissolved in culture medium to reach a final concentration of 10 mM.

Isolation of primary myoblasts and myotubes formation

Gastrocnemius muscles from two-to-three months old *Zeb1*$^{skm-/-}$ and control mice were dissected and put immediately in ice-cold PBS. Muscles were then digested in 0.5 U/mg of Collagenase Type I (Sigma-Aldrich) and Dispase II (Sigma-Aldrich) solution in PBS. The digested tissue was then centrifuged twice and the resulting pellet was re-suspended in primary myoblasts growth medium (80% Ham's F10 (Lonza) supplemented with 20% FBS (Sigma-Aldrich), 1% Pen/Strep and 2.5 ng/ml basic FGF (Miltenyi Biotec, Bergisch Gladbach, Germany). The cell suspension was pre-plated twice for 1 hour in a non-coated 60 mm culture dish, to enrich the myoblast population and allow the preferential adherence of fibroblasts. Next, cells well plated on 12-well plates coated with 5 μg/ml Laminin and 0.002% Collagen type I. The day after plating, the growth medium was supplemented with 2 μM of 4-Hydroxytamoxifen (4-OHT, Sigma-Aldrich) to induce HSA-Cre-ER^{T2} activation. Once primary myoblasts reached confluence, the growing medium was replaced by Differentiation Medium (DM, DMEM with 2% HS and 1% P/S) supplemented with 2 μM of 4-OHT. Myoblasts were differentiated for 4 days before to assess their gene expression.

siRNA transient transfection

For knockdown of gene expression, C2C12 and 293T cells were plated onto 12-well plates and, when they reached 60-70% confluency, they were transfected for 5 hours with 50 nM of a control siRNA (siCtrl) or specific siRNA oligonucleotides against the gene of interest (Table 1), using 4 μl of RNAiMAX (Thermo-Fisher Scientific, Carlsbad, CA). For C2C12 myotubes transfection, when cells reached 100% confluence, Growth Medium (DMEM 15% FBS) was replaced with Differentiation Medium (DMEM 2% Horse serum). At day three and four of differentiation, myotubes were transfected with 50 nM of siCtrl or specific siRNA oligonucleotides against the gene of interest, as described above. 48 hours after transfection, cells were collected and processed for further analysis.

Table 1

siRNA oligonucleotides

Gene Target	Upstream sequence	Reference
siCtrl	UAUAGCUUAGUUCGUAACC	(Siles et al., 2013)
si*Zeb1-A*	GACCAGAACAGUGUUCCAUGUUUAA	(Siles et al., 2013)
si*Zeb1-B*	AACUGAACCUGUGGAUUAU	(Siles et al., 2013)
si*Ctbp*	GAACUGUGUCAACAAGGACTT	(Siles et al., 2013)
si*Foxo3*	Pool of 3 siRNAs [Santa Cruz Biotechnologies (sc-37888)] CAUGCGCGUUCAGAAUGAAtt GAACGUUGUUGGUUUGAAUtt GAAGGAAGGUGUUAUAUCAtt	

Plasmids

Firefly luciferase reporters used in the study were obtained from the following researchers: wild-type 0.4, 1.0, and 3.5 kb fragments of the mouse *Fbxo32* promoter fused to firefly luciferase (pGL3pAT1-0.4, pGL3pAT1-1.0, and pGL3pAT1-3.5, respectively) were obtained from SH Lecker (Harvard Medical School, Boston, MA, USA) (Sandri et al., 2004); wild-type 4.4 kb fragment of mouse *Trim63* promoter subcloned into the pGL3 firefly luciferase vector from B-C Oh (Lee Gil Ya Cancer and Diabetes Institute, Incheon, Korea) (Cai et al., 2004); and, a heterologous luciferase reporter (L8G5-luc) containing five binding sites for yeast Gal4 (UAS) and eight sites for bacterial LexA (LexAOp) proteins from J-L Baert (Université des Sciences et Technologies, Lille, France) (Lemercier et al., 2000; Maurer et al., 2003). In addition, the following expression vectors were used: pECE-*Foxo3* from P Coffer (University Medical Center Utrecht, The Netherlands) (van der Vos et al., 2012), pEMSV-MyoD from AB Lassar (Dana-Farber Harvard Cancer Center, Harvard University, Boston, MA, USA) (Davis et al., 1987), pcDNA3-*Zeb1* from K Miyazono (University of Tokyo, Japan) (Shirakihara et al., 2007), Gal4 and Gal4-*Foxo3* from H Ito (Keio University School of Medicine, Tokyo, Japan) (Nakae et al., 2012) ; LexA (PBXL3), LexA-*ZEB1* (PBXL3-*ZEB1*), LexA-*ZEB1*-CID (PBXL3-*ZEB1*-CID), and LexA-*ZEB1*-CID_{mut} (PBXL3-*ZEB1*-CID_{mut}) (A. A. Postigo & Dean, 1999b, 1999a), and LexA-Foxo3 from FM Stanley (New York University School of Medicine, NY, USA) (Jag et al., 2009). SV40-β-galactosidase and pBluescript SK vectors were obtained commercially from Clontech (Takara, Kyoto, Japan), and Stratagene (Agilent, Santa Clara, CA), respectively.

Immunohistochemistry

Gastrocnemius muscles were dissected, mounted on corks, embedded in Tissue-Tek® O.C.T. Compound (Electron Microscopy Sciences, Hatfield, PA, USA), and frozen in liquid nitrogen cooled isopentane and stored at -80ºC. Next, 8 µm cryosections were prepared (Leica Cryostat CM 1950, Leica Biosystems, Wetzlar, Germany), fixed for 20 min in ice-cooled acetone and permeabilized in 0.25% Triton X-100 in PBS for 30 min. At least one slide from each sample used for immunohistochemistry (IHC) was routinely stained with hematoxylin and eosin. To

block endogenous peroxidase, slides of mouse muscle samples were incubated with 0.3% hydrogen peroxide in PBS and with a non-specific binding blocking solution (NSBBS) [5% goat normal serum (Jackson ImmunoResearch Europe Ltd., Cambridgeshire, England, UK), 4% BSA in PBS, 0.5% Tween 20] followed by the corresponding primary (overnight at 4°C) and HRP-conjugated secondary (1 h at room temperature) antibodies. ZEB1 antibodies, clone H102 for *Zeb1* +/- mouse model, and clone HPA027524 for *Zeb1*$^{skm-/-}$ mouse model, were used at 1/100 or 1/150 dilution, respectively. The immunohistochemistry reaction was developed with a DAB substrate kit (Vector Labs, Burlingame, CA) before slides were counterstained with hematoxylin and mounted in Di-N-butylPhthalate in Xylene solution (DPX, Sigma-Aldrich). Staining was evaluated in a Nikon Olympus BX41 microscope and images processed with ImageJ software (NIH, Bethesda, MD).

Immunofluorescence

Gastrocnemius muscles from wild-type and *Zeb1* +/- mice were embedded, frozen, cryo-sectioned and fixed as described for IHC. Fixed samples of gastrocnemius muscles, were then incubated with 0.1% $NaBH_4$ to block non-specific autofluorescence and with NSBBS to reduce non-specific antibody signal. Slides were then incubated with the corresponding primary (overnight at 4°C) and fluorochrome-conjugated secondary (1 h at room temperature) antibodies. The primary antibodies listed in Table 2 were used as follows: Atrogin-1 (AP2041, 1/100 dilution), and laminin (48H-2, 1/80). Their respective secondary antibodies were used as follows: anti-rabbit Dylight 488 (1/250), and donkey anti-rat rodamine Red-X (1/250). Slides were then mounted with Prolong Gold® Antifade Reagent with DAPI (Thermo Fisher). Staining was evaluated in a Nikon Eclipse E600 microscope (Minato, Tokyo, Japan). For immunofluorescence experiments in C2C12 myotubes, cells were plated onto 12-well plates, washed with PBS and permeabilized in 0.25% Triton X-100 in PBS for 30 min. After washing cells again with PBS, myotubes were first incubated for 1-3 h with the same blocking NSBBS solution described above followed by overnight incubation at 4°C with a polyclonal antibody against Atrogin-1 (AP2041, dilution 1/100). Wells were then washed with PBS, incubated for 90 min

with a donkey anti-rabbit Dylight 488 (1/250 in blocking solution), washed again and a drop of Prolong Gold® Antifade Reagent with DAPI (Thermo Fisher) was added before visualization in an inverted Zeiss Axiovert 200 (Oberkochen, Germany) microscope. All immunofluorescence images were processed with ImageJ software (NIH, Bethesda, MD).

Table 2

Primary and secondary antibodies

Antibodies		
Primary Abs	**Source**	**Clone (Catalog Number)**
Atrogin-1	ECM Biosciences	AP2041
GAPDH	Cell Signaling	14C10
Laminin	Santa Cruz Biotechnologies	48H-2 (sc-59854)
MuRF1	Santa Cruz Biotechnologies	C-11 (sc-398608)
MYOD1	Santa Cruz Biotechnologies	G-1 (sc-377460)
ZEB1	Santa Cruz Biotechnologies	H-102 (sc-25388)
ZEB1	Santa Cruz Biotechnologies	E20-X (sc-10572)
ZEB1	Atlas Antibodies (Sigma-Aldrich)	HPA027524
Secondary Abs	**Source**	**Catalog Number**
Anti-rabbit Alexa Fluor 488	Jackson ImmunoResearch	711-545-152
Anti-rabbit -HRP	Jackson ImmunoResearch	111-035-144
Anti-mouse-HRP	Jackson ImmunoResearch	715-035-151
Anti-rat Rhodamine Red-X	Jackson ImmunoResearch	712-295-153

Assessment of myofiber cross-sectional area and C2C12 myotube diameter

Gastrocnemius samples from wild-type and *Zeb1* (+/-) mouse model after 5 and 17 days of unilateral hindlimb immobilization were assessed for myofiber area (referred as cross-sectional area, CSA). Samples were stained for hematoxylin/eosin and the area of at least 160 fibers was measured using ImageJ software (NIH, Bethesda, MD). In *Zeb1*$^{f/f}$ and *Zeb1*$^{skm-/-}$ mouse model, gastrocnemius muscles of fed and fasted animals were stained for ATPase and the cross-sectional area of at least 100 fibers was measured using ImageJ software (NIH, Bethesda, MD). The diameter of C2C12 myotubes cultured in either differentiation or atrophic medium was quantified using ImageJ software. The diameter of each individual myotube was calculated as the average of ten measurements along its length. At least 100 myotubes from ten fields at 20X magnification were assessed.

RNA extraction and qRT-PCR analysis

Total RNA from gastrocnemius muscles and C2C12 cells was extracted using TRIzol (Life Technologies, Thermo Fisher). RNA was retrotranscribed with random hexamers using High-Capacity cDNA Reverse Transcription kit (Applied Biosystems, Thermo Fisher). mRNA levels were determined by qRT-PCR using SYBRGreen GoTaq® qPCR Master Mix (Promega Corp., Madison, WI) in a LightCycler ® 96 real-time PCR apparatus (Roche, Rotkreuz, Switzerland). Results were analyzed using LightCycler 96 SW1.1 software (Roche) by the ΔΔCt method using *Gapdh* as reference gene. Primers used to amplify the different genes examined in the study are detailed in Table 3.

Table 3

DNA primers used in qRT-PCR

Gene	Forward 5' – 3'	Reverse 5' – 3'	Reference
Ctsl	GTGGACTGTTCTCACGCTCAAG	TCCGTCCTTCGCTTCATAGG	(Milan et al., 2015)
4ebp1	CACGCTCTTCAGCACCAC	GGAGGCTCATCGCTGGTAG	(Ninfali et al., 2018)
Fbxo32	GCAAACACTGCCACATTCTCTC	CTTGAGGGGAAAGTGAGACG	(Milan et al., 2015)
Foxo3	GATAAGGGCGACAGCAACAG	CTGTGCAGGGACAGGTTGT	(Nowak et al., 2007)
Gabarapl1	CATCGTGGAGAAGGCTCTA	ATACAGCTGGCCCATGGTAG	(Milan et al., 2015)
Myod1	TGGGATATGGAGCTTCTATCGC	GGTGAGTCGAAACACGGATCAT	(Dogra et al., 2006)
Nrf2	GCAACTCCAGAAGGAACAGG	AGGCATCTTGTTTGGGAATG	(Milan et al., 2015)
Psma1	CATTGGAATCGTTGGTAAAGAC	GTTCATCGGCTTTTTCTGC	(Ninfali et al., 2018)
Gapdh	CGACTTCAACAGCAACTCCCACTCTTCC	TGGGTGGTCCAGGGTTTCTTACTCCTT	(Banerjee et al., 2013)
Trim63	TGTCTGGAGGTCGTTTCCG	ATGCCGGTCCATGATCACTT	(Castillero et al., 2009)
Zeb1	AACTGCTGGCAAGACAAC	TTGCTGCAGAAATTCTTCCA	(Siles et al., 2013)
Atgl	AACACCAGCATCCAGTTCAA	GGTTCAGTAGGCCATTCCTC	(Chakrabarti & Kandror, 2009)
Sod2	CCGAGGAGAAGTACCACGAG	GCTTGATAGCCTCCAGCAAC	(H. J. Lee et al., 2015)
Ampkα	CTTGACGTGGTGGGAAAAAT	ATAATCAAATAGCTCTCCTCCAGA	Own design
Nrf1	TGGGTAGCTTCCATTTTTGG	AAGGGGAGTCTTCATCAGCA	Own design
Tfam	CCAAAAAGACCTCGTTCAGC	CTTCAGCCATCTGCTCTTCC	Own design
Pgc1α	TTGCTAGCGGTTCTCACAG	TAAGACCGCTGCATTCATTG	Own design

	A		
Pgc1β	GGACGCCAGTGACTTTGACT	TTCATCCAGTTCTGGGAAGG	Own design
Mfn1	CCTGAGGGAAGGCCCTGT	AGTAACTGGCCGAAGATTGC	Own design
Mfn2	CTCAGGAGCAGCGGGTTTAT	GAGAGGCGCCTGATCTCTTC	(Ramamoorthy et al., 2015)
Uqcrb	TTTCAGCATCAAGCAAGTGG	TCAGGTCCAGGGCTCTCTTA	Own design
Uqcrc1	GGGGCAAAAACATCCTTAGG	ATCCGGCTCTCCCACTCAGC	(Ramamoorthy et al., 2015)
Uqcr11	TGCTGAGCAGGTTTCTAGGC	TCCTTCTTAAACTTGCCGTTG	(Ramamoorthy et al., 2015)
Uqcrc2	CATCTTGCTTTGCTGTCTGC	GCAGAGGCACTCCTCCAG	Own design
Uqcrfs1	GAGCCACCTGTTCTGGATGT	CAAGAACTTCAGCACGACGA	Own design
Uqcrq	GGCACGTGATCTCCTACAGC	GCAGGCCGTCTACTTGTCAT	Own design
Cox5a	GGGTCACACGAGACAGATGA	GGAACCAGATCATAGCCAACA	(Yoon et al., 2010)
Cox5b	CGTCCATCAGCAACAAGAGA	AGATAACACAGGGGCTCAGT	(Ramamoorthy et al., 2015)
Cox4i1	TTCAGTTGTACCGCATCCAG	TGGGGCCATACACATAGCTC	Own design
Bnip3	AAAGGGGGAATTTTCTCAGC	AACACCCAAGGACCATGCTA	Own design
Beclin1	GGCCAATAAGATGGGTCTGA	GCTGCACACAGTCCAGAAAA	Own design
Lc3b	CTGACCACGTGAACATGAGC	AACCATTGGCTTTGTTGGAG	Own design
Myh7	AGTCCCAGGTCAACAAGCTG	TTCCACCTAAAGGGCTGTTG	(Siles et al., 2013)
Myh2	CGATGATCTTGCCAGTAATG	ATAACTGAGATACCAGCG	(Siles et al., 2013)
Myh4	ACAGACTAAAGTGAAAGCC	CTCTCAACAGAAAGATGGAT	(Siles et al., 2013)

Pink1	ATCCAGAGGCAGTTCATG GT	TTAAGATGGCTTCGCTGGAG	(Akundi et al., 2011)
Parkin	AAACCGGATGAGTGGTGA GT	AGCTACCGACGTGTCCTTGT	(Bouman et al., 2011)

Western blots

C2C12 myotubes and surgically dissected gastrocnemius were washed with ice-cold PBS and resuspended in RIPA lysis buffer (150 mM NaCl, 50 mM Tris pH 8.0 0.1% NP40, 0.5 % SDS, 2 mM EDTA) containing protease inhibitors (10 µg/ml aprotinin, leupeptin, pepstatin A and PMSF) as previously described (Shirakihara et al., 2007). Lysates were sonicated in a Sonics Vibra-Cell™ CV188 instrument (Misonix Inc., Farmingdale, NY), clarified by centrifugation and quantified by Bradford assay. Lysates were then boiled and loaded onto 10 % polyacrylamide gels and transferred to a PVDF membrane (Immobilon-P, Millipore, Bedford, MA, USA). Membranes were blocked with 5 % non-fat milk in TBST (20 mM Tris pH 7.5, 150 mM NaCl, 0.1% Tween 20) buffer and split into two sections at the level indicated in the Figure Legend. The upper section was used to detect ZEB1 (HPA027524, dilution 1/500) while the lower section was used to detect MuRF1 (C-11, 1/900) and GAPDH (14C10, 1/4000). After washing several times with TBST buffer, membranes were incubated with their respective HRP-conjugated secondary antibodies. The chemiluminescence reaction was developed with Clarity Western ECL (Bio-Rad).

Promoter analysis and mutagenesis of the *Fbxo32* promoter

Consensus binding sites for ZEB1 in mouse *Fbxo32* and *Trim63* promoters were identified using MacVector 16.0.8 software (MacVector Inc, Apex, NC, USA). FOXO3 binding sites in both promoters were described elsewhere (Sandri et al., 2004) and/or identified using MacVector 16.0.8 software. The ZEB1 binding site at -85 bp

(CACGTG) of the 0.4 kb *Fbxo32* promoter luciferase reporter (Sandri et al., 2004) was mutated to a sequence (CACTCA) known not to bind to ZEB1 (Sekido et al., 1994). Site-directed mutagenesis was performed as previously described (Ester Sánchez-Tilló et al., 2011, De Barrios, et al., 2017). Briefly, the 0.4 kb *Fbxo32* luciferase reporter was amplified using *PfuUltra* High-Fidelity DNA polymerase (Stratagene-Agilent) and oligos described in Table 4. DNA was then digested with DpnI and transformed into chemically competent bacteria.

Table 4

Oligonucleotides for site directed mutagenesis

Gene Target	Sequence
Upper strand	GAGCCTATAAACAAAGCCACTCAGCCTCGGGGCGCGGGGGG
Lower strand	CCCCCCGCGCCCCGAGGCTGAGTGGCTTTGTTTATAGGCTC

Chromatin Immunoprecipitation Assays

Chromatin immunoprecipitation (ChIP) assays were performed using EpiQuick ChIP kit (Epigentek, Farmingdale, NY, USA) as per manufacturer's instructions. Briefly, C2C12 myoblasts, starved, and non-starved myotubes were incubated for 20 min with 1% formaldehyde solution (Electron Microscopy Sciences, Hatfield, PA, USA) at room temperature followed by incubation with 1.25 mM glycine. Lysates were sonicated in an Ultrasonic Liquid Processor (Misonix Inc. Farmingdale, NY, USA). Settings were as follows: 25 amplitude, 7 min (on for 10 s, off for 20 s on ice). Goat anti-mouse/human ZEB1 (4 μg, clone E-20X), mouse MYOD1 (4 μg, clone G-1) and their corresponding normal goat and mouse IgG (4 μg, Jackson ImmunoResearch Europe Ltd.), respectively, were used. Design of primers for qRT-PCR was conducted using MacVector software (MacVector Inc). DNA fragments were

quantified by qRT-PCR as detailed above using the primers detailed in Table 5. In all qRT-PCRs, values shown represent relative binding in relation to input and are the average of at least three independent ChIP experiments, each one performed in triplicate.

Table 5

Oligonucleotides for ChIP assays

Promoter Region	Forward 5' → 3'	Reverse 5' → 3'
Fbxo32 promoter ZEB1 binding site (-85 bp) (-105/+48 bp)	GGCGAGCCTATAAAC AAAGCCAC	CTCCTGACTCTGGGAATG CTGAG
Nrf1 promoter ZEB1 binding site (-43720 bp) (-43772/-43598 bp)	GGCTGTCCTGGAACT CACTC	GGCTGTCCTGGAACTCAC TC
Nrf2 promoter ZEB1 binding site (-499 bp) (-657/-450 bp)	TGTGCTTGCACCAAC TGTTT	CCCACTGTTGATCCTCCT CT

Cell line-based transcriptional assays

C2C12 and 293T cells were seeded in 12-well plates and transiently transfected with firefly luciferase reporters for *Fbxo32*, *Trim63* or L8G5 along with pcDNA3-*Zeb1* or pECE-*Foxo3* with 2 µl of Lipofectamine® 3000 (Thermo-Fisher Scientific) per well. Knockdown of gene expression with siRNAs was performed as described above. When cells needed to be transfected with both cDNA expression vectors and siRNAs, cells were first transfected with siRNAs (with RNAiMAX) for 5 h, washed and replaced with fresh medium. Twenty-four hours later, cDNA expression vectors were

transfected (Lipofectamine® 3000) during 5 h. As control, equal molar amounts of the corresponding expression empty vectors and/or siCtrl were also transfected. The total amount of transfected DNA was topped up to the same amount in all conditions with pBluescript SK. To normalize for transfection efficiency, 0.5 µg of SV40-β-galactosidase were co-transfected in each condition. Levels of luciferase and β-galactosidase activity were assayed 48 hours later with Luciferase Assay System kit (Promega Corp.) and Luminiscent β-galactosidase Detection kit II (Clontech, Takara Kusatsu, Shiga, Japan), respectively. Relative luciferase activity (RLU) was determined using Modulus II Glomax microplate reader (Promega Corp.). Data shown correspond to the mean of at least three independent experiments with each transfection conducted as duplicates. When RLU values are represented in a histogram, the control condition is set to a RLU value of 100.

In vivo assessment of the *Fbxo32* promoter transcription

Stock solution (10X, weight/volume) of Pluronic L-64 (Sigma Aldrich) was prepared in pure water and stored at 4ºC. The gastrocnemius muscles of both hindlimbs of wild-type and *Zeb1* (+/-) mice were injected with 25 *µ*g of the 3.5 kb *Fbxo32* promoter, mixed with an equal amount of 2X Pluronic L-64 (derived from 10X stock solution diluted 1:5 in PBS), as described in (Song et al., 2014). After 3.5 days, the left hindlimb was immobilized for 3.5 additional days. At day 7, luciferase activity was assessed by bioluminescent imaging (M. S. Evans et al., 2014). Briefly, mice were anesthetized with 500 mg/kg of Avertin (Sigma-Aldrich) and the plastic cast was removed. Then, mice were injected i.p. with 15 mM of CycLuc1 substrate (Calbiochem®, EMD Millipore, Billerica, MA) in 100 *µ*l of PBS. Ten minutes later, the photon flux signal was collected in a charge-coupled ORCA-II BT imaging system (Hamamatsu Photonics, Hamamatsu City, Japan). Bioluminescence data was analyzed with Wasabi! Imaging Software (Hamamatsu Photonics) and represented as the total photon flux/sec/cm^2 signal emitted by each hindlimb using the signal emitted by the head and trunk as background reference.

Assessment of the activity of mitochondrial complexes

Muscle protein extracts for measuring the enzymatic activity of mitochondrial respiratory chain (MRC) complexes CII+CIII, CIV and citrate synthase (CS), were prepared in mannitol extraction buffer (225 mM mannitol (Sigma Aldrich M-9546), 75 mM sucrose (Sigma Aldrich S9378), 10 nM Tris-HCl, 0.1 mM EDTA). Briefly, 10-20 mg of frozen gastrocnemius muscle were homogenized 3 times at 850 rpm, for 5 seconds in 200 μl of ice-cold mannitol buffer. The homogenized tissue was collected and centrifuged at 650 g for 20 minutes at 4ºC. The supernatant was separated in a new eppendorf and the pellet was re-suspended in other 200 μl of ice-cold mannitol buffer and homogenized and centrifuged again. The two supernatants were mixed and quantified by Bradford assay.

Measurement of mitochondrial CII+CIII, CIV and CS enzymatic activity

The enzymatic activity of mitochondrial respiratory chain (MRC) complexes II+III, IV and Citrate Synthase (CS) were measured spectrophotometrically in mannitol-homogenized gastrocnemius muscle from two-to-three months old *Zeb1*$^{skm-/-}$ and control mice, concentrated at 2 μg/μl.

CII+CIII activity: The combined activity of CII and CIII transfers the electrons from succinate to Cytochrome C. This activity can be measured by following the increasing absorbance at 550 nm of the Cytochrome C reduced. The consequential oxidation of Cytochrome C is inhibited by KCN, which is added in the reaction solution (Succinate 20mM, K2HPO4 pH 7.5 20mM, BSA 2 mg/ml, KCN 1mM). Briefly, 20 μl of 2 μg/μl mannitol-homogenized tissue were added to 880 μl of the reaction solution. Samples were incubated for 5 minutes at 37ºC. A blank sample (mannitol buffer only) was also incubated. After 5 minutes, the reaction was started by adding 100 μl of the Cytochrome C 1 mM in the reaction solution and the absorbance at 550 nm was measured for 3 minutes, every 20 seconds. The activity of at least six mice for each genotype was measured.

CIV activity: The complex IV of the respiratory chain transfers electrons from reduced cytochrome C to oxygen. This activity can be measured by monitoring the decreasing absorbance at 550 nM of 100% reduced cytochrome C solution

(Potassium phosphate buffer 50 mM, pH7, and 100 μM cytochrome C). Briefly, 980 μl of reduced solution were incubated for 5 minutes at 37ºC. After 5 minutes, the reaction solution was started by adding 20 μl of 2 μg/μl concentrated mannitol-homogenated tissue. The decreasing absorbance was measured at 550 nm for 3 minutes, every 15 seconds. The activity of at least five mice for each genotype was measured.

CS activity: CS is an enzyme belonging to the tricarboxylic acid (TCA) cycle, widely used as a reliable marker of mitochondrial content. CS catalyzes the formation of citrate from oxaloacetate and acetyl-coA. The reduced CoA, which is formed in the reaction, transforms the 5,5'-dithiobis-2-nitrobenzoic acid (DNTB) in 2-nitro-5-thiobenzoic acid (TNB), which absorbs at 412 nm (Reaction solution: 100μM DNTB, 100mM Tris-HCL pH 8.1, 300 μM Acetyl-coA, 500 μM). Briefly, 20 μl of 2 mg/ml mannitol-homogenized tissue were added to 930 μl of the reaction solution. After 5 minutes of incubation at 37ºC, the basal absorbance at 412 nm was measured for 4 minutes, every 15 seconds. The reaction was then started by adding 50 μl of 10 mM Oxaloacetate in Tris-HCL 100 mM pH 8.1. The increasing absorbance of the reaction was measured for 4 minutes, every15 seconds. The activity of at least six mice for each genotype was measured.

The CII+CIII and CIV activity were normalized to citrate synthase (CS) activity. The absorbance changes along time of CII+CIII, CIV and CS activities were monitored in a HITACHI-U2900 spectrophotometer, at 37ºC, using the UV-Solution software 2.2 (Hitachi High Technologies, Ibaraki, Japan). The results were calculated as nanomoles of consumed substrate or generated product per minute and milligram of protein (nmol/min·mg protein) and expressed as fold increase versus age matched controls, arbitrarily set to 1.

High-resolution respirometry

High-resolution respirometry was performed at 37°C using polarographic oxygen sensors in a two-chamber Oxygraph-2k system according to manufacturer's instructions (OROBOROS Instruments, Innsbruck, Austria). The high-resolution oxygraph permits to measure oxygen concentration and oxygen consumption in

biological samples, with high resolution and sensitivity. Gastrocnemius muscles of *Zeb1*$^{skm-/-}$ and control mice were extracted and immediately put in ice-cold biopsy preservation solution (BIOPS) buffer (CaK_2EGTA 2.77 mM; K_2EGTA 7.23 mM; Na_2ATP 5.77 mM; $MgCl_2$ 6.56 mM; Taurine 20 mM; Na_2Phosphocreatine 15 mM; Imidazole 20 mM; DTT 0.5 mM; MES 50 mM; pH 7.1) Muscle fibers were delicately separated and then permeabilized in ice-cold BIOPS buffer with 5 *µ*g/ml saponin, for 30 minutes at 4ºC, in agitation. The permeabilized fibers were then placed for 10 minutes in agitation in ice-cold mitochondria respiratory buffer (MIRO5) (EGTA 0.5 mM; $MgCl_2$ 3mM; K-lactobionate 60 mM; Taurine 20 mM; KH_2PO_4 10 mM; HEPES 20 mM; Sucrose 110 mM; BSA 1 mg/ml). 3.5 to 4.5 mg of permeabilized fibers from each genotype were weighted and put in oxygraphy chambers. In each experiment a *Zeb1*$^{skm-/-}$ and control mice, in basal or fasted condition, were analysed. Manual titration of OXPHOS substrates and inhibitors was performed using Hamilton syringes (Hamilton Company, Reno, NV, USA). Oxygen consumption rates were calculated using DatLab software v5.1.1.9 (Oroboros Instruments, Innsbruck, Austria) and expressed as picomoles per second per mg of tissue. The quantities and volume to assess respiratory activity of each complex are detailed below:

Substrate	**Concentration**	**Volume used**
Glutamate	1 M	20 *µ*l
Malate	0,5 M	8 *µ*l
ADP	0,5 M	40 *µ*l
Pyruvate	0,25 M	40 *µ*l
Succinate	1 M	20 *µ*l
Rotenone	2 mM	1 *µ*l
Malonate	1 M	10 *µ*l
G3P	0,5 M	43 *µ*l
Antimycin-A	20 mM	25 *µ*l
Ascorbate	0,2 M	42,5 *µ*l
TMPD	6 mM	42,5 *µ*l
KCN	5.2 mg/ml	17 *µ*l

SDH staining

For succinate dehydrogenase (SDH) staining, 8 μm cryosections were air dried for ten minutes at room temperature and then incubated for 20 minutes at 37ºC in SDH staining solution (5 mM EDTA, 1 mM KCN, 0.2 mM Phenazine methosulfate (PMS), 50 mM Succinic Acid, 1.5 mM Nitro Blue Tetrazolium (NBT); pH 7.6). Sections were then rinsed three times during five minutes each in distilled water and mounted with aqueous mounting medium (ProLong^{TM} Glass Antifade Mountant, Life Technologies). SDH intensity was measured using ImageJ software (NIH, Bethesda, MD) in at least five different pictures for each mouse, at 20X magnification. At least seven different mice for each genotype and condition were analyzed.

Assessment of fiber type composition by ATPase staining

For ATPase staining, 8μm cryosections were air-dried for ten minutes and then pre-incubated in acidic solution (pH 4.5) for 5 minutes at room temperature. This acidic pre-incubation permits to distinguish between slow-twitch (type I) appearing darkest, fast fatigue-resistant (type IIa), the lightest, and fast-fatigable (type IIb), with an intermediate color, fibers. After washing in deionized water, sections were incubated for 25 minutes in ATP solution (60 mg of ATP (Sigma-Aldrich) in 6 ml of 0.1 M sodium barbital (Sigma-Aldrich), 21 ml of distillate water and 3 ml of 0.18 M $CaCl_2$) at room temperature. Sections were then washed in three changes of 1% $CaCl_2$ and incubated ten minutes in 2% Cobalt Chloride (Sigma-Aldrich) followed by ten minutes' incubation in 5 mM sodium barbital. Next, they were washed in deionized water and incubated 30 seconds in 2% Ammonium Sulfide (Sigma-Aldrich). Sections were dehydrated in ascending concentration of ethanol and, after clearing in two changes of xylene, they were mounted in DPX mounting medium. Fiber type composition was measured using ImageJ software (NIH, Bethesda, MD). The three different fiber types were counted in a total of at least 600 fibers for each mouse, at 4X magnification pictures. The relative abundance of each fiber type was calculated relative to the total number of fibers counted. Bars represent the mean with s.e.m of at least four different mice for each genotype and condition.

Assessment of reactive oxygen species by DHE

The DHE oxidative dye was used to measure the in situ gastrocnemius production of superoxide anion. Muscle cryosections (10 μm thick) were air-dried for ten minutes and then incubated for 30 minutes at 37ºC with 2.5 μM DHE in PBS. DHE is freely permeable to cells and in the presence of superoxide anions it is oxidized to Ethidium Bromide and produces a red fluorescence by intercalating to DNA. The DHE intensity was measured using ImageJ software (NIH, Bethesda, MD) creating a mask over DAPI, in at least five different pictures for each mouse, at 20X magnification. Bars represent the mean with s.e.m of at least four different mice for each genotype and condition.

Staining of lipids by Oil Red O (ORO)

Neutral lipids were stained in 8 μm gastrocnemius cryosections with the fat soluble lysochrome ORO ($C_{26}H_{24}N_4O$), as described elsewhere (Mehlem, Hagberg, Muhl, Eriksson, & Falkevall, 2013). Briefly, a starting concentration of 5% ORO dye in isopropyl alcohol was diluted 1,5:1 in distilled water, where ORO is minimally soluble. The solution was leaved to thicken ten minutes at 4ºC, and then filtrated in 0.45 μm filter to remove precipitates. Next, cryosections were incubated for 10 minutes at R/T with ORO solution, permitting the hydrophobic dye to move from solution to lipids within the muscle, and counterstained 15 seconds in hematoxylin. Sections were then washed for 20 minutes under running tap water to remove ORO excess and mounted in aqueous medium. At least 7 captures (40X magnification) for each mice and condition were analyzed using ImageJ software (NIH, Bethesda, MD). Bars represent the mean with s.e.m of at least six different mice for each genotype and condition.

RESULTS

RESULTS

Chapter I. Expression, role and mechanism of action of ZEB1 in muscle atrophy induced by immobilization

ZEB1 protects skeletal muscle from sparing upon immobilization

To investigate a potential role of ZEB1 in muscle atrophy, we first examined whether its downregulation has an effect on muscle mass loss in response to immobilization. Two-to-three month-old wild-type and *Zeb1* (+/-) mice were subjected to unilateral hindlimb immobilization for up to 17 days and the weight of both gastrocnemius muscles, from the immobilized and non-immobilized hindlimbs, was assessed over time. As expected, and respect to the control non-immobilized counterpart, gastrocnemius muscles in the immobilized hindlimb displayed a progressive weight loss (Figure 10A and Figure 10B). Notably, muscle sparing by immobilization was larger in *Zeb1* (+/-) mice than in wild-type mice (Figure 10A and Figure 10B).

These data suggest that ZEB1 expression protects skeletal muscle from an otherwise excessive atrophy in response to immobilization.

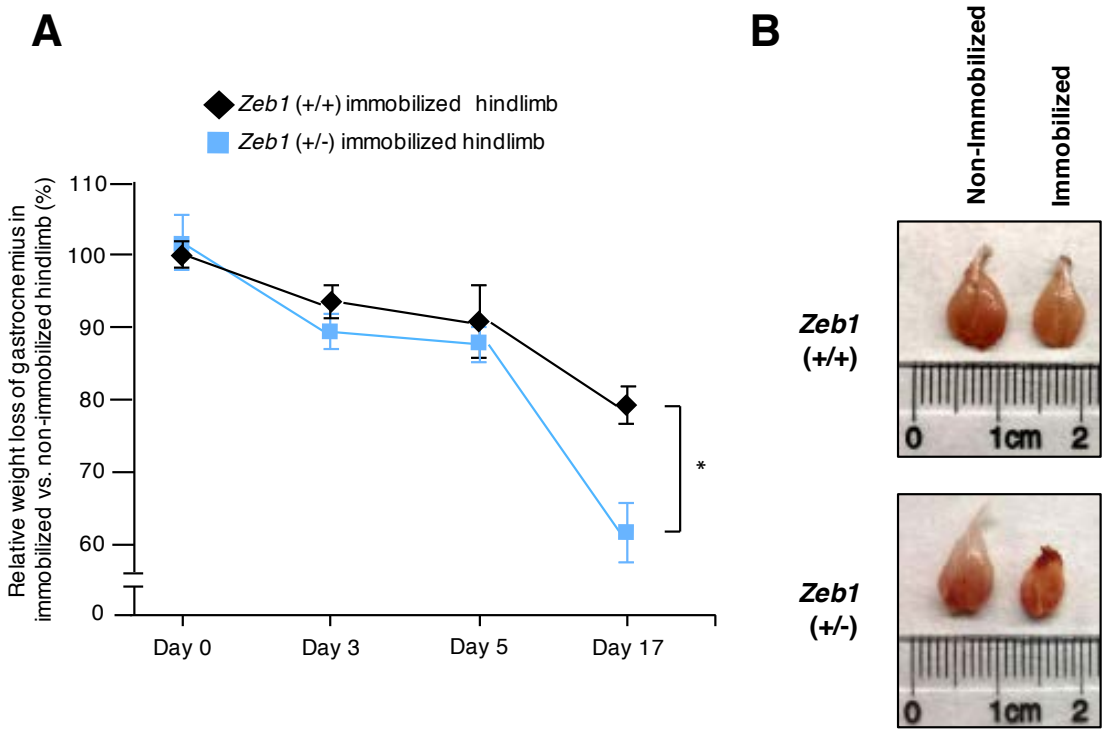

Figure 10: ZEB1 protects skeletal muscle from sparing upon immobilization. **(A)** Two-to-three-month old wild-type and *Zeb1* (+/-) mice were subjected to unilateral hindlimb immobilization for different periods as described in Materials and Methods. At each time point, mice were euthanized and the weight of their immobilized gastrocnemius muscles was assessed with respect to that in the contralateral non-immobilized hindlimb. The weight of the gastrocnemius in the immobilized hindlimb vis-à-vis that in the non-immobilized at the start of the protocol (day 0) was set arbitrarily to 100. At least 5 mice of each genotype were examined. **(B)** As in (A), representative images of non-immobilized and immobilized gastrocnemius muscles from wild-type and *Zeb1* (+/-) mice at day 17 of the immobilization protocol.

Muscle atrophy is manifested by an increase in the number of smaller size myofibers and/or a decrease of larger ones. Staining with hematoxylin/eosin, and immunofluorescence staining for the structural protein laminin revealed a smaller size in the myofibers of immobilized *Zeb1* (+/-) gastrocnemius muscles compared to wild-type counterparts (Figure 11A and Figure 11B). Fiber cross-sectional area (CSA) analysis confirmed that, upon immobilization, *Zeb1* (+/-) muscles contained a larger share of fibers of less than 800 μm^2 and a lower share of fibers of 800 μm^2 or more than wild-type muscles (Figure 11C and Figure 11D).

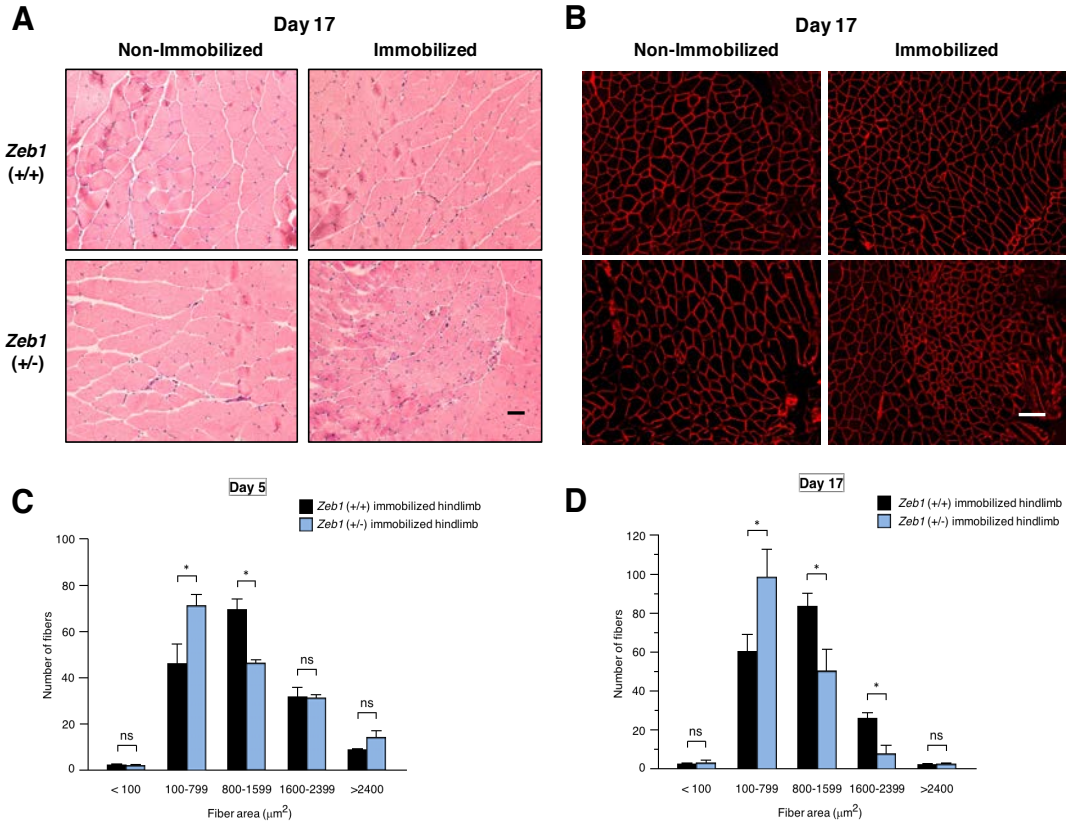

Figure 11: ZEB1 protects skeletal muscle from sparing upon immobilization. **(A)** Wild-type and *Zeb1* (+/-) mice were subjected to unilateral hindlimb immobilization during 17 days, euthanized and their gastrocnemius muscles stained for hematoxylin/eosin. Scale bar: 50 μm. **(B)** As in (A) but sections were stained with an antibody against laminin (clone 48H-2). Scale bar: 100 μm. **(C)** Myofiber cross-sectional analysis in the immobilized gastrocnemius of wild-type and *Zeb1* (+/-) mice at day 5 of the immobilization protocol. Myofiber area was assessed as described in Materials and Methods. A total of 160 myofibers were measured from at least 8 mice, half from each genotype. **(D)** As in (C) but the myofiber area was measured on day 17 of the immobilization protocol.

Next, we examined whether ZEB1 expression is modulated during hindlimb immobilization. Immobilization resulted in a slight increase in ZEB1 mRNA and protein (Figure 12A and Figure 12B). ZEB1 was expressed at the nuclei of some myofibers (Figure 12C) and the number of ZEB1-positive nuclei in gastrocnemius muscles from both genotypes was similar in the immobilized and non-immobilized hindlimbs (Figure 12D).

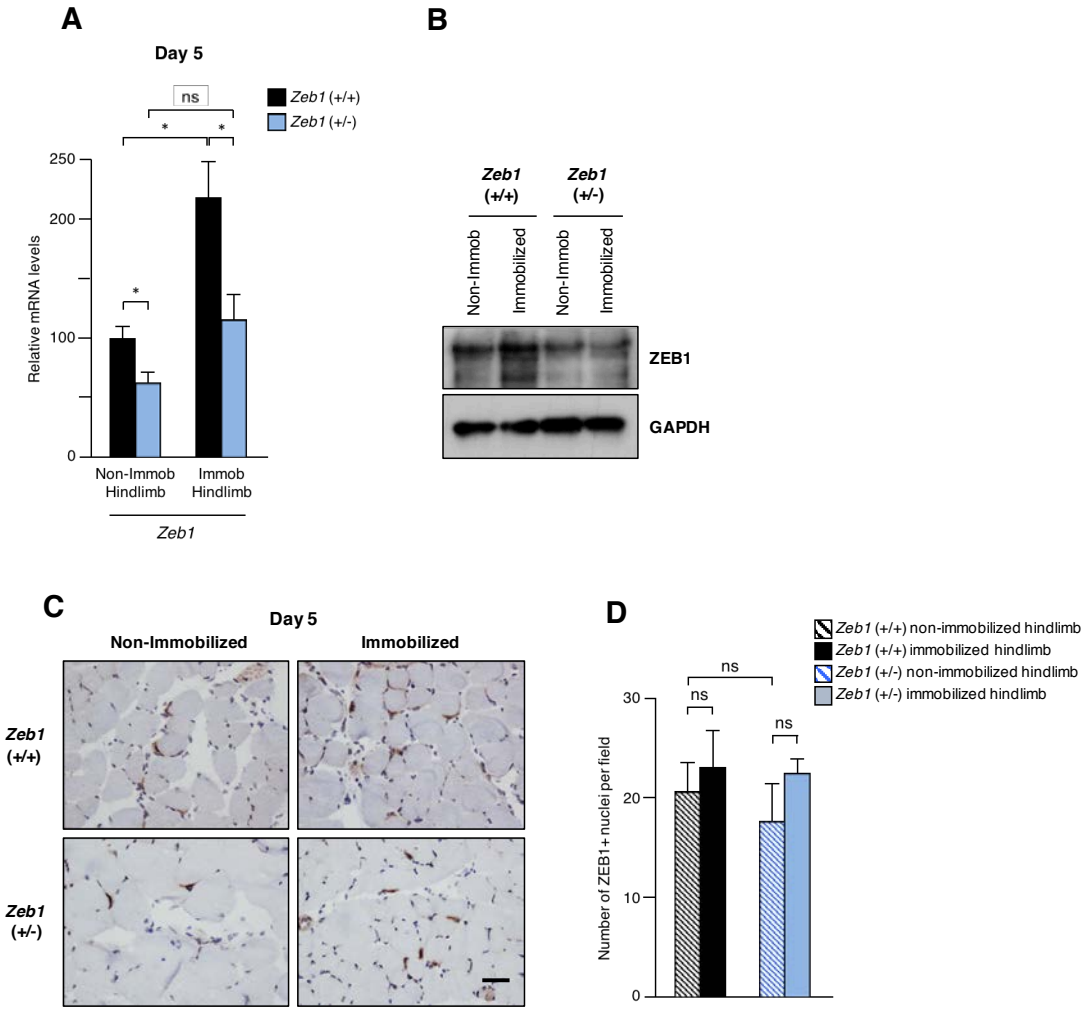

Figure 12: ZEB1 protects skeletal muscle from sparing upon immobilization **(A)** *Zeb1* expression slightly increases upon immobilization. Wild-type and *Zeb1* (+/-) mice were subjected to unilateral hindlimb immobilization for 5 days. At that time, mice were euthanized and *Zeb1* mRNA levels were assessed in the immobilized and non-immobilized gastrocnemius by quantitative real time PCR (qRT-PCR) using Gapdh as a reference gene. The results are the mean with standard error of at least five mice for each genotype and condition. **(B)** As in (A) but ZEB1 expression was assessed at the protein level by Western blot. Gastrocnemius muscle lysates were blotted for ZEB1 (clone HPA027524) along with GAPDH (clone 14C10). The blots shown are representative of three independent experiments. **(C)** As in (A), but the ZEB1 expression was assessed by immunohistochemistry (clone H102) at day 5. Captures are representative of at least five mice for each genotype and condition. Scale bar: 40 μm. **(D)** Immobilization does not alter the number of ZEB1 positive nuclei. The absolute number of nuclei positive for ZEB1 per 20X magnification field was calculated in four fields. Data are the average of four mice for each genotype and condition.

ZEB1 inhibits the in vivo expression of atrogenes

We next investigated whether ZEB1 regulates the expression of atrogenes. Although muscle weight loss in response to immobilization progressively increases over time,

the expression of Atrogin-1 and MuRF1 peaks at around day 3 post-immobilization and declines afterward (Bodine et al., 2001).

Wild-type and *Zeb1* (+/-) mice were subjected to unilateral hindlimb immobilization and their gastrocnemius muscles examined for Atrogin-1/*Fbxo32* mRNA and protein expression. Levels of Atrogin-1/*Fbxo32* expression were similar in the non-immobilized gastrocnemius muscles from both genotypes. However, its induction upon immobilization was larger in *Zeb1* (+/-) muscles (Figure 13A and Figure 13B).

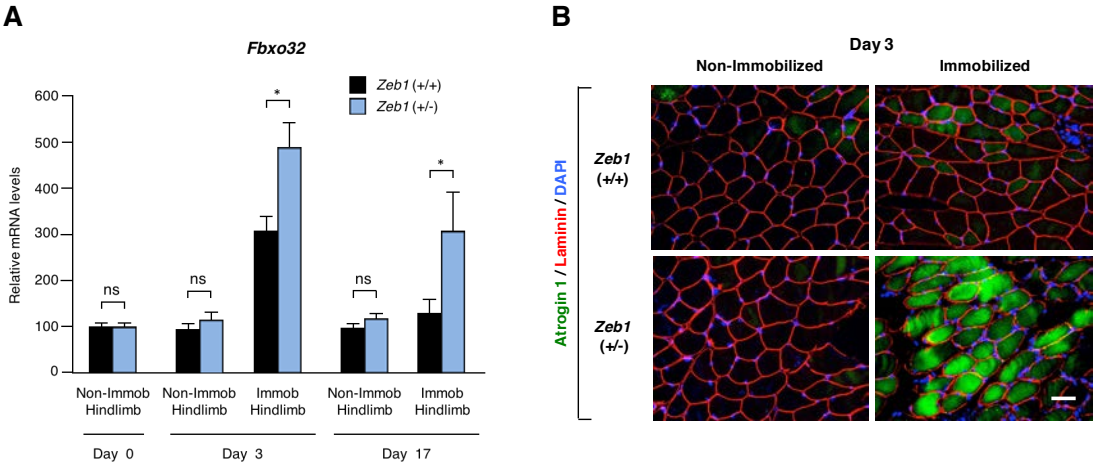

Figure 13: Zeb1 inhibits the in vivo induction of atrogenes upon immobilization. **(A)** Wild-type and *Zeb1* (+/-) mice were subjected to unilateral hindlimb immobilization during 3 and 17 days and their immobilized and non-immobilized gastrocnemius were then examined for *Fbxo32* mRNA expression by qRT-PCR with respect to Gapdh. *Fbxo32* mRNA levels in the non-immobilized hindlimb at day 0 were arbitrarily set to 100 with all other data genotypes and conditions referred to them. Data represent the mean of at least 5 mice for each genotype and condition. **(B)** The gastrocnemius of mice from both genotypes after three days of the unilateral hindlimb immobilization protocol were stained with antibodies against Atrogin-1 (clone AP2041), laminin (clone 48H-2), and counterstained for DAPI for nuclear staining. Scale bar: 50 μm.

A similar pattern was observed for MuRF1/*Trim63*; non-immobilized gastrocnemius muscles from both genotypes expressed equivalent levels of this atrogene but immobilization induced higher *Trim63* mRNA and MuRF1 protein levels in *Zeb1* (+/-) gastrocnemius muscles than in wild-type counterparts (Figure 14A and Figure 14B).

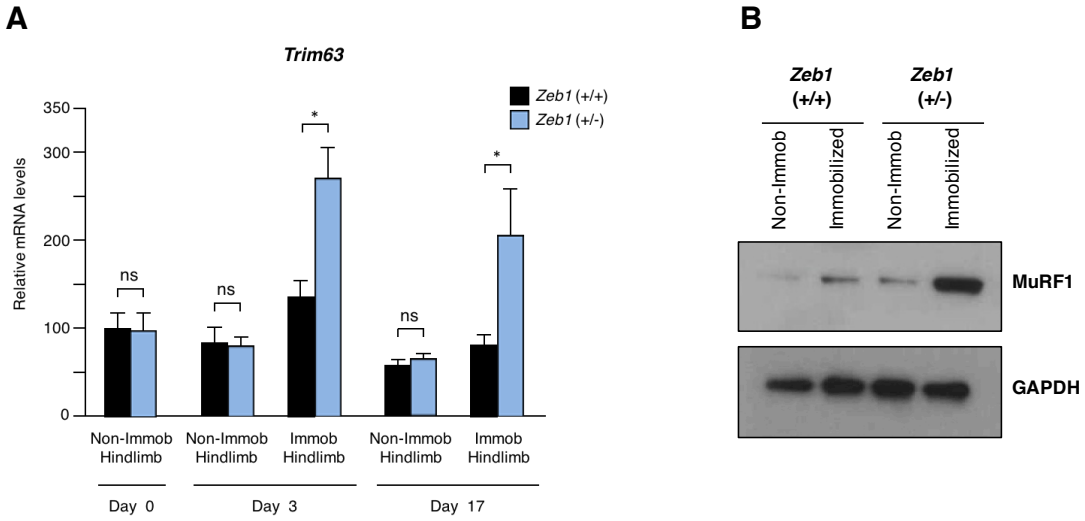

Figure 14: Zeb1 inhibits the in vivo induction of atrogenes upon immobilization. **(A)** As in Figure 13A, but for Trim63. **(B)** As in Figure 13B but the lysates from gastrocnemius of mice from both genotypes after three days of the unilateral hindlimb immobilization protocol were blotted for MuRF1 (clone C11) along with GAPDH (clone 14C10) as a loading control. The blots shown are representative of three independent experiments.

Altogether, these results indicate that ZEB1 inhibits Atrogin-1/*Fbxo32* and MuRF1/*Trim63* expression in *vivo.*

Several conditions induce muscle atrophy, like immobilization, bed rest, denervation, fasting or cancer. Atrogin-1 and MuRF1 are the archetypal atrogenes but many other genes are also induced during muscle atrophy. The set of atrogenes upregulated in response to different atrophy-inducing conditions is largely, although not completely, overlapping. We tested whether ZEB1 regulates some of these other atrogenes. The immobilized and non-immobilized gastrocnemius of wild-type and *Zeb1* (+/-) mice were examined for the expression of atrogenes involved in different cellular processes, namely: proteasome system [proteasome subunit, alpha type 1 (*Psma1*)], autophagy [Cathepsin L (*Ctsl*), GABA A-receptor associated protein-like 1 (*Gabarapl1*)], protein synthesis [eukaryotic translation initiation factor 4E binding protein 1 (*4ebp1*)], and oxidative stress [nuclear factor E2 related factor 2 (*Nrf2*)]. Although with different temporal patterns and at lower levels than in the case of *Fbxo32* and *Trim63*, expression of these atrogenes increased in immobilized wild-type gastrocnemius but, as for *Fbxo32* and *Trim63,* their induction was higher in *Zeb1* (+/-) muscles (Figure 15).

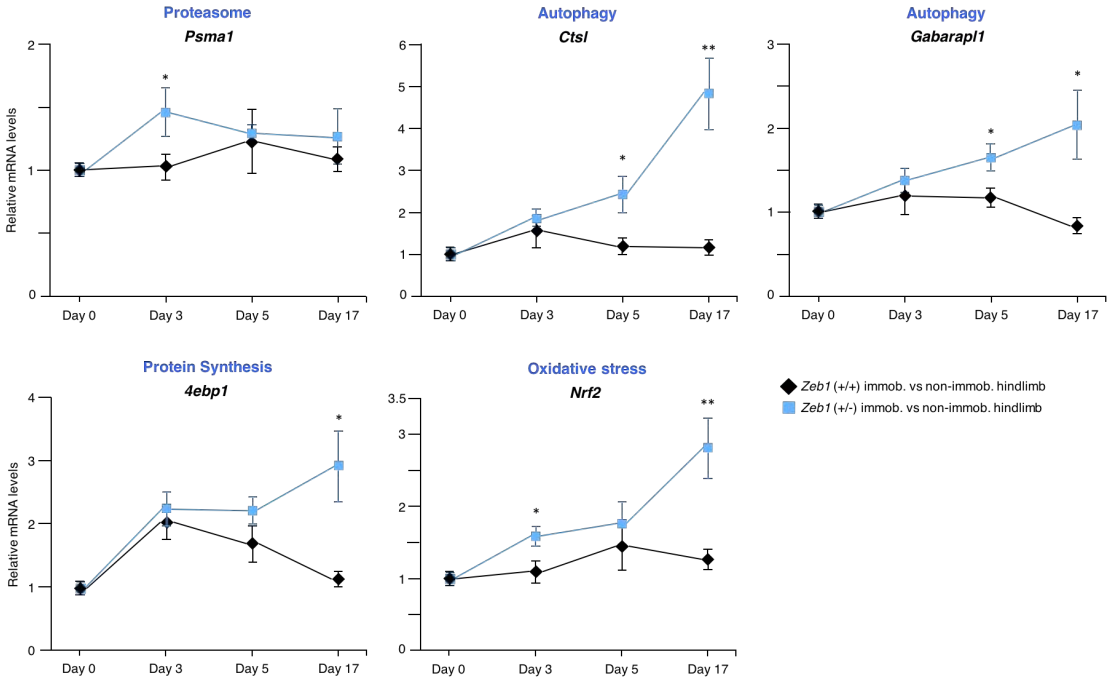

Figure 15: Zeb1 inhibits the in vivo induction of atrogenes upon immobilization. Wild-type and *Zeb1* (+/-) mice were subjected to the unilateral hindlimb immobilization protocol for 3, 5, and 17 days. At the end of each time point, mice were euthanized and the mRNA levels for *Psma1*, *Ctsl*, *Gabarapl1, 4ebp1, and Nrf2* were assessed by qRT-PCR. For each gene, mRNA levels shown correspond to that in the gastrocnemius of the immobilized with respect to the contralateral non-immobilized hindlimb. The gene expression in the non-immobilized gastrocnemius at days 3, 5, and 17 was similar to that on day 0 shown. At least five mice from each genotype and day were analyzed.

Altogether, these results indicate that atrogenes are under negative regulation by ZEB1, whose expression prevents unrestricted atrogene overexpression in response to immobilization.

ZEB1 inhibits atrogene expression and size reduction in starved C2C12 myotubes

We sought to confirm the role of ZEB1 in muscle atrophy using the C2C12 cell myogenic model, which has been widely employed to study gene expression during both muscle differentiation and atrophy (Blau et al., 1983). When grown in high serum (hereafter referred as growth medium), C2C12 cells maintain a proliferating myoblast-like phenotype (see representative pictures in Figure 16 and a scheme in Figure 17A). Only when cells exit the cell cycle upon reaching confluence and are

switched into a low-serum medium (differentiation medium) they fuse and form terminally differentiated multinucleated myotubes. When C2C12 myotubes are starved of serum, glucose, and amino acids (atrophic medium), they undergo a rapid reduction in their mean myotube diameter.

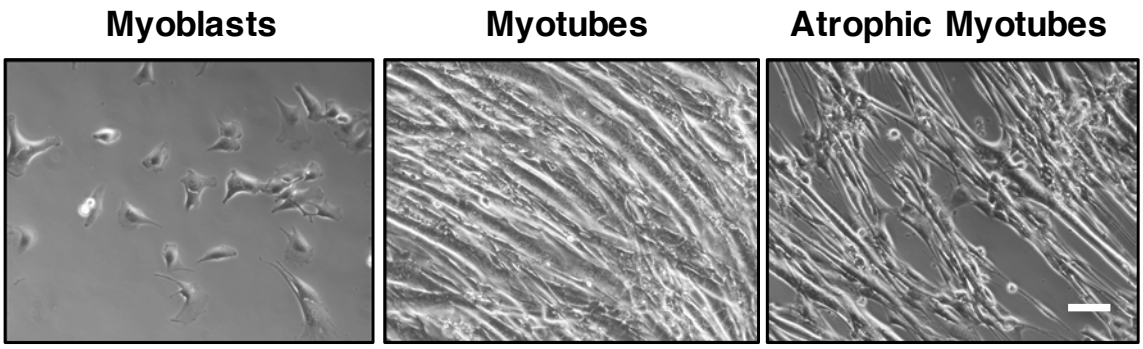

Figure 16: ZEB1 inhibits atrogene expression and size reduction in starved C2C12 myotubes
When C2C12 cells are grown in the growth medium, cells maintain a proliferating myoblast-like phenotype. Once they reach confluence and are cultured in differentiation medium they fuse to form terminally multinucleated myotubes. When C2C12 myotubes are cultured in atrophic medium, they undergo a reduction in myotube diameter. Scale bar: 50 μm.

At days three and four of their differentiation, C2C12 myotubes were transfected with either a siRNA control (siCtrl) or any of two siRNA sequences previously validated to specifically knockdown *Zeb1* (si*Zeb1*-A, si*Zeb1*-B) (Siles et al., 2013) (Figure 17A and Figure 17B). On day 5, the differentiation medium was replaced by atrophic medium for up to 8 hours (Figure 17A).

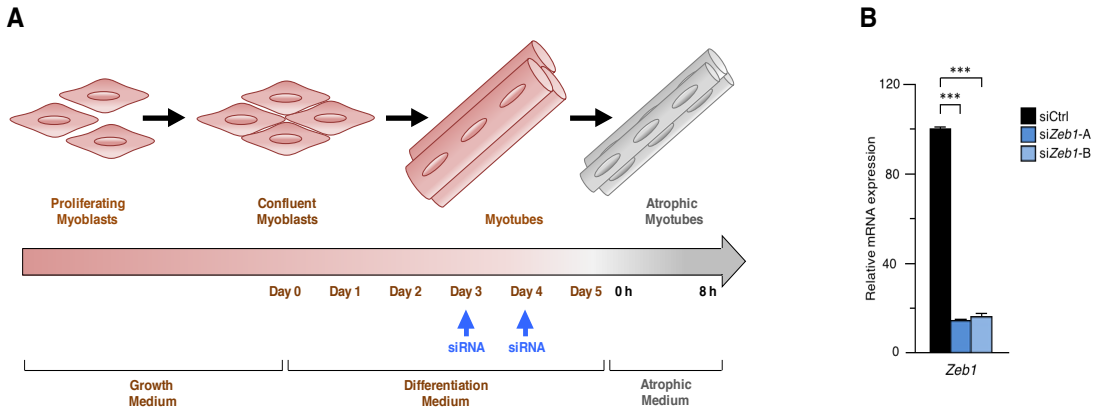

Figure 17: ZEB1 inhibits atrogene expression and size reduction in starved C2C12 myotubes **(A)** Scheme of the starvation-induced atrophy protocol in C2C12 myotubes. C2C12 myotubes were transfected with siCtrl or any of two siRNA sequences previously validated to specifically knockdown Zeb1 and their differentiation medium was replaced by atrophic medium for up to 8 h. **(B)** C2C12 myotubes were transfected with a control siRNA (siCtrl) or with either of two previously validated siRNAs against *Zeb1* (si*Zeb1*-A and si*Zeb1*-B) (Siles et al., 2013). mRNA levels were assessed by qRT-PCR with respect to Gapdh.

In line with our *in vivo* results above, the diameter reduction induced by the atrophic medium was larger in C2C12 myotubes that had been knocked down for *Zeb1* (Figure 18A and Figure 18B). Likewise, *Zeb1* mRNA and protein expression slightly increased when C2C12 myotubes were cultured in atrophic medium (Figure 18C and Figure 18D). Altogether these data indicate that ZEB1 inhibits muscle atrophy both *in vivo* and in the C2C12 cell model.

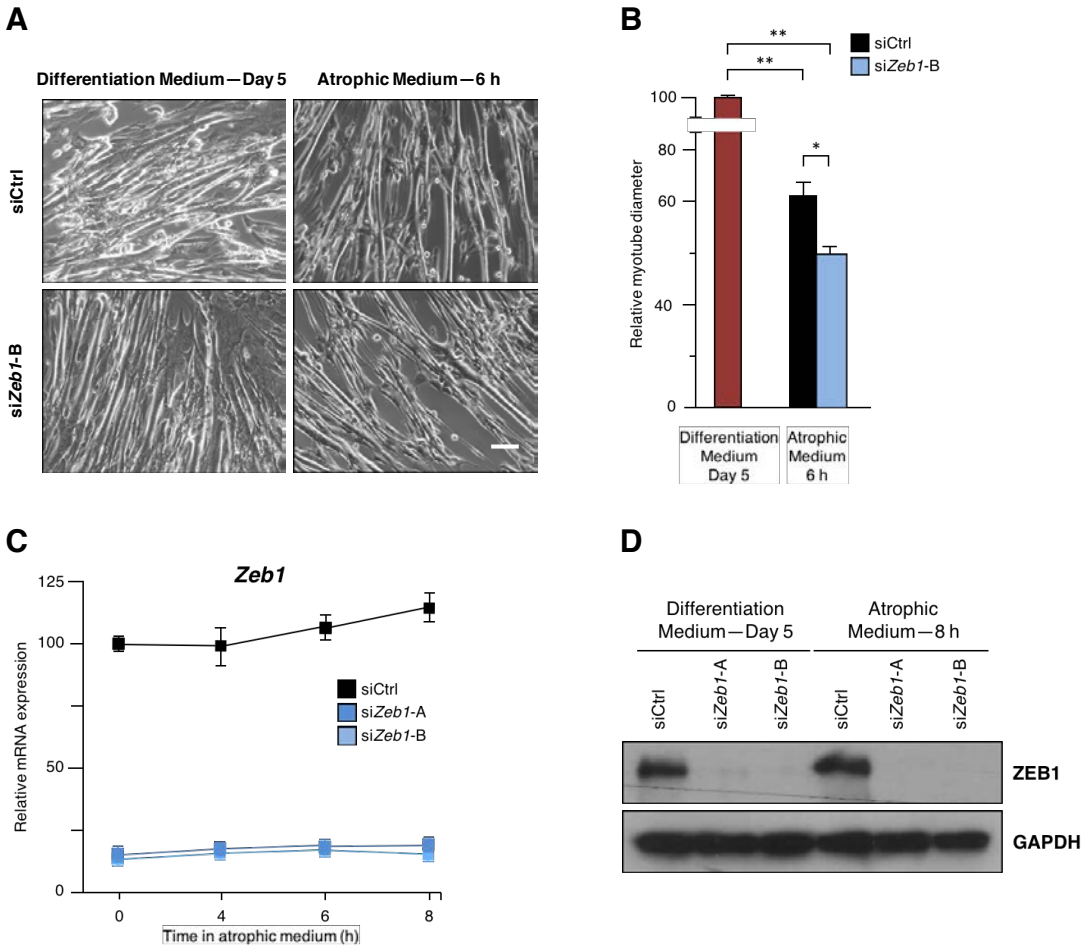

Figure 18: ZEB1 inhibits atrogene expression and size reduction in starved C2C12 myotubes. **(A)** Representative captures of C2C12 myotubes transfected with siCtrl or si*Zeb1*-B following incubation in differentiation medium or atrophy medium. Scale bar: 50 μm. **(B)** The diameter of C2C12 myotubes subjected to the protocol in (A) was assessed as described in Materials and Methods. Myotube diameter in the differentiation medium on day 5 was arbitrarily set at 100. Data represent the average of at least 3 experiments. **(C)** *Zeb1* mRNA levels in C2C12 myotubes interfered with siCtrl, si*Zeb1*-A or si*Zeb1*-B and cultured in the atrophic medium for the indicated periods were assessed by qRT-PCR with respect to Gapdh. *Zeb1* expression in cells interfered with siCtrl at 0 h of atrophic medium was arbitrarily set to 100. Data are representative of four independent experiments. **(D)** As in (A), lysates from C2C12 non-atrophic and atrophic myotubes. The blots shown are representative of four independent experiments.

The inhibition of atrogenes by ZEB1 was also examined in the C2C12 model. In line with the results above, and compared to C2C12 atrophic myotubes interfered with siCtrl, knockdown of *Zeb1* resulted in higher mRNA and protein levels of Atrogin-1/*Fbxo32* and MuRF1/*Trim63* (Figure 19A-C).

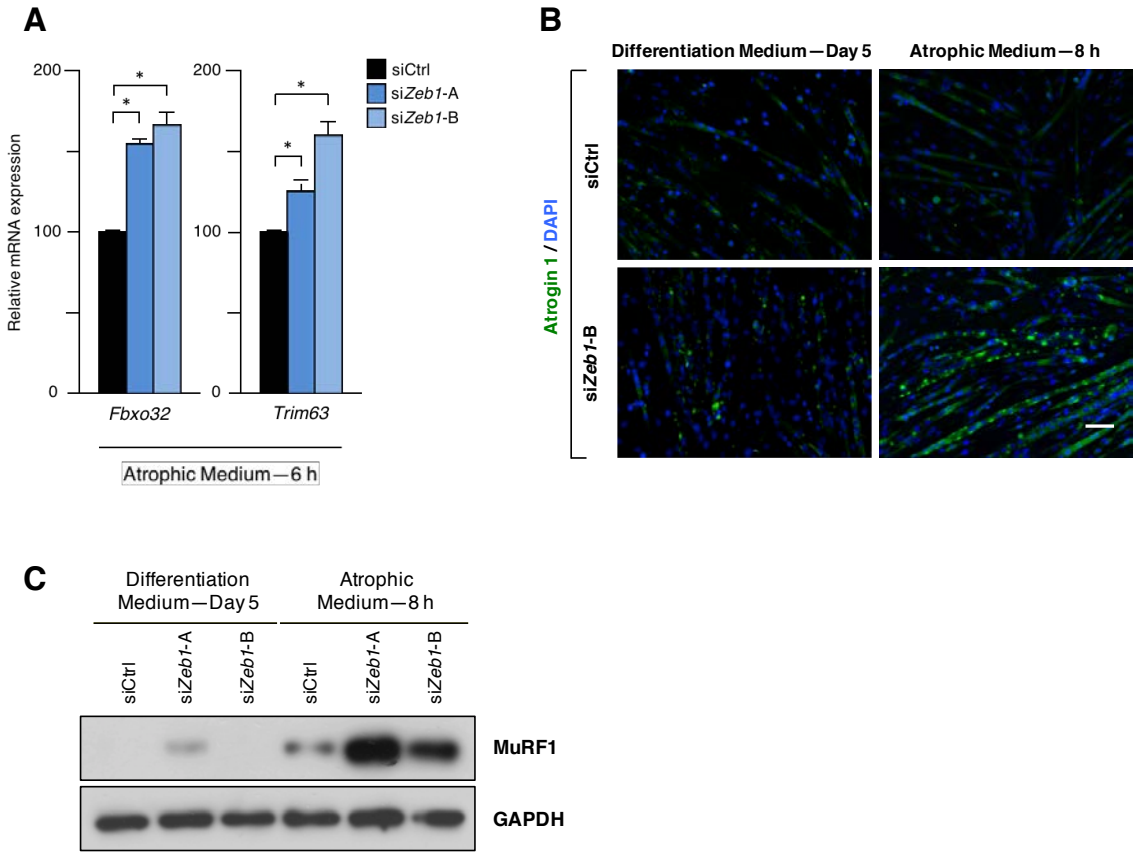

Figure 19: ZEB1 inhibits atrogene expression and size reduction in starved C2C12 myotubes. **(A)** C2C12 myotubes were interfered with siCtrl, si*Zeb1*-A or si*Zeb1*-B and transferred to atrophy medium. Expression of *Fbxo32* and *Trim63* was assessed by qRT-PCR using Gapdh as a reference gene. Data represent the average of at least three independent experiments. **(B)** C2C12 non-atrophic and atrophic myotubes were stained for Atrogin-1 (clone AP2041) along with DAPI for nuclear staining. Pictures shown are representative of three independent experiments. Scale bar: 50 μm. **(C)** Lysates from C2C12 non-atrophic and atrophic myotubes were assessed for MuRF1 expression (clone C11) along with GAPDH (clone 14C10) as a loading control. The blots shown are representative of four independent experiments.

Stage-dependent binding and repression of the *Fbxo32* promoter by ZEB1

The expression of most atrogenes is activated by transcription factors of the *Forkhead box O* (Foxo) family (e.g., FOXO1, FOXO3, and FOXO4). FOXO3 triggers muscle atrophy through protein degradation via activation of the ubiquitin-proteasome system as well as via autophagy-dependent clearance of organelles. The regulatory regions of many atrogenes contain multiple binding sites for FOXO proteins and, accordingly, progressively larger fragments of the *Fbxo32* promoter—

that contain an increasing number of FOXO3 binding sites—displayed a parallel larger activation in response to FOXO3 overexpression (Figure 20).

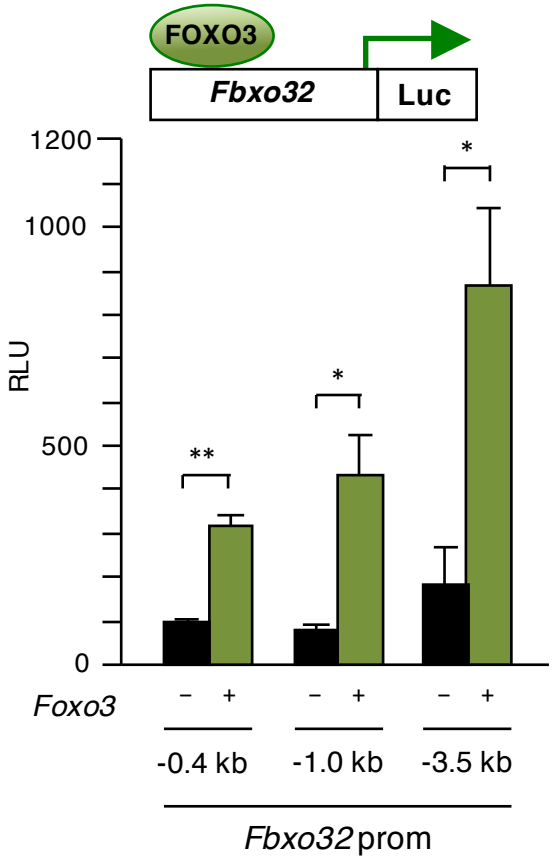

Figure 20: ZEB1 represses the Fbxo32 promoter through CtBP-dependent inhibition of FOXO3 transcriptional activity. Transcriptional activity of different fragments of the *Fbxo32* promoter both under basal conditions and in response to Foxo3 overexpression. C2C12 cells were transfected with equal molar amounts of luciferase reporters containing the 0.4 kb, 1.0, and 3.5 kb fragments of the mouse *Fbxo32* promoter along with Foxo3 or equal molar amounts of the corresponding empty vector.

ZEB1 regulates gene expression by binding to E-box and E-box-like sequences (CANNTG) in the regulatory regions of its target genes. Analysis of the *Fbxo32* and *Trim63* promoters revealed the existence of several consensus binding sites for ZEB1, particularly in the former where many FOXO3 consensus sites are located in close proximity to ZEB1's (Figure 21A). ZEB1 and MYOD1 partially overlap in their DNA sequence recognition with ZEB1 repressing key muscle differentiation genes in a reverse temporal pattern vis-à-vis MYOD1. Thus, during the myoblast stage, ZEB1 binds to E-boxes in the promoters of differentiation genes and represses its transcription but, as differentiation proceeds, MYOD1 accumulates and displaces ZEB1 from these E-boxes.

To investigate whether ZEB1 regulation of *Fbxo32* involves direct binding to its promoter we examined ZEB1's capacity to bind to a consensus binding site

located at -85 bp of the *Fbxo32* promoter in myoblasts, myotubes and atrophic myotubes. Interestingly, we found that in myoblasts and atrophic myotubes, but not in non-atrophic myotubes, an anti-ZEB1 antibody—but not its specie-matched IgG control— immunoprecipitated a fragment of the *Fbxo32* promoter containing the -85 bp binding site (Figure 21B). This stage-specific binding of ZEB1 to the *Fbxo32* promoter was reversely mirrored by the pattern of binding of MYOD1; an anti-MYOD1 antibody—but not its respective IgG control—immunoprecipitated the *Fbxo32* promoter in myotubes but not in atrophic myotubes or in myoblasts.

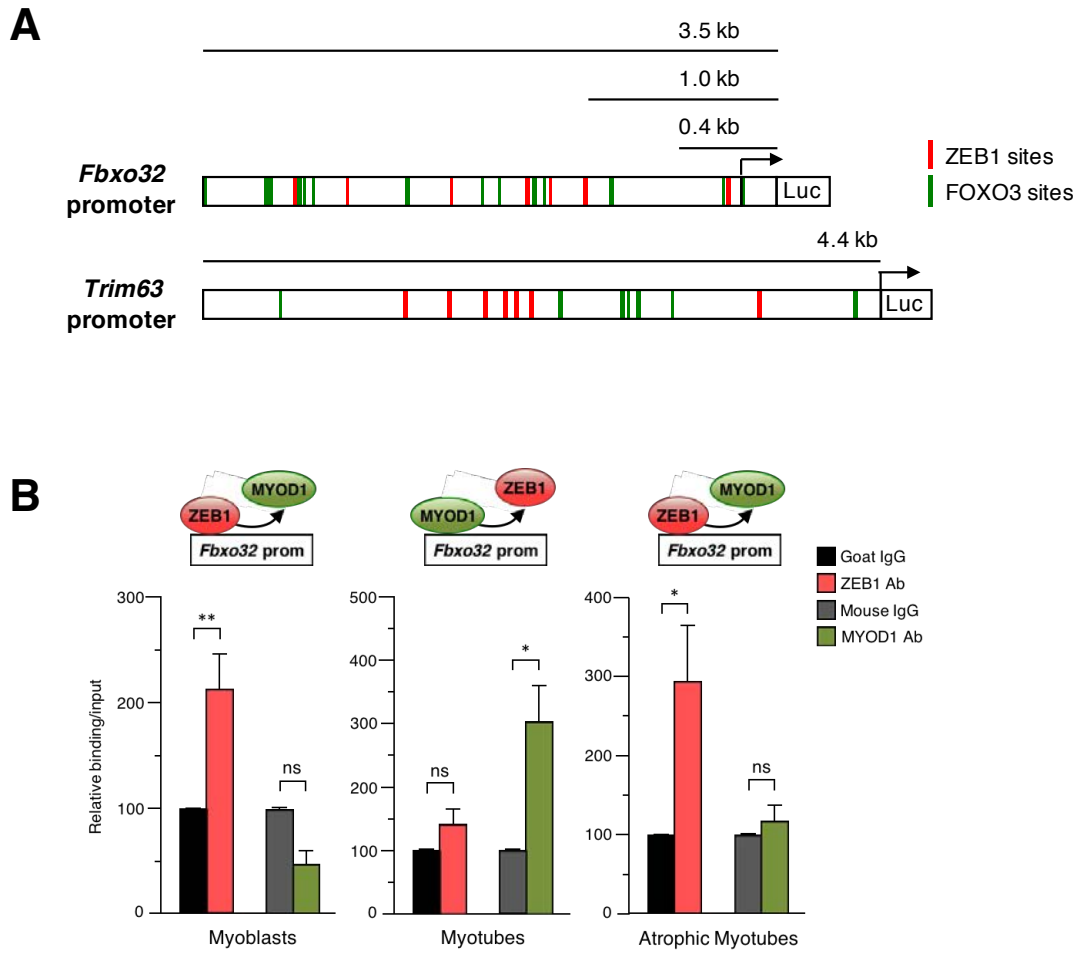

Figure 21: Stage-dependent inhibition of the Fbxo32 and Trim63 promoters by ZEB1 is mediated by CtBP-dependent repression of FOXO3 transcriptional activity. **(A)** Schematic representation of the consensus sites for ZEB1 (red boxes) and FOXO3 (green boxes) in the first 3.5 kb and 4.4 kb of the mouse *Fbxo32* and *Trim63* promoters, respectively. Consensus binding sequences for ZEB1 in the *Fbxo32* promoter were identified at –2899 bp, -2584 bp, -1894 bp, -1395 bp, -1254 bp, -1011 bp, and -85 bp. Consensus binding sites for ZEB1 in the *Trim63* promoter were identified at -4488 bp, -4444 bp, -3078 bp, -2792 bp, -2566 bp, -2416 bp, -2358 bp, -2254 bp, and –777 bp. Consensus binding sites for FOXO3 in *Fbxo32* and *Trim63* promoters were previously identified in (Sandri et al., 2004) or assessed as described in Materials and Methods. **(B)** ZEB1 binds

to the mouse *Fbxo32* promoter in myoblasts and atrophic myotubes but not in myotubes. DNA from C2C12 myoblasts, myotubes, or atrophic myotubes was immunoprecipitated with antibodies against ZEB1 (clone E-20X), MYOD1 (clone G-1) or their matched IgG controls (goat and mouse IgG, respectively). Immunoprecipitated DNA was then amplified by qRT-PCR in a region of the *Fbxo32* promoter containing a ZEB1 consensus binding site at – 85 bp. The condition immunoprecipitated with the IgG control was set to 100. Data represent the average of at least three experiments.

We next examined the transcriptional activity of the *Fbxo32* promoter following either the knockdown or overexpression of *Zeb1*. C2C12 cells were transfected with 0.4 and 1.0 kb fragments of the *Fbxo32* promoter fused to luciferase along with an expression vector for FOXO3 to induce its transcription. As expected, FOXO3 activated both *Fbxo32* promoter reporters (Figure 22A and Figure 22B). Compared to siCtrl, si*Zeb1*-A and si*Zeb1*-B further increased FOXO3-mediated induction of the *Fbxo32* promoter (Figure 22A and *left panel* of Figure 22B), indicating that the *Fbxo32* promoter is under negative transcriptional regulation by endogenous ZEB1. In turn, exogenous overexpression of *Zeb1* downregulated FOXO3-mediated induction of the *Fbxo32* promoter luciferase reporter (Figure 22B, *right panel*). When *Foxo3* was knocked down with a specific siRNA, overexpression of *Zeb1* had no significant effect on the transcriptional activity of the 0.4 kb *Fbxo32* promoter reporter (Figure 22C-D). Mutation of the ZEB1 binding site at the -85 bp site in the context of the 0.4 kb *Fbxo32* luciferase reporter to a sequence known not to bind ZEB1 reduced the effect of both *Zeb1* knockdown and *Zeb1* overexpression on *Fbxo32* transcription (Figure 22B). ZEB1-mediated repression of the 0.4 kb *Fbxo32* promoter reporter was also released by overexpression of MYOD1 (Figure 22E).

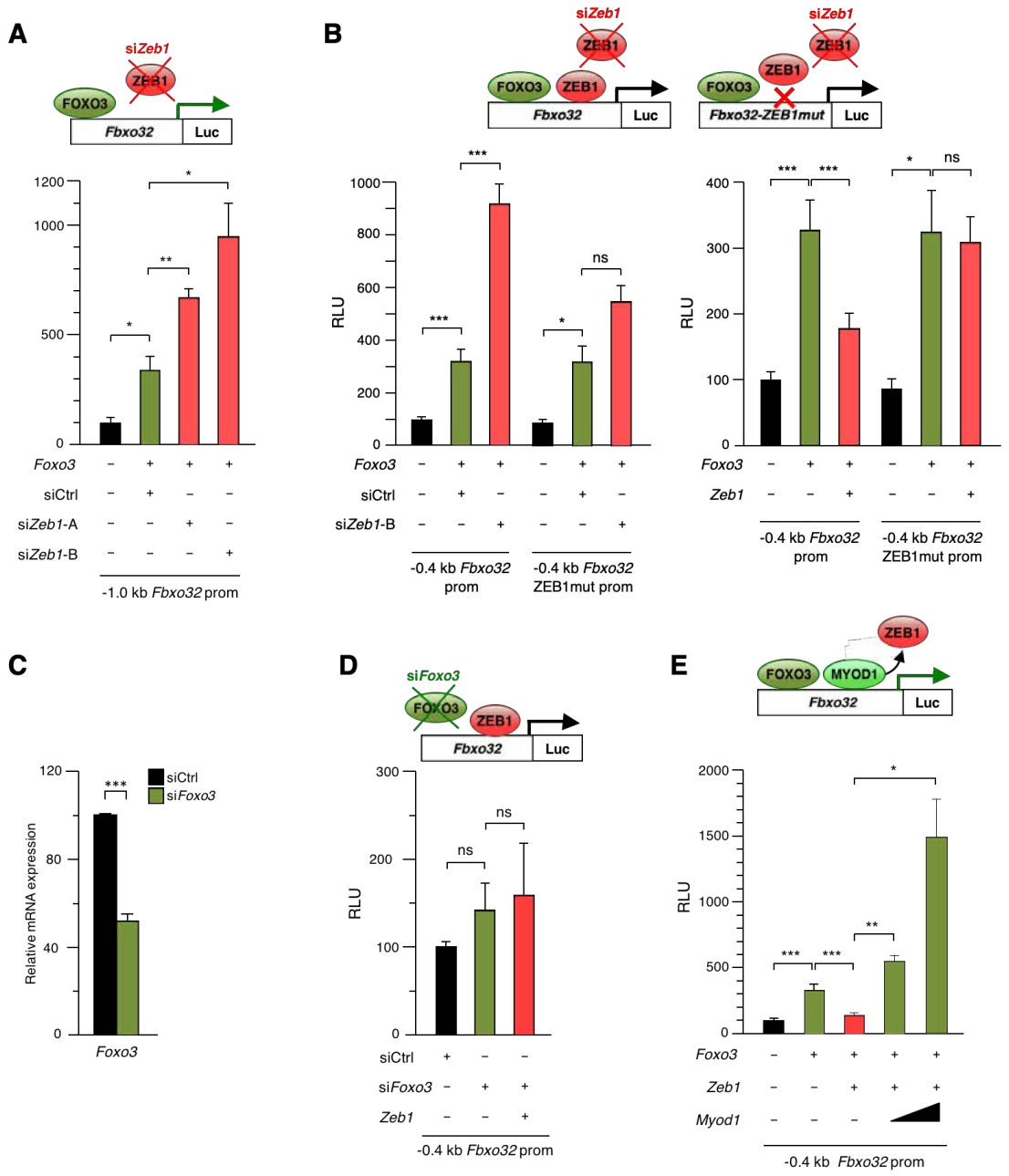

Figure 22: Stage-dependent inhibition of the Fbxo32 and Trim63 promoters by ZEB1 is mediated by CtBP-dependent repression of FOXO3 transcriptional activity. **(A)** Transcription of the *Fbxo32* promoter is under negative regulation by endogenous ZEB1. A luciferase reporter containing a 1.0 kb fragment of the mouse *Fbxo32* promoter (Sandri et al., 2014) was co-transfected in C2C12 cells along with an expression vector for FOXO3 (or the corresponding molar amount of the empty expression vector) to induce *Fbxo32* transcription. Throughout this Figure, the effect of overexpressing the indicated genes (*Foxo3* in this panel) is shown with respect to their corresponding empty vectors. Where indicated, cells were also transfected with 50 nM of either siCtrl, si*Zeb1*-A or si*Zeb1*-B. Transfections and assessment of Relative luciferase units (RLU) were performed as described in Materials and Methods. The first condition was arbitrarily set to 100. Data represent the average of three independent experiments. **(B)** Left panel: As in (A) but cells were instead transfected with a luciferase reporter containing a 0.4 kb fragment of the mouse *Fbxo32* promoter (Sandri et al., 2004) or version of it where only the ZEB1 binding site at -85 bp has been mutated to a sequence known to not bind ZEB1 (see Materials and Methods for details). Right panel: As in the left panel, but an expression vector for *Zeb1* (or the corresponding molar amount of the empty expression vector) were also transfected. The first condition was arbitrarily set to 100. Data represent the average of

three independent experiments. **(C)** C2C12 cells were transfected with 50-100 nM of either siCtrl or a pool of three siRNAs against *Foxo3* (si*Foxo3*). mRNA levels were assessed by qRT-PCR with respect to Gapdh. Data are the mean of four independent experiments. **(D)** C2C12 cells were transfected with a luciferase reporter containing a 0.4 kb fragment of the mouse *Fbxo32* promoter, an expression vector for *Zeb1* (or the corresponding molar amount of the empty expression vector) and/or 50-100 nM of either siCtrl or a pool of three siRNAs against *Foxo3* (si*Foxo3*). **(E)** Overexpression of MYOD1 displaces ZEB1 from its binding to the 0.4 kb *Fbxo32* luciferase reporter. As in the right panel of (B) but the expression vector for *Myod1* (or the corresponding molar amount of the empty expression vector) were transfected along with Zeb1. The first condition was arbitrarily set to 100. Data shown are the mean of three independent experiments.

ZEB1 inhibits the *Fbxo32* and *Trim63* promoters through CtBP-dependent repression of FOXO3 transcriptional activity

ZEB1 represses transcription of its target genes by recruitment of non-DNA binding transcriptional co-repressors, chiefly of CtBP. In that line, a siRNA against *Ctbp* increased the *Fbxo32* promoter activity (Figure 23A). The large increase in *Fbxo32* transcription induced by si*Ctbp* suggests that *Fbxo32* is under negative regulation by other CtBP-binding factors besides ZEB1. ZEB1 repression of *Fbxo32* was also partially relieved by blocking of CtBP activity with 2-keto-4-methylthiobutyrate (MTOB), an intermediate in the methionine salvage pathway that binds and inactivates CtBP (Figure 23B).

Next, we examined the potential regulation of *Trim63* by ZEB1 at the transcriptional level. Knockdown of *Zeb1* and *Ctbp* upregulated FOXO3-induced transcription of the *Trim63* reporter (Figure 23C) indicating that, as for *Fbxo32*, MuRF1 expression is inhibited at the transcriptional level by endogenous ZEB1 and CtBP.

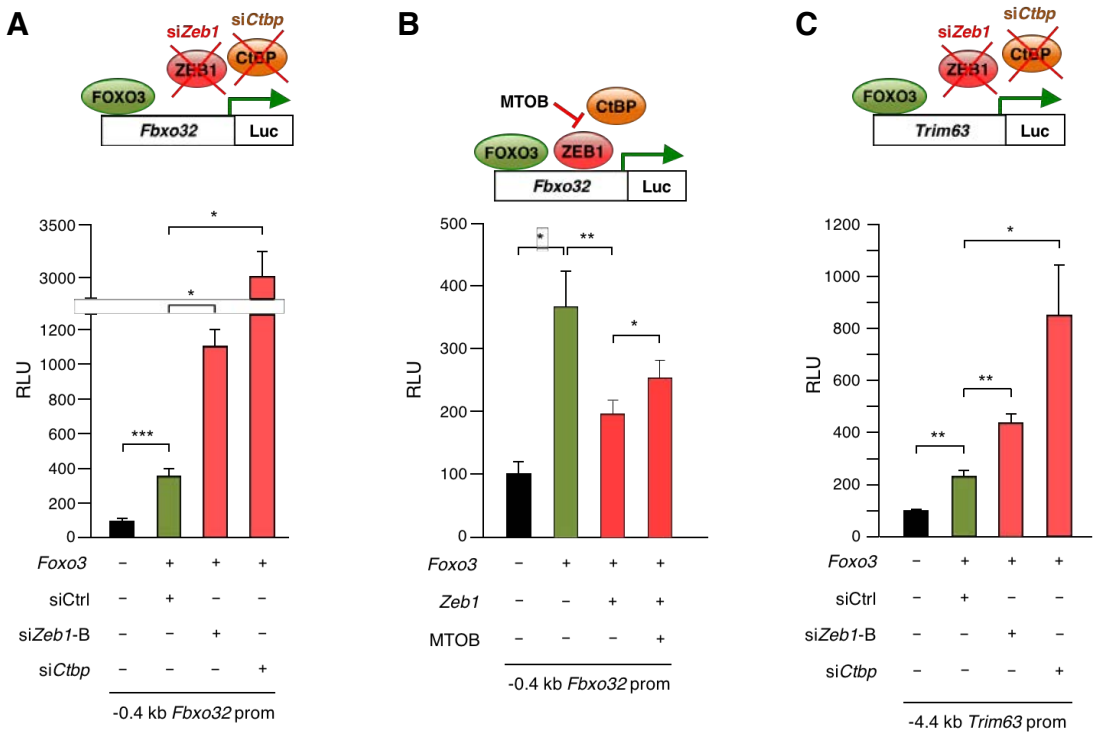

Figure 23: Stage-dependent inhibition of the Fbxo32 and Trim63 promoters by ZEB1 is mediated by CtBP-dependent repression of FOXO3 transcriptional activity. **(A)** Transcription of the *Fbxo32* promoter is under negative regulation by endogenous CtBP. As in Figure 22A but cells were transfected with a siRNA against *Ctbp*. The first condition was arbitrarily set to 100. Data represent the average of three independent experiments**. (B)** C2C12 cells were transfected with a luciferase reporter containing a 0.4 kb fragment of the mouse *Fbxo32* promoter, an expression vector for *Foxo3* (or equal molar amounts of the empty vector), and/or an expression vector for *Zeb1* (or the corresponding molar amount of the empty vector), and in the presence or absence of 10 mM of MTOB. Data are the mean of three independent experiments. **(C)** As in (A) but cells were instead transfected with a luciferase reporter containing a 4.4 kb fragment of the mouse *Trim63* promoter. The first condition was arbitrarily set to 100. Data are the average of at least three independent experiments.

ZEB1 repression of several atrogenes (Figure 15) suggests that ZEB1 modulates the activity of a common activator of muscle atrophy. The results above also indicate that ZEB1 represses FOXO3-induced activation of the *Fbxo32* and *Trim63* promoters. We, therefore, investigated whether ZEB1 directly represses FOXO3-mediated transcriptional activity using a heterologous luciferase reporter (L8G5-luc) that contains binding sites for yeast Gal4 (Gal4-UAS) and bacterial LexA (LexAOp) proteins (scheme on top of Figure 24A). The cDNA of *Foxo3* fused to the DNA binding domain of Gal4 (Gal4-*FOXO3*) activated the basal transcription of the L8G5-luc reporter (Figure 24A). In turn, the cDNA of *Zeb1* fused to the DNA binding

domain of LexA (LexA-*ZEB1*) repressed Gal4-*FOXO3*-induced transcriptional activation of the L8G5-luc reporter (Figure 24A). In line with the results above with the *Fbxo32* and *Trim63* promoters (Figure 23A and C), knockdown of *Ctbp* with a siRNA partially relieved the repression of Gal4-*FOXO3* by LexA-*ZEB1* (Figure 24A). A similar result was obtained when the cDNA of *Foxo3* was instead fused to the DNA binding domain of LexA and that of ZEB1 to Gal4 (Figure 24B). *Foxo3*-mediated transcription in this heterologous system was also repressed by a ZEB1 fragment containing only its CtBP-interacting domain (CID) fused to Gal4 (Gal4-*ZEB1*-CID) (Figure 24B). However, mutation of the three CtBP sites within ZEB1's CID (Gal4-ZEB1-CID$_{mut}$) abrogated transcriptional repression of FOXO3 by *ZEB1*-CID.

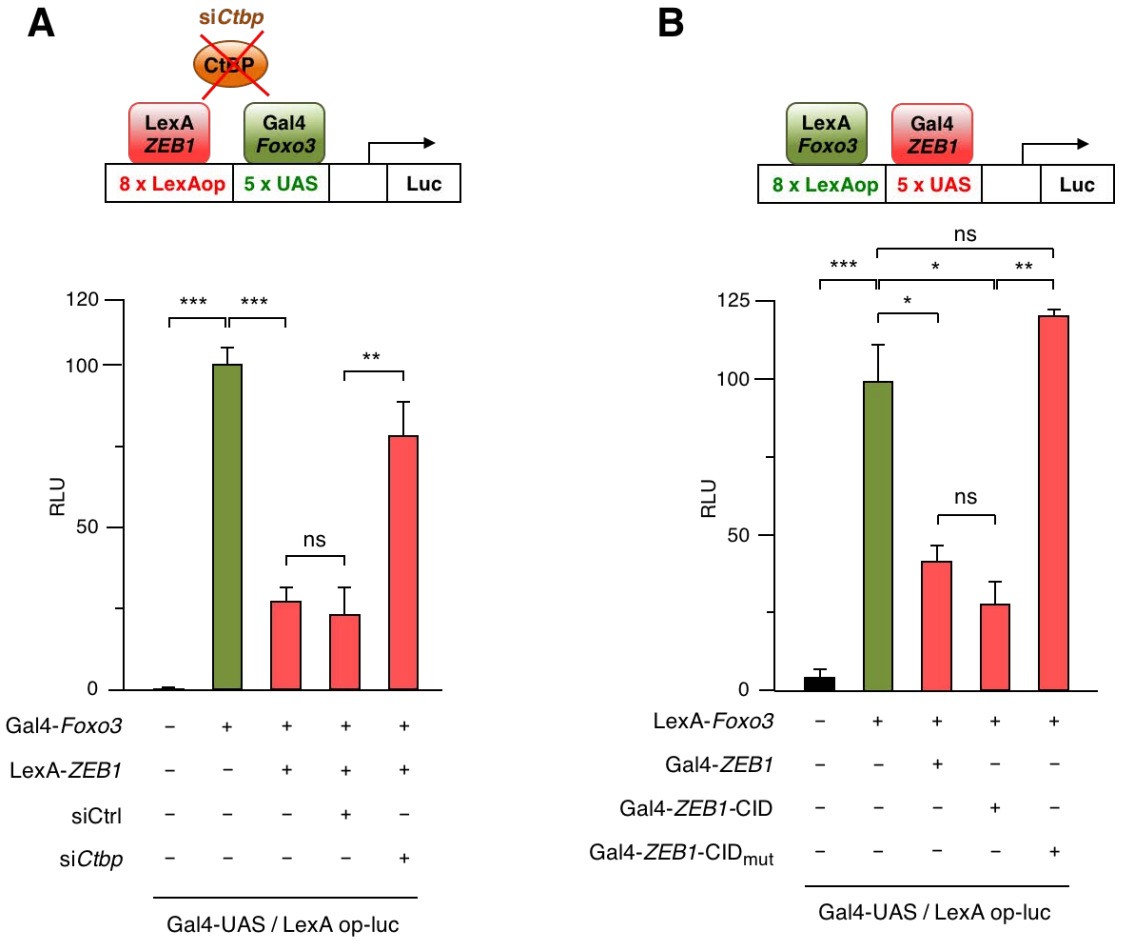

Figure 24: Stage-dependent inhibition of the Fbxo32 and Trim63 promoters by ZEB1 is mediated by CtBP-dependent repression of FOXO3 transcriptional activity. **(A)** FOXO3 transcriptional activity is repressed by ZEB1 and CtBP. 293T cells were transfected with a reporter containing LexA operon and Gal-UAS sites (L8G5-luc) along with Gal4-FOXO3 and/or LexA-ZEB1 (or their corresponding empty vectors). Where indicated, cells were transfected with 10-20 nM of either siCtrl or si*Ctbp*. The condition overexpressing only Gal4-Foxo3 was arbitrarily set to 100. Data

represent the average of five independent experiments. **(B)** ZEB1 represses FOXO3 transcriptional activity through a CtBP-dependent mechanism. As in (A) but the Gal4 and LexA fusion proteins were swapped: ZEB1, ZEB1-CID and ZEB1-CIDmut were fused to Gal4 whereas *Foxo3* was fused to LexA. Cells were transfected with L8G5-luc, LexA-Foxo3, Gal4-ZEB1, Gal4-ZEB1-CID and/or ZEB1-CIDmut. The condition overexpressing only LexA-Foxo3 was arbitrarily set to 100. Data are the average of three independent experiments.

The conclusions from these results are twofold: first, ZEB1 inhibits *Foxo3*-mediated induction of atrogenes; and second, ZEB1 has the intrinsic capacity to repress *Foxo3* transcriptional activity through, at least in part, the recruitment of the CtBP co-repressor.

In vivo repression of the *Fbxo32* promoter by endogenous ZEB1

Lastly, we examined the *in vivo* regulation of the *Fbxo32* promoter by endogenous ZEB1 (see scheme in Figure 25A). Both hindlimbs of wild-type and *Zeb1* (+/-) mice were injected with the *Fbxo32* promoter fused to luciferase. After 3.5 days, the left hindlimb was immobilized during 3.5 additional days while the right hindlimb remained non-immobilized. At day 7, luciferase signal emission was assessed by whole-body bioluminescence imaging. In line with the above results, the luminescence signal emitted by the *Fbxo32* promoter was higher in the immobilized hindlimb of *Zeb1* (+/-) mice than in that of wild-type counterparts. These results indicate that endogenous ZEB1 also inhibits the transcription of the *Fbxo32* promoter *in vivo* (Figure 25B and Figure 25C).

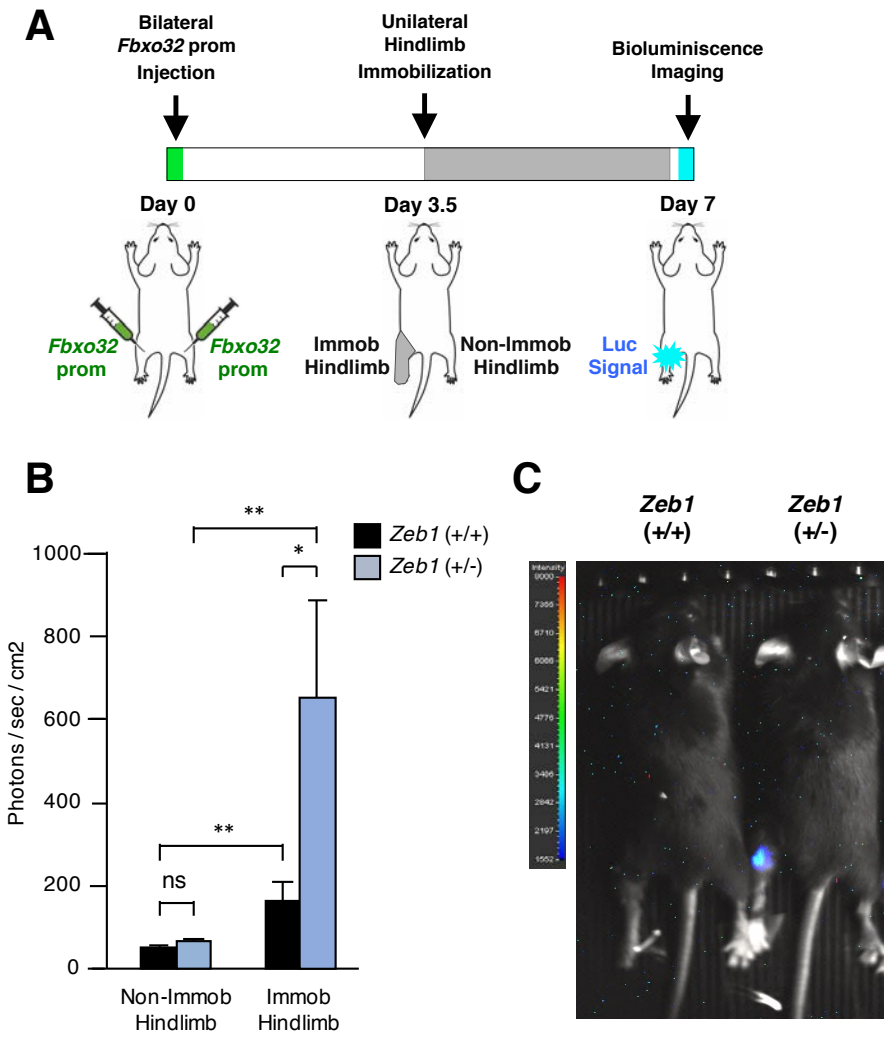

Figure 25: In vivo repression of the Fbxo32 promoter by endogenous ZEB1. **(A)** Graphic representation of protocol for the in vivo assessment of ZEB1 regulation of the *Fbxo32* promoter. Both hindlimbs of wild-type and *Zeb1* (+/-) mice were injected with a 3.5 kb fragment of the *Fbxo32* promoter fused to luciferase. After 3.5 days, mice were subjected to unilateral (left) hindlimb immobilization for 3.5 additional days. At day 7, *Fbxo32* promoter activity was assessed in vivo by whole-body bioluminescence imaging. See Materials and Methods for details. **(B)** ZEB1 inhibits the *Fbxo32* promoter in vivo. In both genotypes, the bioluminescence signal emitted by the *Fbxo32* promoter is higher in the immobilized hindlimb than in the non-immobilized hindlimb. However, immobilization induced greater bioluminescence signal in *Zeb1* (+/–) mice than in wild-type mice. Data represent the average of seven mice of each genotype. **(C)** Bioluminescence signal rendered by a representative mouse for each genotype on day 7.

➔ *Note: The data in Chapter I have been published in Nucleic Acids Research. 2018 Oct 10; 46(20):10697-708.*

Chapter II. Generation and characterization of transgenic *Zeb1*$^{skm-/-}$ mice

Generation of transgenic *Zeb1*$^{skm-/-}$ mice

To investigate the specific role of ZEB1 in adult skeletal muscle, we generated a conditional *Zeb1* knockout mouse in collaboration with the CNB-CBMSO Transgenesis Service at CSIC's *Centro Nacional de Biotecnologia*, in Madrid. We introduced loxP sequences flanking *Zeb1* exon 6, with the CRISPR technique (See scheme in Figure 26). The exon 6 codifies for a large portion of the ZEB1 protein and, upon Cre deletion, the exon 5 splices to exon 7, leading to a truncated form of the protein. Mice bearing floxed *Zeb1* alleles, called here *Zeb1*$^{f/f}$, were then crossed with mice that express the tamoxifen-inducible Cre-ER^{T2} recombinase selectively in myofibers under the human skeletal actin promoter (HSA)-Cre-ER$^{T2\ (tg/0)}$ (Schuler et al., 2005). In *in vitro* primary culture, (HSA)-Cre-ER^{T2} is expressed in completely formed myotubes, but not in myoblasts or fusing myocytes, after tamoxifen treatment (Guerci et al., 2012).

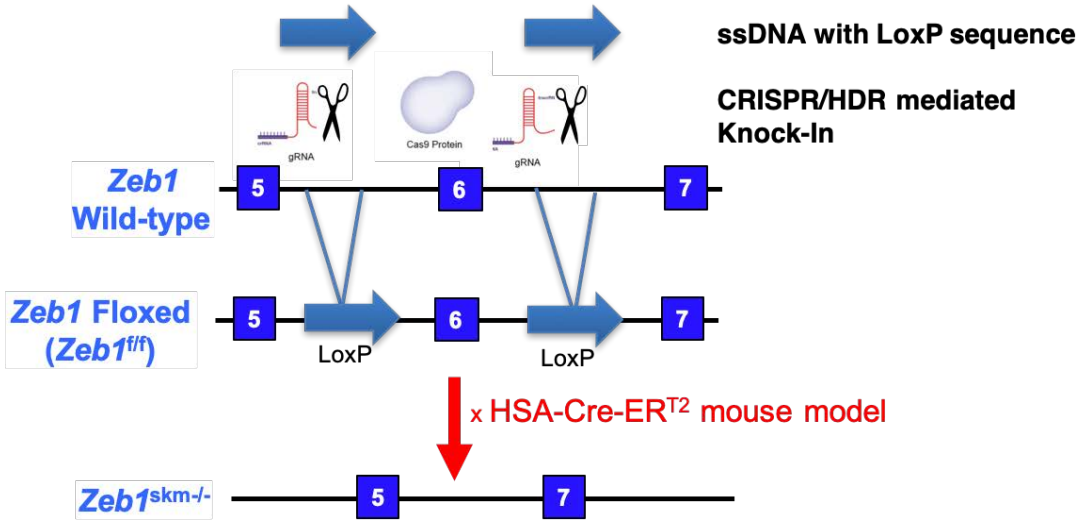

Figure 26: Scheme of transgenic generation of the Zeb1 flox mouse model

Two-to-three months old mice *Zeb1*$^{f/f}$ and *Zeb1*$^{f/f}$/HSA-Cre-ER$^{T2(tg/0)}$ of both sex were intraperitoneally injected with tamoxifen for five days, to generate control or *Zeb1*$^{skm-/-}$ mice respectively. After 5 days of the last tamoxifen injection, mice were sacrificed and *Zeb1* transcript and protein levels were analyzed in the gastrocnemius muscle of both genotypes (Figure 27A and Figure 27B). Compared to age-matched control mice, *Zeb1* mRNA and protein expression decreased to half levels in *Zeb1*$^{skm-/-}$ gastrocnemius muscles (Figure 27A and Figure 27B). It should be noted here that, in addition to myofibers that express HSA promoter (and, therefore, activate HSA-Cre-ER^{T2} when treated with tamoxifen), skeletal muscle contains others cell types that do not express HSA (and that are therefore not subjected to HSA-Cre-ER^{T2} promoter), namely satellite cells, fibroblasts, endothelial and adipose cells.

To confirm the efficient *Zeb1* deletion in our model, we isolated primary myoblasts from gastrocnemius muscle of control and *Zeb1*$^{skm-/-}$ mice and we differentiated them into myotubes *in vitro*. We treated myoblasts and myotubes with 4-Hydroxytramoxifen for 5 days and analyzed the *Zeb1* mRNA levels of control- and *Zeb1*$^{skm-/-}$-derived primary myoblasts and myotubes. Compared to myoblasts and myotubes not expressing HSA, *Zeb1*$^{skm-/-}$ myotubes were knockdown for *Zeb1* mRNA expression (Figure 27C), indicating an efficient HSA-Cre recombinase activity in completely formed myotubes/myofibers.

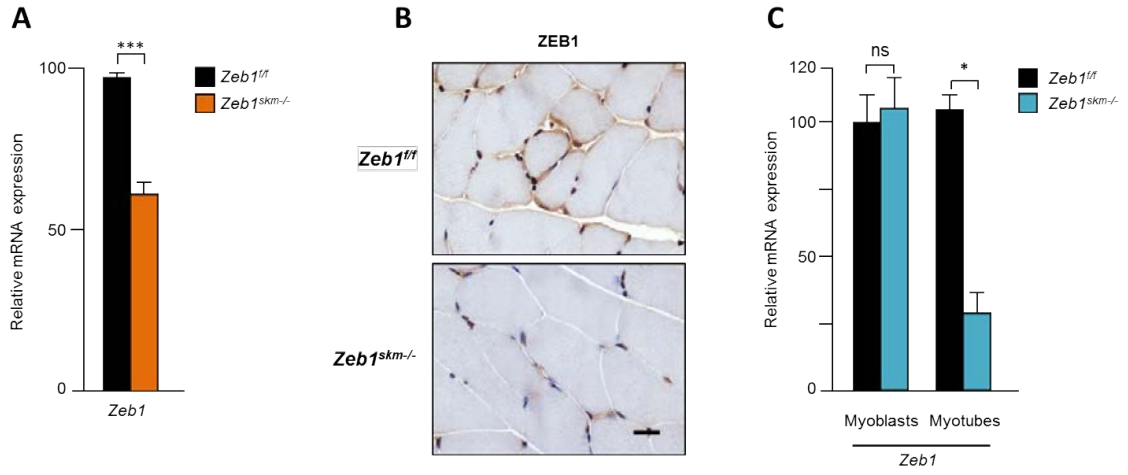

Figure 27: ZEB1 is downregulated in Zeb1$^{skm-/-}$ gastrocnemius. *Zeb1*$^{f/f}$ control and *Zeb1*$^{skm-/-}$ mice were intraperitoneally injected with tamoxifen for 5 days. After 5 days of last tamoxifen injection, mice were sacrificed and *Zeb1* transcript and protein levels were analyzed. **(A)** *Zeb1* mRNA levels in *Zeb1*$^{f/f}$ control and *Zeb1*$^{skm-/-}$ total gastrocnemius muscle. Bars represent the average with sem of at least six different mice for each genotype. **(B)** ZEB1 expression was assessed by immunohistochemistry (clone HPA027524) after 5 days from the last tamoxifen injection. Captures are representative of at least six mice for each genotype and condition. Scale bar: 20μm. **(C)** Primary myoblasts were isolated from total gastrocnemius muscle of 5 days' tamoxifen injected *Zeb1*$^{f/f}$ control and *Zeb1*$^{skm-/-}$ mice and cultured with 4-Hydroxytamoxifen. Myoblasts were then differentiated in differentiation medium (DM) with 4-Hydroxytamoxifen for five days. *Zeb1* mRNA levels were assessed in myoblasts and five days differentiated myotubes. Bars represent the average with sem of at least 3 different experiments. The *Zeb1* expression level in control myoblasts was arbitrarily set to 100.

Zeb1 deficient muscles present lower lipid storage and different fiber type composition

From a macroscopic analysis, we observed that *Zeb1*$^{skm-/-}$ mice fed *ad libitum* weighed about 10% less than age-matched control mice (
Figure 28A). We examined muscle lipid content in gastrocnemius of *Zeb1*$^{f/f}$ control and *Zeb1*$^{skm-/-}$ mice by staining cryosections with the lysochrome oil red O (ORO), which is a widely used fat-soluble diazol dye that stains neutral lipids and cholesteryl esters, but not biological membranes (Mehlem et al., 2013). We found that the gastrocnemius muscle of *Zeb1*$^{skm-/-}$ mice exhibited significantly lower lipid content compared to control mice (

Figure 28B). Moreover, the adipose triglyceride lipase (*Atgl*) mRNA expression, the lipase enzyme responsible for mobilization of fatty acids and diacylglycerols from IMTG stores, was lower in *Zeb1*$^{skm-/-}$ mice compared to controls (Figure 28C).

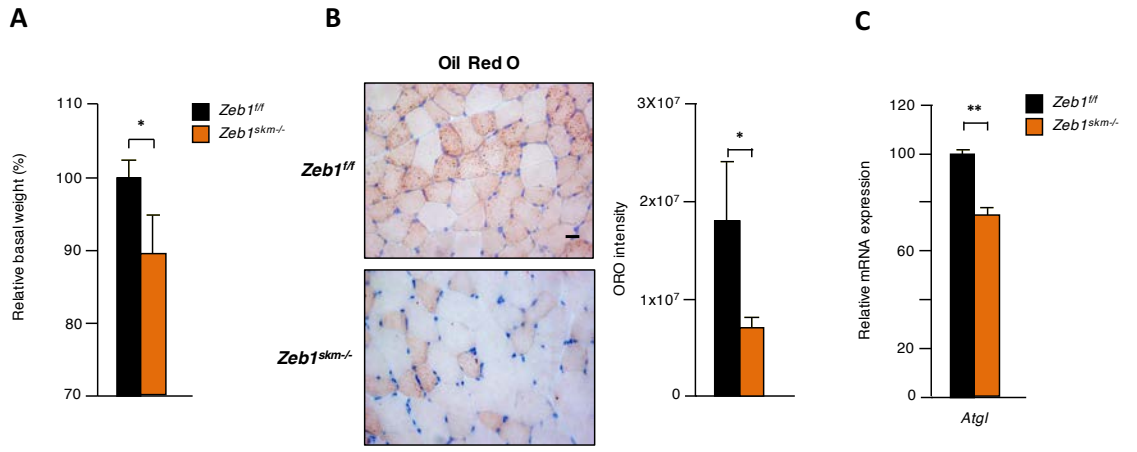

Figure 28: Zeb1 deficient muscles present lower lipid content. **(A)** *Zeb1*$^{f/f}$ *control and Zeb1*$^{skm-/-}$ mice were injected intraperitoneally with tamoxifen for 5 days. After 5 days from the last tamoxifen injection, mice were weighed. The basal weight of control mice was arbitrarily set to 100. Bars represent the mean of at least 6 different mice for each genotype. **(B)** Lipid content of *Zeb1*$^{f/f}$ control and *Zeb1*$^{skm-/-}$ mice, injected intraperitoneally with tamoxifen, was stained by ORO staining and ORO intensity was measured with ImageJ software. Captures are representative of at least six different mice for each genotype. The chart represents the mean ± sem of ORO intensity measured in five different captures of at least six mice for each genotype. Scale bar: 20μm. **(C)** *Atgl* mRNA expression was measured in total gastrocnemius of tamoxifen injected *Zeb1*$^{f/f}$ control and *Zeb1*$^{skm-/-}$ mice. The expression levels in control mice were arbitrarily set to 100. Bars represent the mean with sem of at least six different mice for each genotype.

Within skeletal muscle, lipid accumulation and ATGL expression are situated almost exclusively in slow-twitch, oxidative, type I fibres, rather than in fast-twitch, more glycolytic type II fibres (Malenfant et al., 2001; Jocken et al., 2008). To investigate a potential role of ZEB1 in muscle fiber composition, we performed histochemical staining for ATPase, which allows to distinguish the three major fiber types: slow or type I, fast fatigue resistant or type IIa and fast fatigable or type IIb. Interestingly, the percentage of slow type I fibers and the expression of the slow skeletal muscle fiber MHC gene (*Myh7*) were significantly lower in *Zeb1*$^{skm-/-}$ gastrocnemius compared to controls (Figure 29A-C). No differences were found in

the percentage of type IIb and IIa and their respective MHC genes (*Myh4* and *Myh2* respectively*)* (Figure 29A-C). Of note, ZEB1 accumulates more in slow fibers, in fact slow soleus muscle expresses double *Zeb1* mRNA levels compared to fast tibialis anterioris and mixed gastrocnemius muscle (Figure 29D).

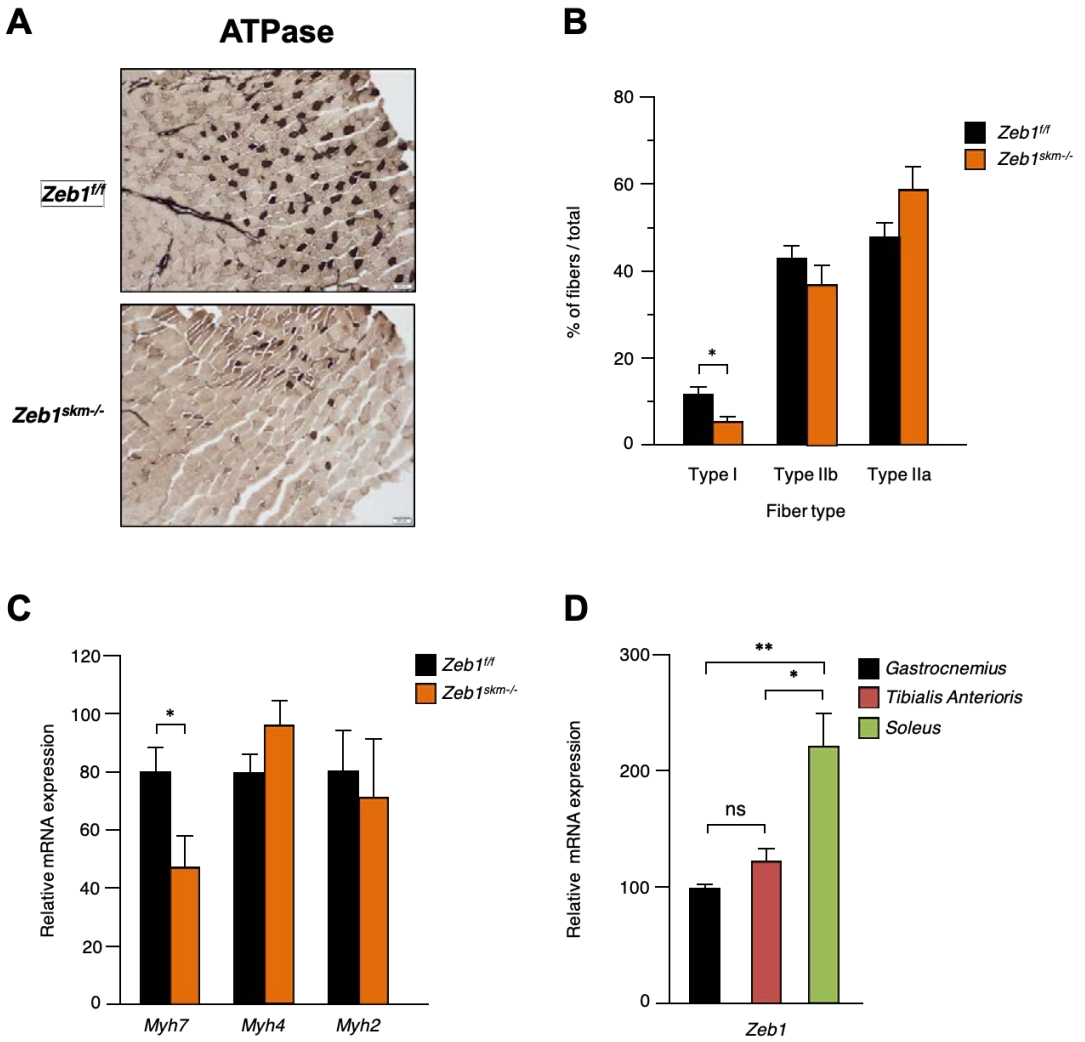

Figure 29: Zeb1 deficient muscles have less slow type I fibers. **(A)** ATPase staining in gastrocnemius muscle of *Zeb1*$^{f/f}$ control and *Zeb1*$^{skm-/-}$ mice, after 5 days of the last tamoxifen injection. Slow-twitch type I fibers appear the darkest, fast-fatigue resistant-type IIa fibers appear the lightest and fast-fatigable, or type IIb, fibers present an intermediate brown color. Captures are representative of at least six different mice for each genotype. Scale bar: 200μm. **(B)** The relative abundance of each fiber type was measured in gastrocnemius muscle from *Zeb1*$^{f/f}$ control and *Zeb1*$^{skm-/-}$ mice with ImageJ software. A total of at least 400 fibers for each mouse were counted. The fiber percentage was calculated relative to the total number of fibers counted for each mouse. Bars represent the mean with sem of at least six mice for each genotype. **(C)** mRNA expression of fiber specific MHC genes *Myh7*, *Myh4* and *Myh2* were analyzed in total *Zeb1*$^{f/f}$ control and *Zeb1*$^{skm-/-}$ gastrocnemius muscle extract, 5 days after the last tamoxifen injection. Bars represent the mean with sem of at least six mice for each genotype. **(D)** *Zeb1* expression in gastrocnemius (mixed), tibialis anterioris (fast) and soleus (slow) muscles. Bars represent the average with sem of at least 4 mice.

We next evaluate if fiber types I, IIa and IIb presented some morphological differences between control and *Zeb1*$^{skm-/-}$ mice. We did not find changes in the total CSA average and in the CSA of each fiber type in gastrocnemius sections from both genotypes (Figure 30A-B).

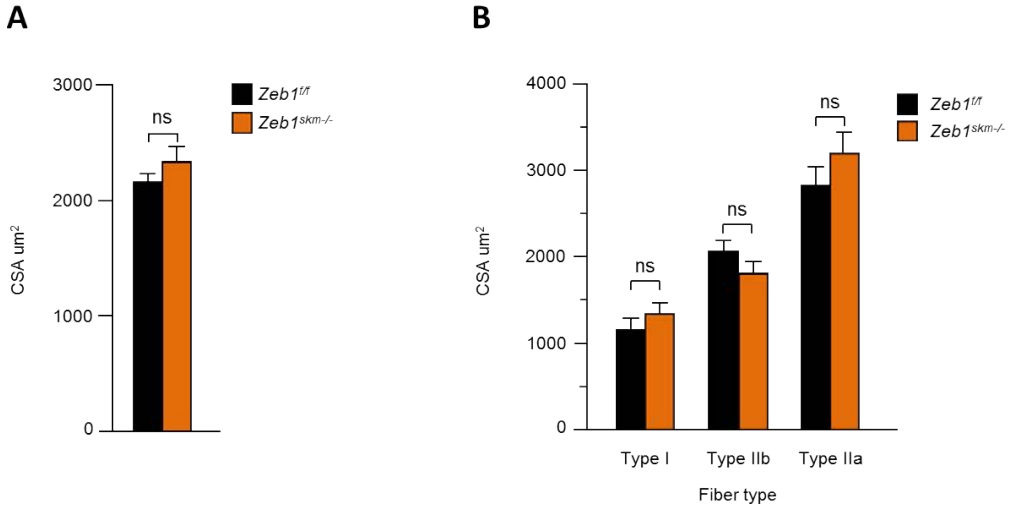

Figure 30: Zeb1 deficient muscles do not change their fiber's CSA. The average total cross-sectional area **(A)** and the myofiber type-specific CSA **(B)** of at least 100 fibers for each mouse was measured with ImageJ software, 5 days after the last tamoxifen injection, in *Zeb1*$^{f/f}$ and *Zeb1*$^{skm-/-}$ gastrocnemius muscles. Bars represent the mean with sem of at least five mice for each genotype.

Taken together, these results indicate that ZEB1 contributes to maintaining slow-twitch type I fibers abundance in adult gastrocnemius muscle, likely by regulating *Myh7* gene, but *Zeb1* knockdown does not result in fiber morphological changes. Moreover, the lower percentage of slow type I fibers in *Zeb1*$^{skm-/-}$ mice reflects a decreasing in skeletal muscle intramuscular lipid accumulation and *Atgl* expression, which typically accumulate in slow type I fibers.

Muscle fibers in *Zeb1*$^{skm-/-}$ mice exhibit less oxidative stress and lower *Pgc1β* expression

Oxidative metabolism is the main source of oxidative stress. Reactive oxygen species (ROS) are continuously produced as a product of incomplete reduction of oxygen in the mitochondrial respiratory chain (Muller et al., 2000). Since *Zeb1*$^{skm-/-}$ mice presented less percentage of more oxidative type I slow fibers, we evaluated ROS production in control and *Zeb1* deficient gastrocnemius muscles, by measuring intracellular superoxide anion (O_2^-) levels with DHE staining. Dihydroethidium (DHE) is a cell membrane permeable dye, which reacts with superoxide anions to form ethidium, a red fluorescent product that intercalates into DNA (Carter et al., 1994). The gastrocnemius muscle of *Zeb1*$^{skm-/-}$ mice had significantly lower intracellular superoxide levels, compared to control mice (Figure 31A). Moreover, the mRNA expression of the manganese superoxide dismutase (*Sod2*), a mitochondrial ROS detoxifying enzyme and an oxidative stress marker, and of the cellular energy sensor AMP-activated protein kinase (*Ampkα*), which can be induced through a non-canonical pathway by mitochondrial ROS (Rabinovitch et al., 2017), were decreased in *Zeb1* lacking fibers compared to controls (Figure 31B).

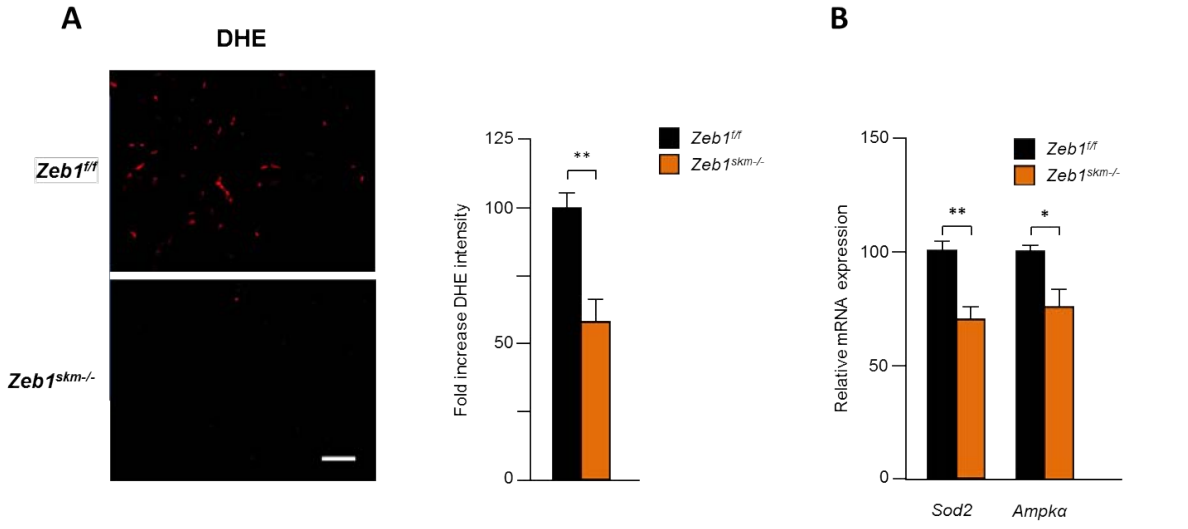

Figure 31: Zeb1 deficient muscles have less reactive oxygen species. **(A)** DHE staining of gastrocnemius muscles from *Zeb1*$^{f/f}$ control and *Zeb1*$^{skm-/-}$ mice. Images are representative of at least five different captures from each mouse. Scale bar: 50μm. Bars represent the fold increase of mean fluorescent DHE intensities with sem, calculated with ImageJ software, of at least six different mice for each genotype. The fluorescent intensity of control mice was arbitrarily set to 100. **(B)** *Sod2* and *Ampkα* mRNA expression in gastrocnemius muscles from *Zeb1*$^{f/f}$ control and *Zeb1*$^{skm-/-}$ mice, 5 days after the last tamoxifen injection. Bars represent the mean with sem of at least six mice for each genotype. The expression levels of control mice were arbitrarily set to 100.

PGC1α and PGC1β co-activators modulate the expression of several genes involved in mitochondrial biogenesis and fiber type composition (Lin et al., 2002; Ramamoorthy et al., 2015). To investigate if ZEB1 regulates fiber type composition, lipid accumulation and ROS production by modulating these key co-activators, we analyzed mRNA expression of both *Pgc1α* and *Pgc1β* by real time PCR. *Zeb1* knockdown induced downregulation of *Pgc1β,* but not *Pgc1α,* mRNA expression (Figure 32A). Although PGC1α and PGC1β regulate an overlapping set of genes, PGC1α, but not PGC1β, induces and sustains the formation of slow-twitch muscle fibers (Lin et al., 2002; Ramamoorthy et al., 2015). PGC1α induces the formation of slow-type I fibers by co-activating several transcription factors, including MEF2C. *Mef2c* mRNA expression was lower in *Zeb1* deficient muscles (Figure 32B), suggesting a possible mechanism by which ZEB1 regulates slow fiber formation.

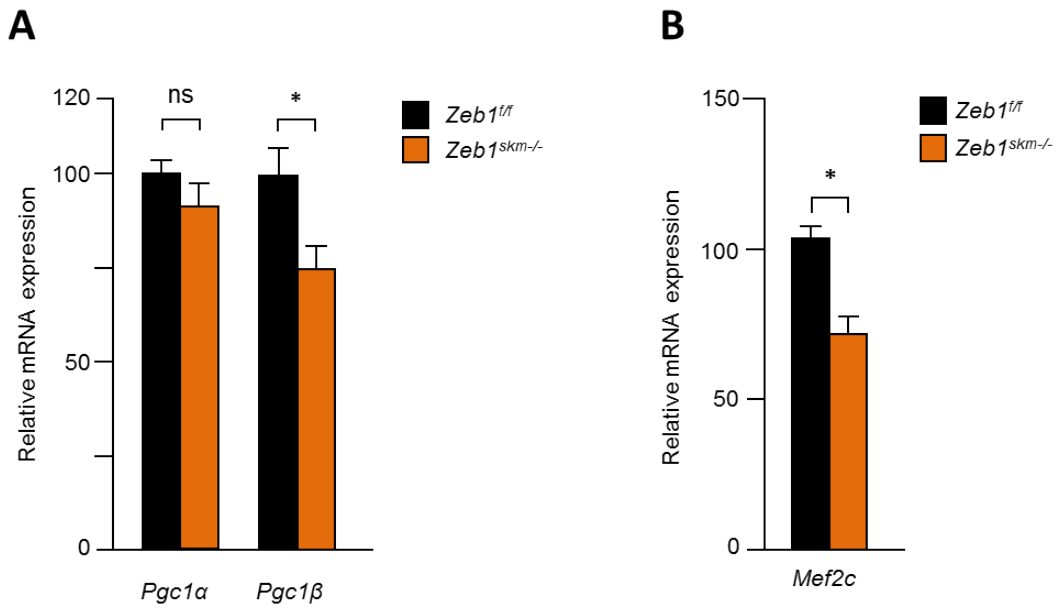

Figure 32: ZEB1 regulates Pgc1β, but not Pgc1α, and Mef2c mRNA expression. *Pgc1α* and *Pgc1β* **(A)** and *Mef2c* **(B)** mRNA expression levels in gastrocnemius muscles from *Zeb1*$^{f/f}$ control and *Zeb1*$^{skm-/-}$ mice, 5 days after the last tamoxifen injection. Bars represent the mean with sem of at least six mice for each genotype. The expression levels of control mice were arbitrarily set to 100.

This result suggests that the lower percentage of slow type I fibers in *Zeb1*$^{skm-/-}$ mice was not due to a modulation in PGC1α content, but rather to other factors, including *Mef2c* and *Myh7* downregulation.

Gain-of-function studies in skeletal muscle of *Pgc1β*$^{skm-/-}$ mice, indicate that *Pgc1β* is required to maintain a healthy population of mitochondria and skeletal muscle oxidative capacity (Ramamoorthy et al., 2015). We measured the muscle mitochondrial respiratory chain capacity in *Zeb1*$^{skm-/-}$ and control mice, fed ad libitum and in resting condition. Two-to-three months old control and *Zeb1*$^{skm-/-}$ mice, injected intraperitoneally for 5 days with tamoxifen, were sacrificed and gastrocnemius muscles of both genotypes were placed into separated O_2K oxygraph chambers (Oroboros Instrument). The substrates and inhibitors reagents, specific for each mitochondrial complex, were sequentially added, to obtain the Oxphos capacity of mitochondrial complex I, I+II, II, III and IV of the respiratory chain, as described in Material and Methods. *Zeb1* deficient muscles presented a decrease in the oxygen consumption rate of complex IV (COX) compared to controls (Figure 33A). No changes were observed in the gene expression of some CIV subunits, like *Cox5a*, *Cox5b* and *Cox4i1* (Figure 33B), suggesting that the lower mitochondrial activity was probably due to less muscle total Oxphos capacity, rather than to CIV transcriptional dysregulation.

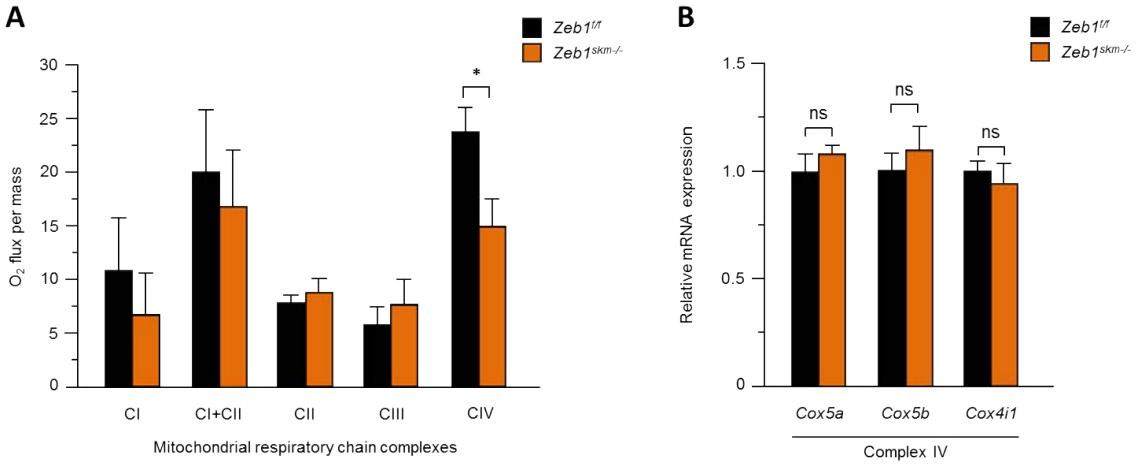

Figure 33: Zeb1 deficient muscles present lower respiratory capacity. **(A)** High-resolution respirometry analysis of permeabilized gastrocnemius fibers from *Zeb1*$^{f/f}$ control and *Zeb1*$^{skm-/-}$ mice. Gastrocnemius muscle from both genotypes was extracted and placed into separated O_2K oxygraph chambers (Oroboros Instrument). The Oxphos capacity of mitochondrial complex I, I+II, II, III and IV of respiratory chain was measured by the sequential addition of the substrates and inhibitors reagents specific for each mitochondrial complex, as described in Material and Methods. Bars represent the mean with sem of at least five mice for each genotype. **(B)** mRNA expression levels of CIV nuclear-encoded genes *Cox5a*, *Cox5b* and *Cox4i1*, in gastrocnemius muscle from *Zeb1*$^{f/f}$ control and *Zeb1*$^{skm-/-}$ mice, 5 days after the last tamoxifen injection. Bars represent the mean with sem of at least six different mice for each genotype. mRNA expression levels of control mice were arbitrarily set to 1.

Chapter III. Expression, role and mechanism of action of ZEB1 in muscle atrophy induced by fasting

ZEB1 protects from fasting-induced muscle atrophy

We sought to investigate if ZEB1 had a potential role also in the atrophic process induced by metabolic changes, like starvation. Two-to-three months old control and *Zeb1*$^{skm-/-}$ mice, treated intraperitoneally with tamoxifen, were subjected to 36 hours of fasting (Scheme in Figure 34A) and the expression levels of *Zeb1* mRNA and protein were analyzed by quantitative real time PCR and immunohistochemistry. Interestingly, like in disuse-induced atrophy, both *Zeb1* mRNA and protein levels increased during fasting in control, but not in *Zeb1*$^{skm-/-}$, gastrocnemius muscles (Figure 34B and Figure 34C).

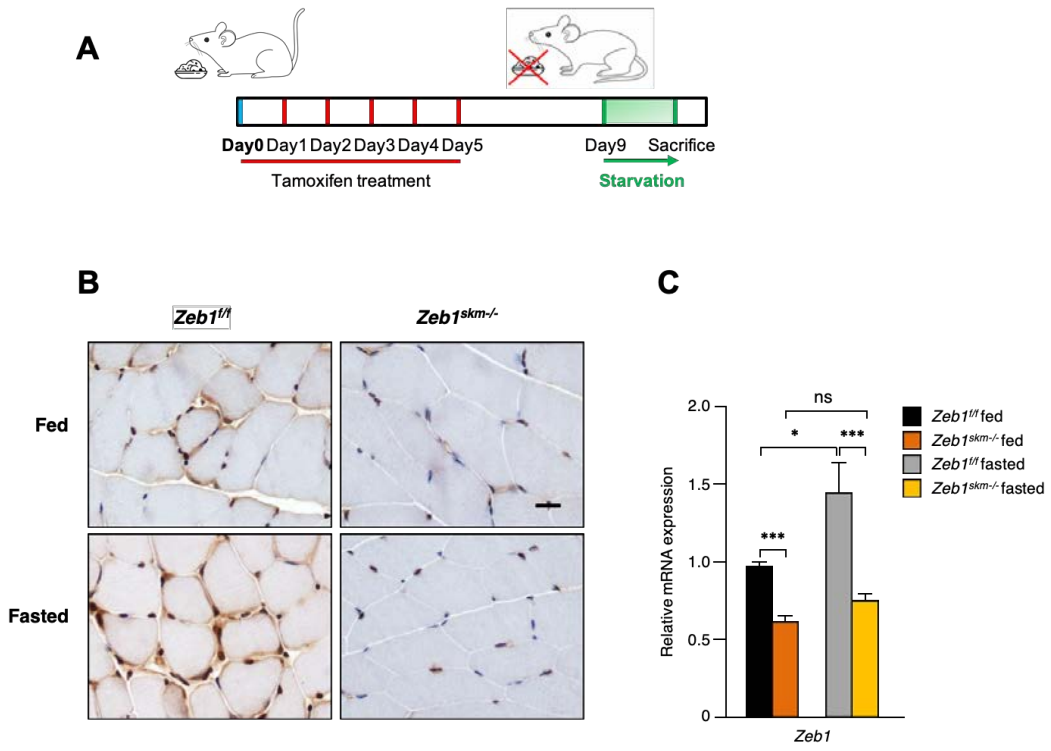

Figure 34: Zeb1 mRNA and protein expression increases during fasting. **(A)** Scheme of the tamoxifen treatment and the fasting protocol used to induce muscle atrophy. **(B)** ZEB1 protein expression was assessed by immunohistochemistry (clone HPA027524) in gastrocnemius muscle from *Zeb1*$^{f/f}$ control and *Zeb1*$^{skm-/-}$ mice fed ad libitum or after fasting. Captures are representative of at least five mice for each genotype and condition. Scale bar: 20μm. **(C)** *Zeb1* mRNA levels in *Zeb1*$^{f/f}$

control and *Zeb1*$^{skm-/-}$ total gastrocnemius muscle in basal condition or after fasting. Bars represent the average with sem of at least six different mice for each genotype and condition.

After fasting, both *Zeb1*$^{skm-/-}$ and control mice suffered a significant decrease in total CSA average, but this decline was more pronounced in *Zeb1*$^{skm-/-}$ fibers (Figure 35A and Figure 35B). Moreover, *Zeb1*$^{skm-/-}$ mice presented a larger number of fibers with CSA <800 μm^2 and a lower number of ones with CSA >2400 μm^2 compared to controls (Figure 35C), suggesting that *Zeb1* deficient muscles suffered a more severe atrophic process.

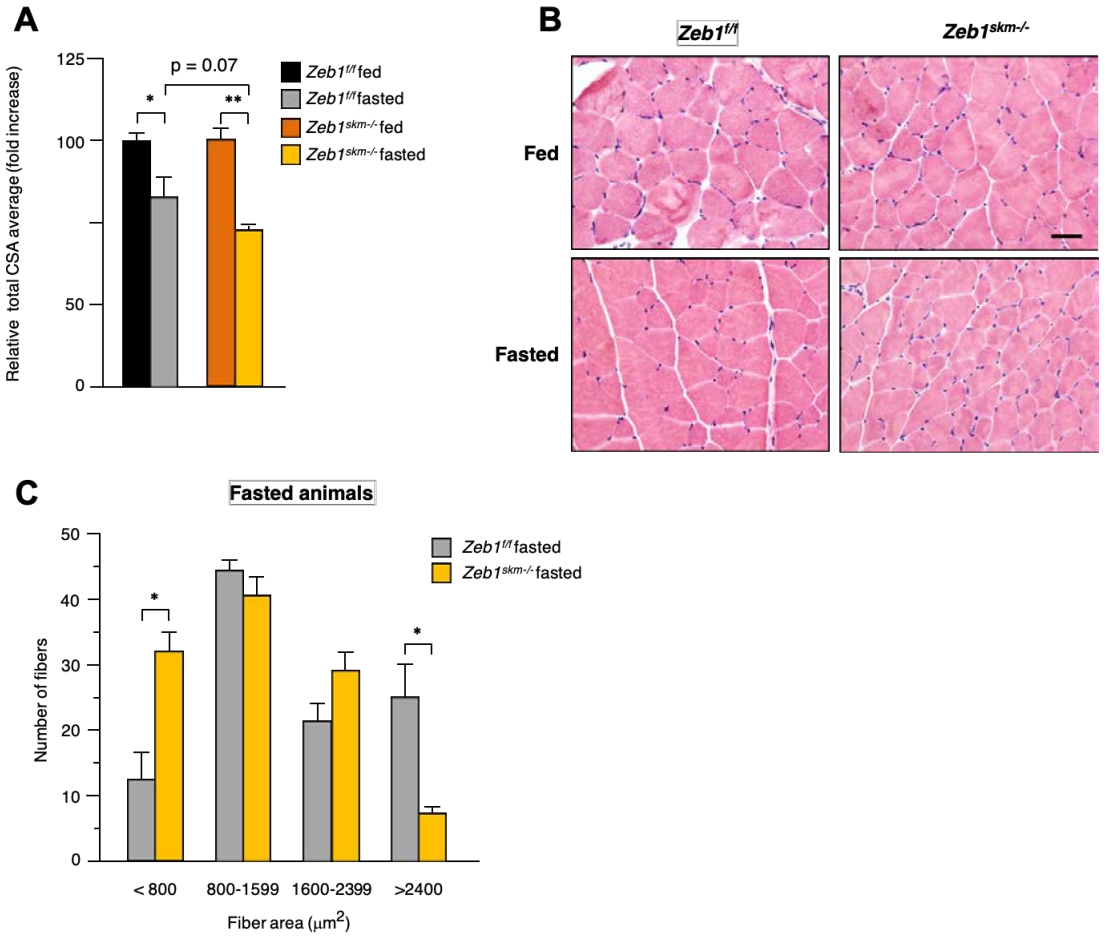

Figure 35: Zeb1 deficient muscles suffer more severe atrophy after fasting. **(A)** Myofiber total cross-sectional area (CSA) analysis in gastrocnemius muscle from *Zeb1*$^{f/f}$ control and *Zeb1*$^{skm-/-}$ mice, in fed-basal condition and after fasting. A total of at least 100 myofibers for each mouse were measured. Bars represent the mean with sem from at least six mice for each genotype and condition. **(B)** *Zeb1*$^{f/f}$ control and *Zeb1*$^{skm-/-}$ mice were treated with tamoxifen for five consecutive days and, after four days from the last tamoxifen injection, they were fasted and then euthanized and their gastrocnemius muscles stained for hematoxylin/eosin. Scale bar: 40 μm. **(C)** Myofibers cross sectional area distribution in fasted *Zeb1*$^{f/f}$ control and *Zeb1*$^{skm-/-}$ gastrocnemius muscles. A total of at

least 100 myofibers for each mouse were measured. Bars represent the mean with sem from at least six mice for each genotype.

This result suggests that, as in the case of immobilization-induced atrophy, ZEB1 protects muscle from an otherwise excessive fasted-induced atrophy.

ZEB1 inhibits muscle atrophy in type I and IIa fibers.

Skeletal muscle is a highly adaptable tissue, able to change its composition and/or morphology depending on the stimulus to which it is subjected. During fasting, when circulating glucose concentration decreases, fatty acids are the major source of energy used by skeletal muscle (Kelley et al., 2005; Cantó et al., 2010). Since in fed-basal condition *Zeb1* deficient muscles presented fewer lipid reserves compared to controls (

Figure 28B), we examined the lipid content in gastrocnemius of fasted control and *Zeb1*$^{skm-/-}$ mice, by ORO staining. The lipid stores decreased during fasting in control mice, while they remained at the same low levels in *Zeb1*$^{skm-/-}$ muscles (Figure 36A). Moreover, both genotypes significantly increased *Atgl* expression versus their respective levels in basal condition (arbitrarily set at 1), indicating an active fatty acid metabolism activation (Figure 36B).

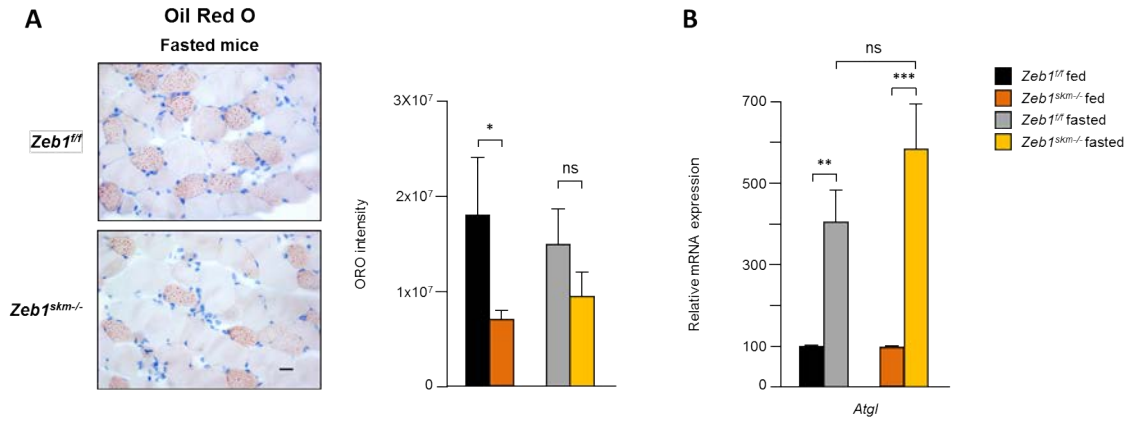

Figure 36: Fasting induces fatty acid oxidation. **(A)** Lipid content of *Zeb1*$^{f/f}$ control and *Zeb1*$^{skm-/-}$ mice after fasting was measured by ORO staining and quantified with ImageJ software. Images are representative of at least five captures for each mouse. Scale bar: 20μm. Bars represent the mean with sem of ORO intensity measured in at least six mice for each genotype. **(B)** *Atgl* mRNA expression was measured in total gastrocnemius of tamoxifen injected *Zeb1*$^{f/f}$ control and *Zeb1*$^{skm-/-}$ mice after fasting. The expression levels in control and *Zeb1*$^{skm-/-}$ mice in basal-fed conditions were

arbitrarily set to 100. Bars represent the mean with sem of at least six different mice for each genotype and condition.

We next performed the ATPase staining in fasted gastrocnemius muscles of control and *Zeb1*$^{skm-/-}$ mice and we analyzed fiber-type specific atrophy intensity by measuring the decrease in the cross-sectional area in each fiber type (I, IIa and IIb). After fasting, *Zeb1*$^{skm-/-}$ mice showed a significant CSA decrease in all three fiber types versus their respective basal conditions, while control mice only suffered a more severe atrophic process in type IIb fibers (Figure 37A and Figure 37B). These results suggest that ZEB1 inhibits muscle atrophy, especially in more oxidative type I and IIa fibers, while in type IIb, which are more sensitive to muscle atrophic conditions (Mizushima et al., 2004), its expression seems dispensable.

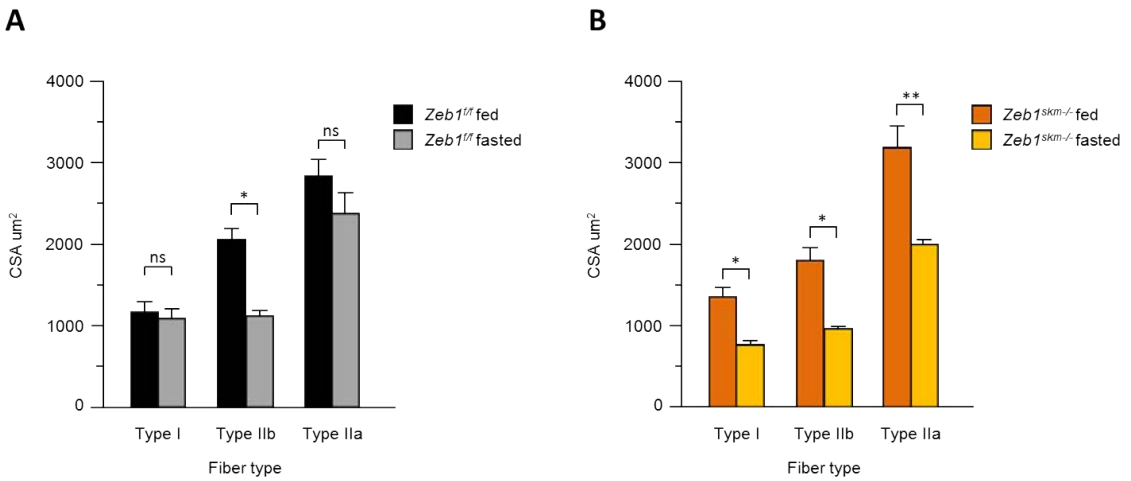

Figure 37: Zeb1 protects type I and IIa fibers from atrophy. Fiber-type specific cross sectional area (CSA) distribution measured in gastrocnemius muscles of *Zeb1*$^{f/f}$ control **(A)** and *Zeb1*$^{skm-/-}$ **(B)** mice in fed-basal condition and after fasting. A total of at least 100 myofibers for each mouse were measured. Bars represent the mean ± sem from at least six mice for each genotype and condition.

Next, we analyzed the fiber type shift during fasting and we found that control muscles suffered a decrease of type IIb and an increase of type IIa fibers, compared to the fed-basal condition (Figure 38A), while *Zeb1* deficient muscles decreased the slow type I fibers without a clear effect in type IIa and IIb (Figure 38B).

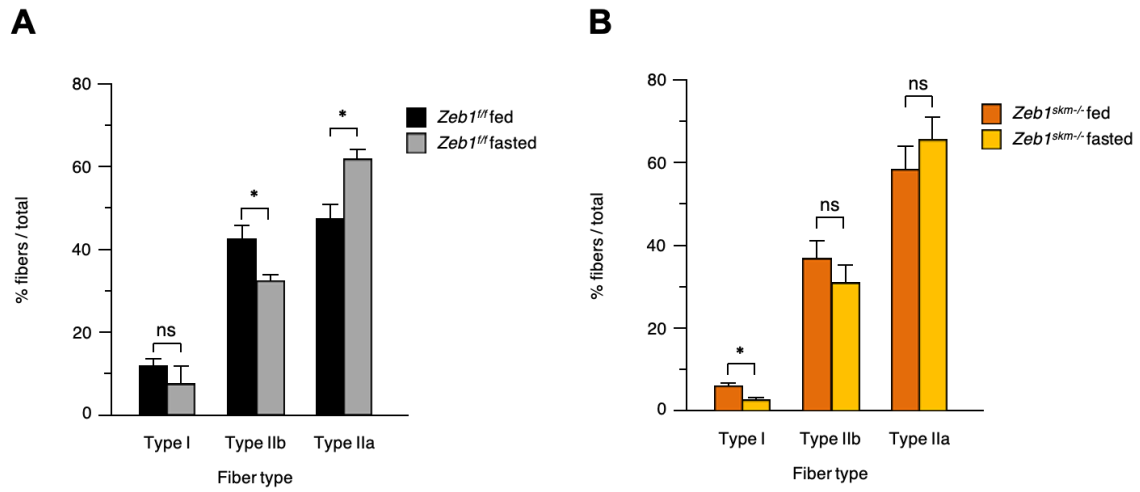

Figure 38: Fiber shift during fasting. Comparison in the percentage of fiber type I, IIb and IIa in *Zeb1*$^{f/f}$ control **(A)** and *Zeb1*$^{skm-/-}$ **(B)** mice in fed-basal condition and after fasting. Bars represent the mean with sem of at least 100 fibers/mouse from six different mice for each genotype and condition.

In atrophic muscles from mice after fasting, the ATPase staining revealed that, as in basal condition, *Zeb1*$^{skm-/-}$ muscles presented a lower number of slow-type I fibers compared to controls (Figure 39A and Figure 39B) with a significantly lower CSA (Figure 39C). *Myh7* mRNA levels decreased in gastrocnemius of control mice during fasting, reaching those of *Zeb1*$^{skm-/-}$ mice. Moreover, fasted control mice increased *Myh4* and decreased *Myh2* mRNA levels, while no differences were seen in the regulation of these genes in *Zeb1* deficient muscles (Figure 39D).

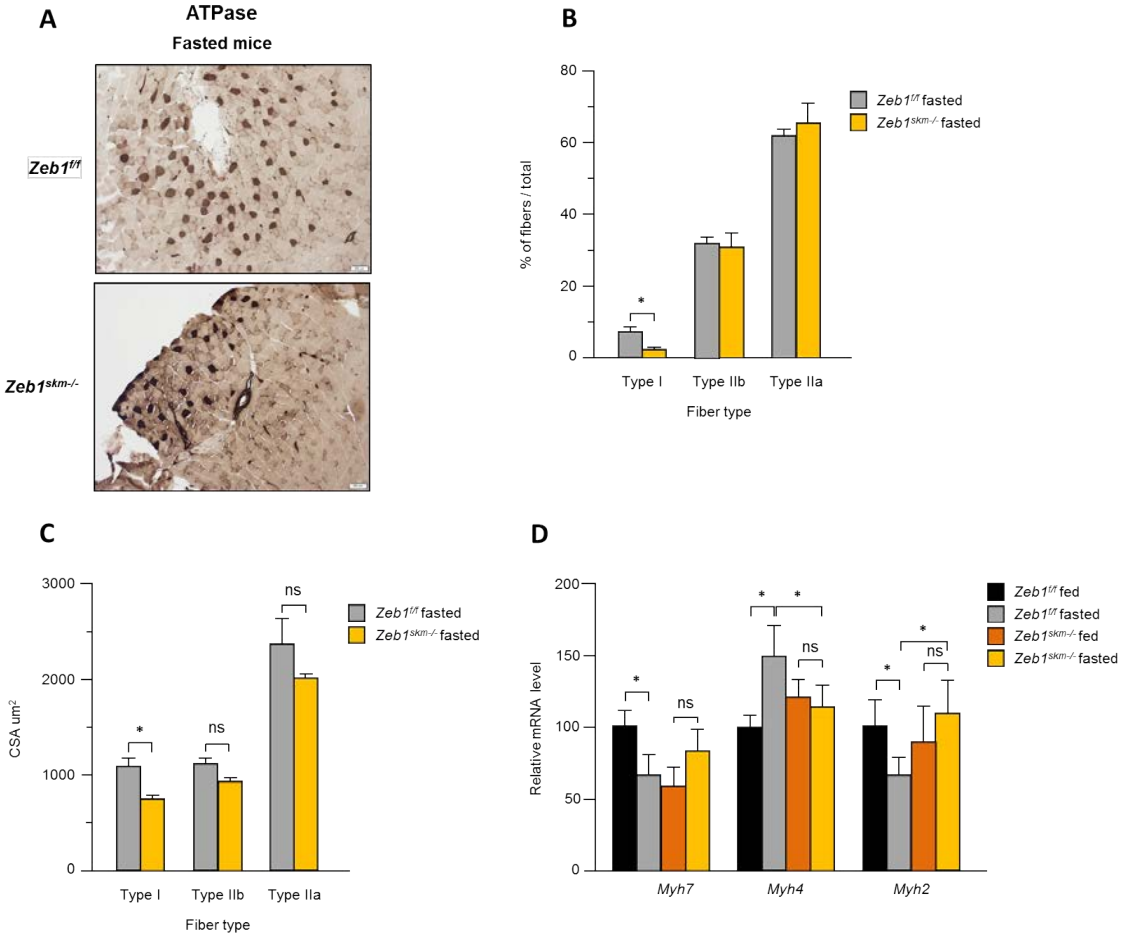

Figure 39: Zeb1 deficient muscles present a dysregulation in fiber shift during fasting. **(A)** ATPase staining in gastrocnemius muscle of *Zeb1*$^{f/f}$ control and *Zeb1*$^{skm-/-}$ mice, after fasting. Slow-twitch type I fibers appear the darkest, fast-fatigue resistant type IIa fibers appear the lightest and fast-fatigable type IIb fibers with an intermediate brown color. Captures are representative of at least six different mice for each genotype. Scale bar: 200μm. **(B)** Bars represent the comparison in the percentage of the three fiber types (I, IIb and IIa) in *Zeb1*$^{f/f}$ control and *Zeb1*$^{skm-/-}$ mice after fasting. Bars represent the mean with sem of at least 100 fibers/mouse from six different mice for each genotype. **(C)** Fiber-type specific myofiber CSA, measured in gastrocnemius muscles of *Zeb1*$^{f/f}$ control and *Zeb1*$^{skm-/-}$ mice after fasting. A total of at least 100 myofibers for each mouse were measured. Bars represent the mean with sem from at least six mice for each genotype. **(D)** mRNA expression of fiber specific MHC genes *Myh7, Myh4* and *Myh2* was analyzed in total *Zeb1*$^{f/f}$ and *Zeb1*$^{skm-/-}$ gastrocnemius muscle, in fed-basal condition and after fasting. Bars represent the mean with sem of at least six mice for each genotype and condition.

Taken together, these data suggest that muscles lacking *Zeb1* suffer a more intense atrophic process, especially in type I and IIa fibers. Moreover, *Zeb1*$^{skm-/-}$ muscles could have dysregulation in the shift of fibers-type during fasting, due to ineffective MHC genes regulation.

ZEB1 protects from fasted-induced ROS by regulating NRFs expression

Muscle atrophy is often accompanied by ROS production, especially mitochondrial ROS, which seem to play an important role in the atrophic process (Pellegrino et al., 2011; Barbieri & Sestili, 2012). We investigated whether *Zeb1* downregulation affected ROS production during the fasted-induced atrophying process by measuring muscle superoxide anion levels in fasted control and *Zeb1*$^{skm-/-}$ mice, by DHE staining. While at basal levels fibers lacking *Zeb1* presented less ROS intensity (Figure 31A), fasted *Zeb1*$^{skm-/-}$ gastrocnemius muscle showed a markedly increasing in superoxide levels compared to controls (Figure 40A). Moreover, *Sod2* and *Ampkα* mRNA levels, which, as explained above, are considered two oxidative stress markers, also significantly increased in *Zeb1*$^{skm-/-}$ versus control mice (Figure 40B).

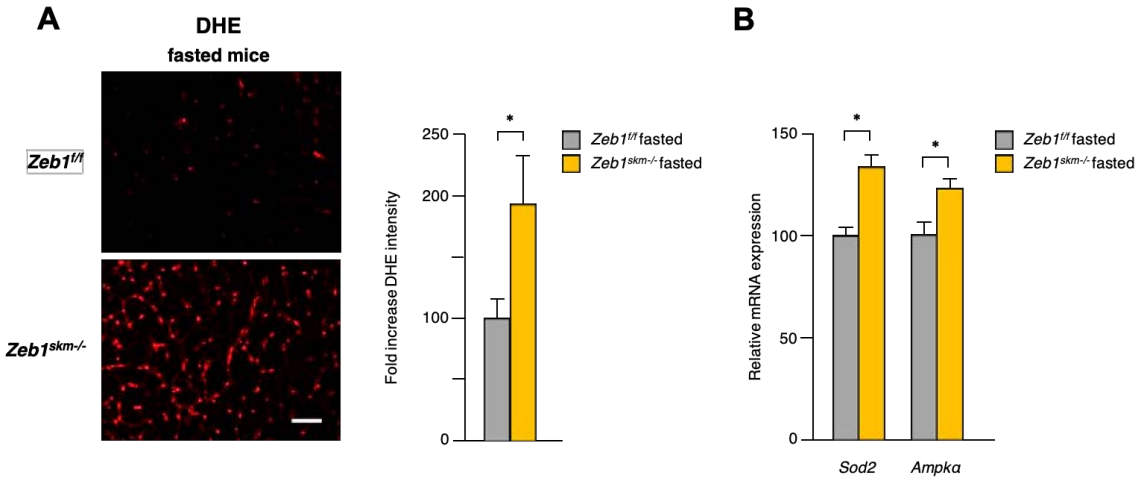

Figure 40: Zeb1 protects against fasted induce ROS. **(A)** DHE staining of gastrocnemius muscles from fasted *Zeb1*$^{f/f}$ control and *Zeb1*$^{skm-/-}$ mice. Images are representative of at least five different captures from each mouse. Scale bar: 50 μm. Bars represent the fold increase of the mean fluorescent intensity with sem of at least six different mice for each genotype. The fluorescent intensity of control mice was arbitrarily set to 100. **(B)** Relative mRNA expression of *Sod2* and *Ampkα* were analyzed in total gastrocnemius muscle extract, from fasted *Zeb1*$^{f/f}$ control and *Zeb1*$^{skm-/-}$ mice. The relative expression in control mice was arbitrarily set to 100. Bars represent the mean with sem of at least six different mice for each genotype.

Since at basal levels *Zeb1*$^{skm-/-}$ mice presented less *Pgc1β* expression (Figure 32A), and it is well established that PGCs co-factors play a key role during metabolically stressing conditions, we evaluated the expression levels of both *Pgc1α* and *Pgc1β* during fasting in *Zeb1*$^{skm-/-}$ and control mice. Unlike what observed in

basal condition, we did not find differences in the *Pgc1β* mRNA level after starvation; in fact, it decreased in both genotypes during fasting, reaching the same expression levels (Figure 41A). We next measured the mRNA levels of nuclear respiratory factors *Nrf1* and *Nrf2*, two master transcription factors that regulate mitochondrial biogenesis and oxidative stress response, and we found that they were both significantly lower induced in *Zeb1*$^{skm-/-}$ gastrocnemius muscle versus controls (Figure 41B). In contrast, the mRNA levels of *Erra,* another mitochondrial master regulator, were higher induced in *Zeb1* lacking muscles after fasting, compared to controls.

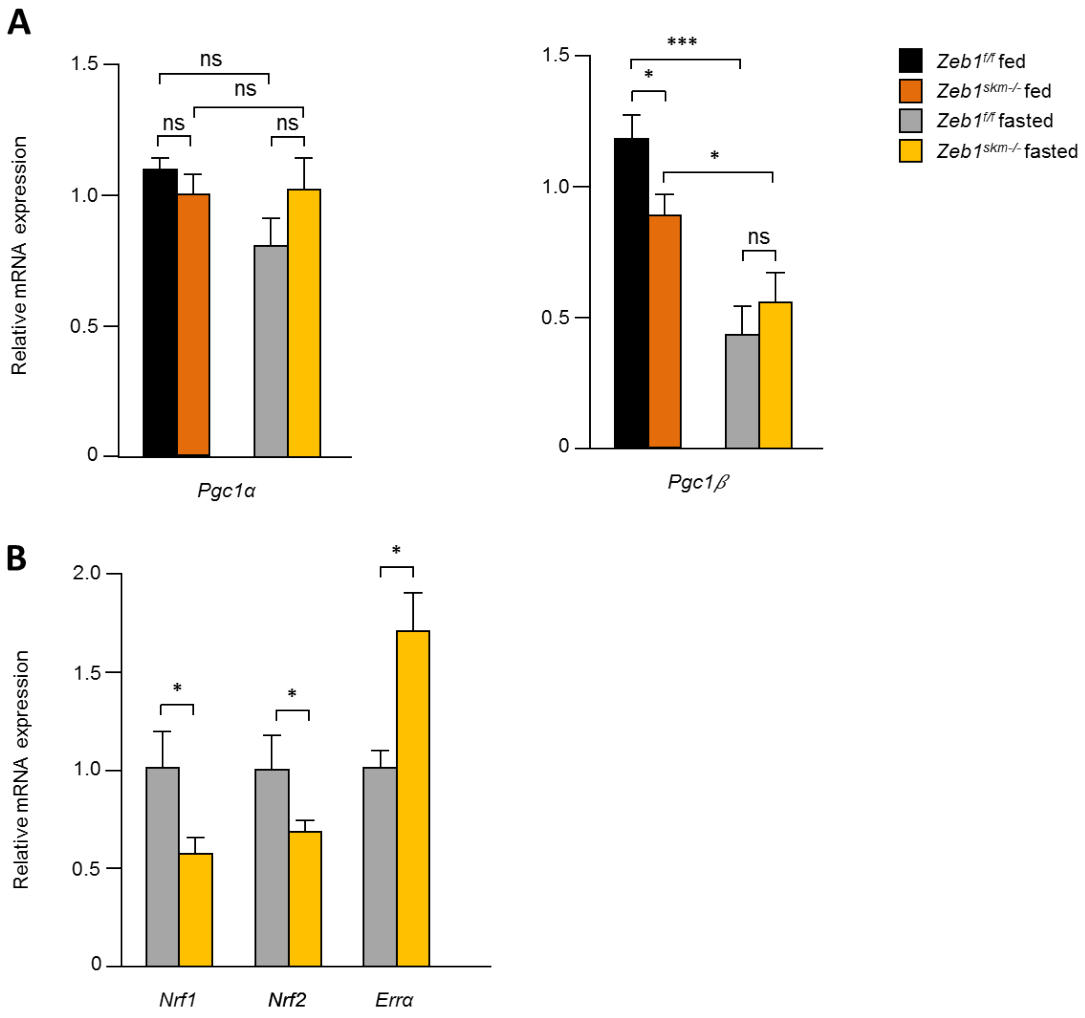

Figure 41: Zeb1 deficient muscles have lower NRFs and higher ERRα induction during fasting. **(A)** Relative mRNA expression of *Pgc1α* and *Pgc1β* were analyzed in total gastrocnemius muscle extract, from *Zeb1*$^{f/f}$ control and *Zeb1*$^{skm-/-}$ mice in fed-basal condition and after fasting. The relative expression in control mice was arbitrarily set to 1. Bars represent the mean with sem of at least six different mice for each genotype and condition. **(B)** As in (A) but relative mRNA expression of *Nrf1*, *Nrf2* and *Erra* were analyzed.

To investigate whether ZEB1 regulation of *NRFs* involved the direct binding to their promoters, we examined the ZEB1's capacity to bind to a CACCTG consensus binding site in both *Nrf1* and *Nrf2* promoters' regions, in the C2C12 myoblasts model. Interestingly, we found that an anti-ZEB1 antibody—but not its specie-matched IgG control— immunoprecipitated a fragment of both *Nrf1* and *Nrf2* promoters containing the CACCTG binding site, suggesting a higher affinity for the *Nrf2* promoter (Figure 42)

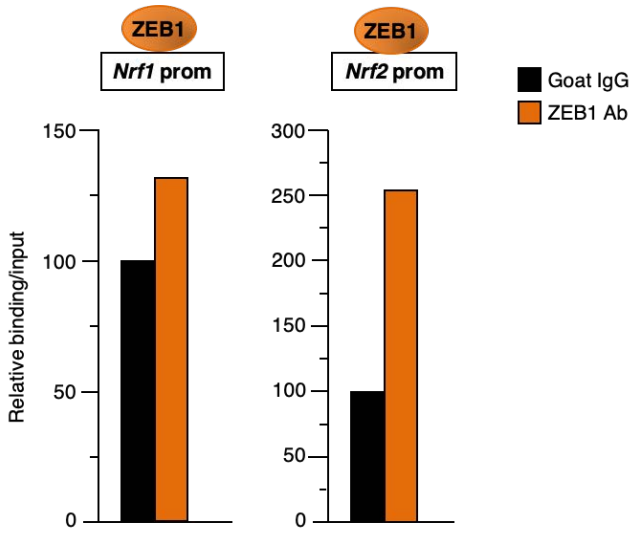

Figure 42: ZEB1 binds Nrf1 and Nrf2 promoters. ZEB1 binds to the mouse *Nrf1* and *Nrf2* promoters in C2C12 myoblasts. The DNA from C2C12 myoblasts was immunoprecipitated with antibodies against ZEB1 (clone C-20) or its matched goat IgG control. Immunoprecipitated DNA was then amplified by qRT-PCR in a region of the *Nrf1* and *Nrf2* promoters containing a ZEB1 consensus-binding site CACCTG. The condition immunoprecipitated with the IgG control was set to 100. Bars show a representative experiment.

Zeb1$^{skm-/-}$ muscles have higher *Mfn1* and *Mfn2* and lower *Pink1* gene expression

As noted in the introduction, during metabolic stress, like during fasting, mitochondria undergo active fusion, by increasing the expression of MFN1 and MFN2, to maintain functional mitochondria (Gomes et al., 2011; Rambold et al., 2011). It was found here that the mRNA levels of *Mfn1* and *Mfn2* were significantly higher in *Zeb1*$^{skm-/-}$ mice versus controls (Figure 43), suggesting that muscles lacking *Zeb1* undergo

mitochondrial fusion to counteract increasing ROS production during the atrophic process.

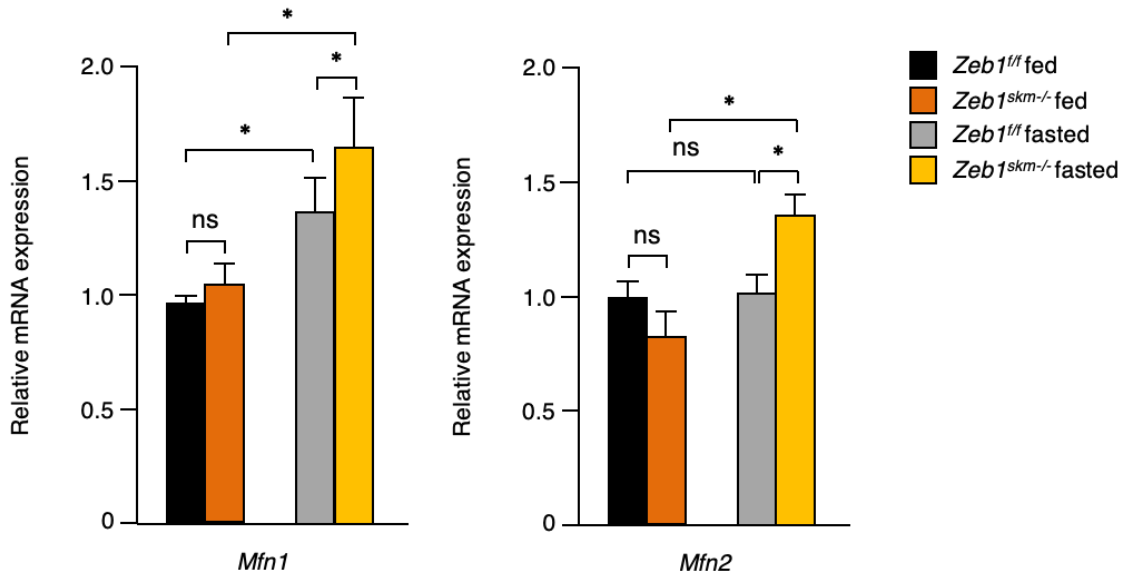

Figure 43: Fibers lacking Zeb1 have a higher increase in mitochondrial fusion genes after fasting. Relative mRNA expression of *Mfn1* and *Mfn2* were analyzed in total gastrocnemius muscle extract, from *Zeb1*$^{f/f}$ control and *Zeb1*$^{skm-/-}$ mice in fed-basal condition and after fasting. The relative expression in control mice was arbitrarily set to 1. Bars represent the mean with sem of at least six different mice for each genotype and condition.

Autophagy is the prevalent mechanism adopted by muscles to counteract nutrient deprivation and to maintain healthy organelles inside atrophic fibers. We analyzed the expression levels of some of the most important autophagy-lysosome and mitophagy factors, including *Beclin1, Bnip3, LC3b, Pink1* and *Parkin*. The expression levels of all of these proteins were significantly increased in atrophied gastrocnemius muscles versus each fed-basal condition, without any significant differences between control and *Zeb1*$^{skm-/-}$ mice except for the mitophagic gene *Pink1* expression (Figure 44), which was slightly, but significantly, lower expressed in fasted *Zeb1*$^{skm-/-}$ muscles compared to controls. This result suggests a possible less efficient mitochondrial autophagy in *Zeb1*$^{skm-/-}$ muscles that could contribute to exacerbate the fiber atrophy.

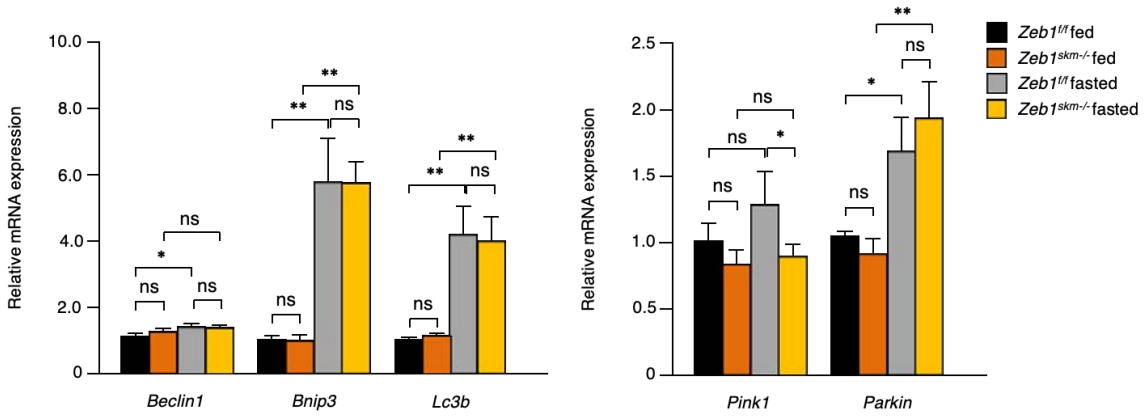

Figure 44: ZEB1 does not modulate autophagy during fasting. Relative mRNA expression levels of the autophagy genes *Beclin1*, *Bnip3*, *Lc3b, Pink1* and *Parkin* were analyzed in total gastrocnemius muscle extract, from *Zeb1*$^{f/f}$ control and *Zeb1*$^{skm-/-}$ mice in fed-basal condition and after fasting. The relative expression of control mice in the fed-basal condition was arbitrarily set to 1. Bars represent the mean with sem of at least six different mice for each genotype and condition.

ZEB1 maintains efficient CIII Oxphos capacity during fasting.

Mitochondrial oxidative metabolism is the cellular major site of ROS production. Complex I (CI) and III (CIII) of the respiratory chain are considered to be the main sources of superoxide anion production. A dysfunction in one or more of these complexes is often accompanied by an increase in ROS production. To evaluate if the higher ROS levels induction in *Zeb1* deficient muscles was due to a dysfunction in some mitochondrial respiratory chain complexes, we measured the mitochondrial respiratory capacity in gastrocnemius fibers from fasted control and *Zeb1*$^{skm-/-}$ mice. The overall mitochondrial respiratory capacity was lower in *Zeb1* deficient muscle, with a significant decrease in the oxygen consumption rate in CIII and CIV complexes (Figure 45).

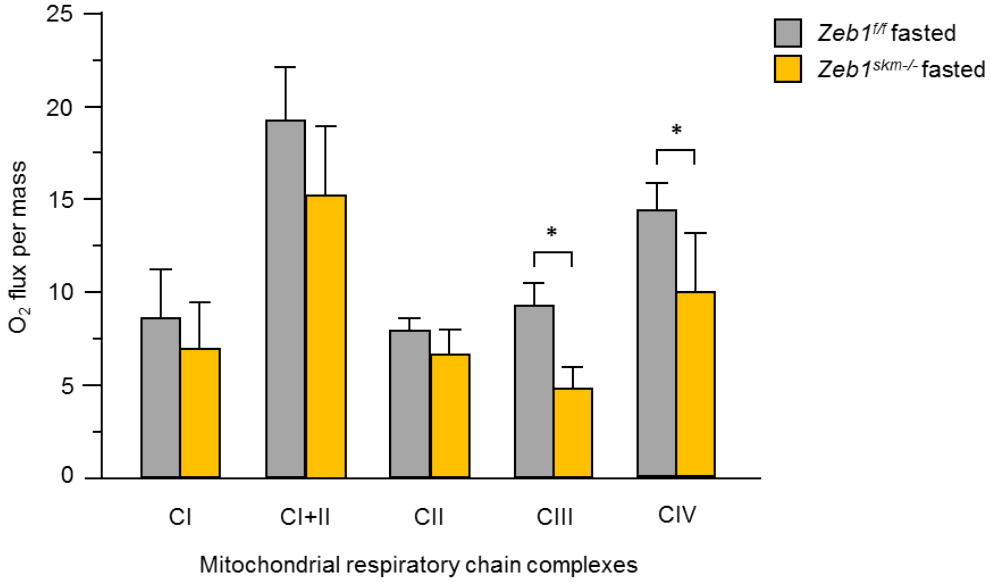

Figure 45: Zeb1$^{skm-/-}$ muscles present lower respiratory capacity after fasting. High-resolution respirometry analysis of permeabilized gastrocnemius fibers from fasted *Zeb1*$^{f/f}$ control and *Zeb1*$^{skm-/-}$ mice. Gastrocnemius muscle from both genotypes was extracted and placed into separated O_2K oxygraph chambers. The substrates and inhibitors reagents, specific for each mitochondrial complex, were sequentially added, to obtain the Oxphos capacity of mitochondrial complex I, I+II, II, III and IV of the respiratory chain, as described in Material and Methods. Bars represent the mean with sem from at least five mice for each genotype.

We then sought to understand if this lower activity was due to a less number of mitochondria or rather to dysfunction in some components of the respiratory chain complexes. The citrate synthase (CS) enzymatic activity, a widely used marker to assess mitochondrial content, did not reveal any significant differences in total mitochondria number from *Zeb1*$^{skm-/-}$ and control mice (Figure 46A). Next, we evaluated the CII+CIII and CIV enzymatic activities (detailed in materials and methods) in homogenates of fasted gastrocnemius muscles from *Zeb1*$^{skm-/-}$ and control mice. The global CII+CIII enzymatic activity was significantly lower in *Zeb1*$^{skm-/-}$ gastrocnemius versus control mice (Figure 46B), while the CIV activity did not change between the two genotypes (Figure 46C).

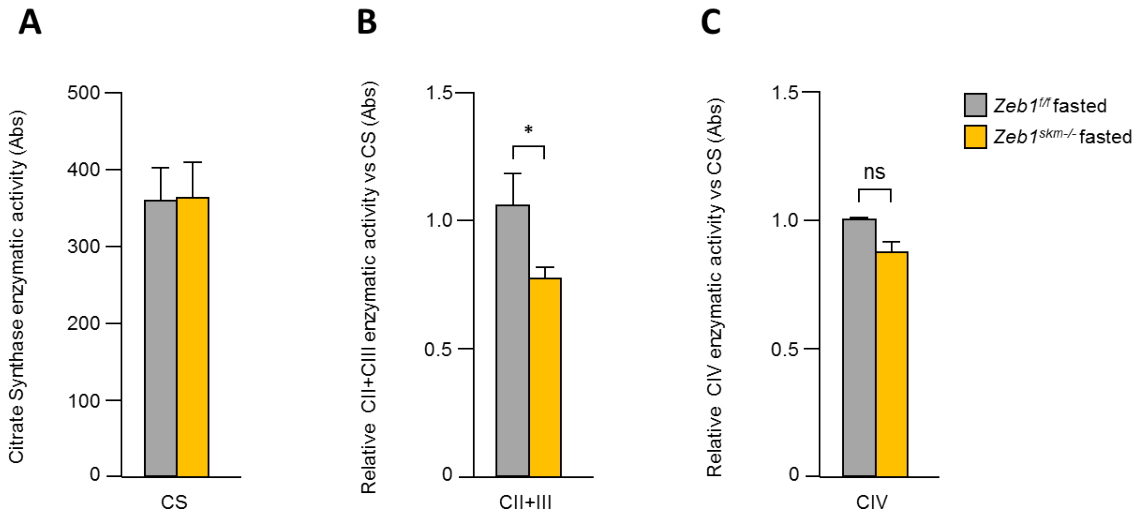

Figure 46: ZEB1 is important to maintain the CIII enzymatic activity. Citrate Synthase **(A)**, complex II + complex III **(B)** and complex IV **(C)** enzymatic activities were measured spectrophotometrically in homogenated gastrocnemius muscle of fasted *Zeb1*$^{f/f}$ control and *Zeb1*$^{skm-/-}$ mice, as described in Materials and Methods. Bars represent the relative average absorbance with sem of at least six different mice for each genotype. CII+CIII and CIV enzymatic activities were normalized versus the CS activity. The relative absorbances of control mice in CII+CIII and CIV activities were arbitrarily set to 1.

Since in the high respiratory capacity analysis the CII did not reveal any differences in the oxygen consumption rate between *Zeb1*$^{skm-/-}$ and control mice (Figure 45), the lower enzymatic activity of CII+CIII was presumably due to the CIII activity, suggesting a possible dysfunction of one or more subunits of this complex.

Mitochondrial CIII is formed from several subunits, which are encoded both from nuclear (nDNA) and mitochondrial (mtDNA) DNA. The mRNA levels of *Tfam*, an important factor in the regulation of mtDNA, did not change between *Zeb1*$^{skm-/-}$ and control mice (Figure 47A), suggesting that mitochondrially encoded CIII subunits were not affected in *Zeb1*$^{skm-/-}$ mice. We measured the expression levels of several CIII nuclear-encoded subunits by real-time qPCR and we found that their transcripts were dysregulated in muscles lacking *Zeb1* versus controls (Figure 47B). Despite that the CIV enzymatic activity remained unchanged between control and *Zeb1*$^{skm-/-}$ mice, the transcript levels of nuclear-encoded subunits *Cox5a* and *Cox5b* were downregulated in *Zeb1* lacking fibers, even if to a lower extent (Figure 47B).

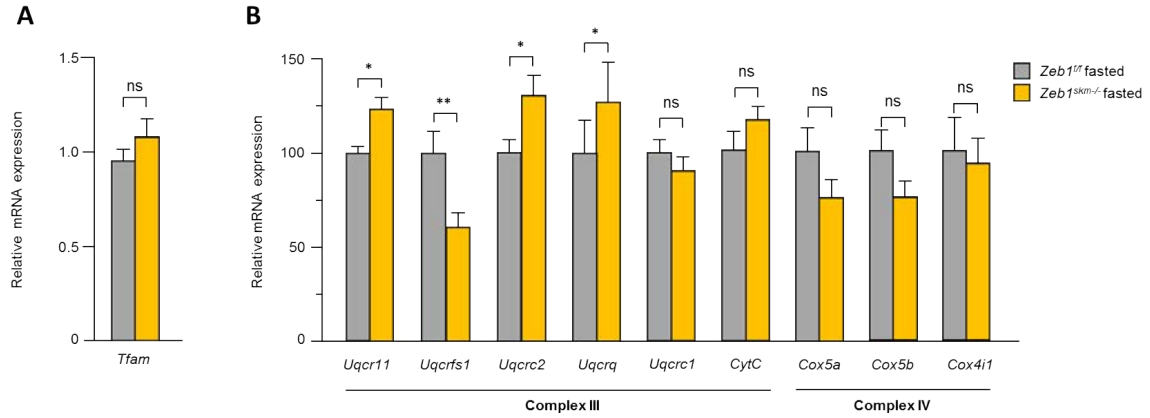

Figure 47: Zeb1$^{skm-/-}$ mice present a dysregulation of nuclear encoded respiratory chain subunits transcripts. **(A)** Relative mRNA expression of *Tfam* was analyzed in total gastrocnemius muscle extract, from fasted *Zeb1*$^{f/f}$ control and *Zeb1*$^{skm-/-}$ mice. The relative expression in control mice was arbitrarily set to 1. Bars represent the mean with sem of at least six different mice for each genotype. **(B)** Relative mRNA expression of CIII (*Uqcr11, Uqcrfs1, Uqcrc2, Uqcrq, Uqcrc1, CytC*) and CIV (*Cox5a, Cox5b, Cox4i1*) nuclear-encoded subunits were analyzed in total gastrocnemius muscle extract, from fasted *Zeb1*$^{f/f}$ control and *Zeb1*$^{skm-/-}$ mice. The relative expression in control mice was arbitrarily set to 100. Bars represent the mean with sem from at least six different mice for each genotype.

An increasing in succinate dehydrogenase (SDH) staining is a hallmark of mitochondrial dysfunction, being often associated with CIII or CIV dysfunction (Lee et al., 2014). The SDH histochemical staining assesses muscle mitochondrial distribution and oxidative capacity, independently of any alteration affecting the mtDNA. We performed an SDH staining in fed and fasted gastrocnemius of *Zeb1*$^{skm-/-}$ and control mice and we found that while at basal levels the two genotypes did not present any differences in SDH intensity, gastrocnemius of fasted *Zeb1*$^{skm-/-}$ mice revealed a more intense SDH staining compared to controls (Figure 48), with some fibers presenting an abnormal accumulation of myofibrillar mitochondria (yellow arrows in Figure 48). The increase in SDH intensity observed in gastrocnemius of *Zeb1*$^{skm-/-}$ mice could be the consequence of the dysregulation in the transcription and enzymatic activity of CIII and CIV mitochondrial complexes, supporting the idea that *Zeb1* deficient fibers have a less efficient mitochondria respiratory capacity to counteract the atrophic process.

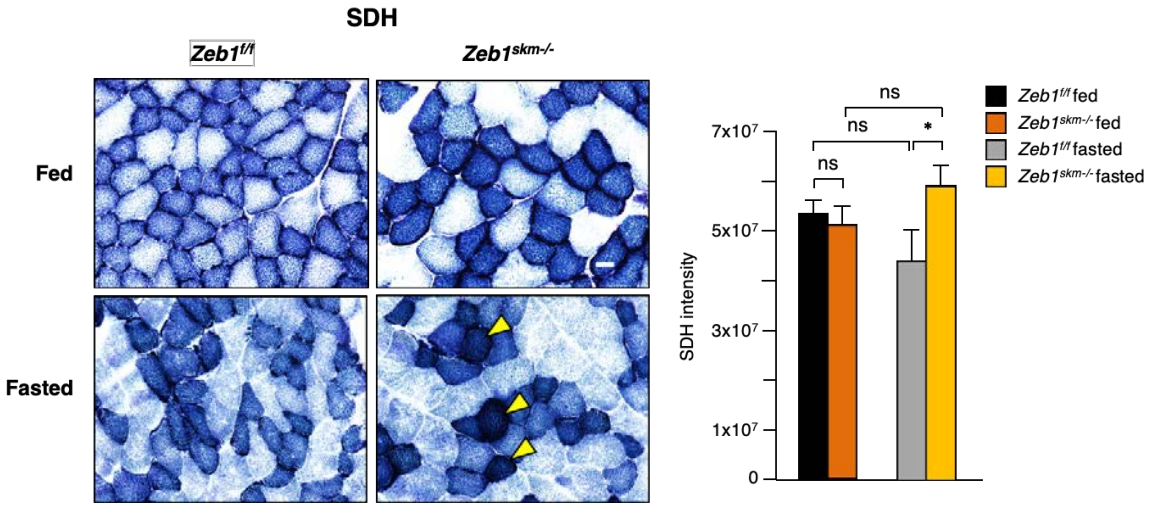

Figure 48: Muscles lacking Zeb1 present abnormal SDH staining. Succinate dehydrogenase (SDH) histological staining of gastrocnemius muscle from *Zeb1*$^{f/f}$ control and *Zeb1*$^{skm-/-}$ mice in fed-basal condition and after fasting. Captures are representative of at least six mice for each genotype and condition. Scale bar: 50 μm. Bars represent the relative SDH intensity with sem, calculated with ImageJ software, in at least five images at 20x magnification for each mouse. At least six mice for each genotype and condition were measured.

The results shown in this dissertation indicate that ZEB1 protects skeletal muscle from immobilization- and fasting-induced atrophy although through different mechanisms. In immobilization-induced atrophy, ZEB1 repressed atrogene expression through CtBP-dependent inhibition of the transcriptional activity of FOXO3. In fasting-induced atrophy, ZEB1 regulates mitochondrial Oxphos activity and ROS production by inducing the NRF1 and NRF2 expression, through direct binding to their promoter regions.

DISCUSSION

DISCUSSION

The molecular mechanisms regulating muscle atrophy are still not fully understood. In this Dissertation, it is shown that ZEB1 inhibits muscle atrophy induced by both hindlimb immobilization and fasting. Full levels of ZEB1 expression protected skeletal muscle from an otherwise unrestrained muscle atrophy and atrogene overexpression in response to immobilization, as occurs when ZEB1 levels are reduced. In the C2C12 myogenic model, ZEB1 knockdown upregulated Atrogin-1 and MuRF1 expression and enhanced the reduction in myotube diameter triggered by growth factor starvation. At the mechanistic level, ZEB1 binds directly to the *Fbxo32 p*romoter in a stage-dependent manner and represses its transcription and that of *Trim63*—both in cell systems and/or *in vivo*—through the CtBP-dependent inhibition of FOXO3 transcriptional activity (see the summary model in Figure 49).

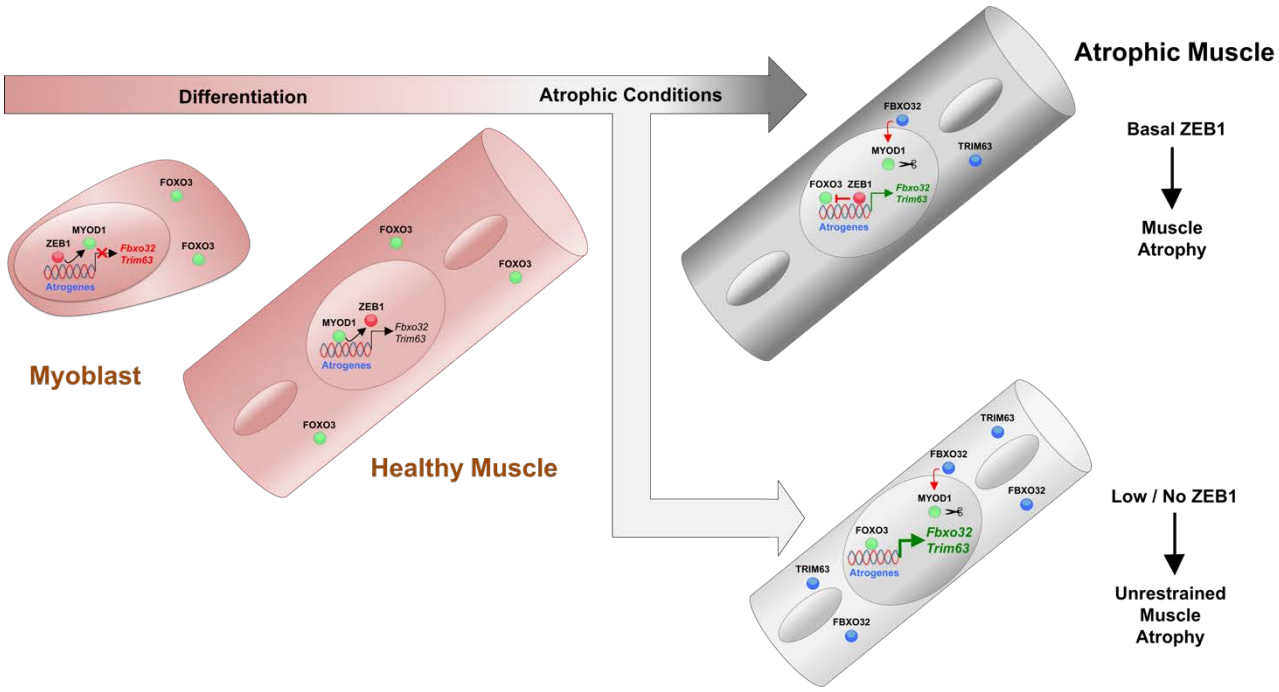

Figure 49: ZEB1 represses atrogene expression. ZEB1 inhibits muscle atrophy and atrogene expression in a stage-dependent manner through the CtBP-mediated repression of FOXO3 transcriptional activity. See the main text for details.

Regulation of muscle fiber size is different during homeostasis and in response to atrophic conditions (Schiaffino et al., 2013), and we found here that under basal (non-immobilized) conditions, *Zeb1* (+/-) muscles displayed equivalent weight and expressed similarly low or non-existing levels of Atrogin-1 and MuRF1 as wild-type counterparts. This can be explained because, in homeostatic (non-immobilized) conditions, ZEB1 does not bind to the *Fbxo32* promoter, that it is instead occupied by MYOD1. Nevertheless, the binding of MYOD1 is not sufficient to induce *Fbxo32* expression, whose transcriptional activation requires FOXO3, which remains in the cytoplasm of fibers in non-immobilized muscles (Sandri et al., 2004; Bonaldo & Sandri, 2013; Schiaffino et al., 2013). In turn, a partial downregulation of *Zeb1*—to around half levels with respect to those in wild-type mice—was sufficient to trigger enhanced muscle atrophy in *Zeb1* (+/-) muscles in response to hindlimb immobilization. In addition, immobilization induced a moderate increase in ZEB1 mRNA and protein expression. This would suggest that the protecting role of ZEB1 against unrestrained muscle atrophy during immobilization depends on a fine threshold of its expression. Interestingly, an analogous expression threshold has been reported for ZEB1's tumor-promoting functions. Thus, a partial downregulation of *Zeb1* in either cancer cells or stromal cells in the tumor microenvironment is enough to completely block the malignant progression of lung, colon and ovarian carcinomas in *Zeb1* (+/-) mice (Liu et al., 2014; Cortés et al., 2017; de Barrios et al., 2017; De Barrios et al., 2019). Likewise, a partial downregulation of *Zeb1* in the dystrophic muscles of the mdx mouse model, increases muscle damage and hampers its regeneration (Siles et al., 2019). In addition, ZEB1 transcriptional activity is regulated by *cis* and *trans m*echanisms that determine its binding to target gene promoters and its recruitment of transcriptional co-activators and co-repressors (reviewed in Sánchez-Tilló et al., 2012).

Muscles need to continuously and finely regulate their protein synthesis and proteolysis in response to atrophic and hypertrophic signals. In that regard, a pleiotropic and tightly regulated protein like ZEB1 can play such a role (reviewed in Sánchez-Tilló et al., 2012; Caramel et al., 2018). Here, we showed that ZEB1 inhibited muscle atrophy in a stage-dependent manner; ZEB1 bound to the *Fbxo32*

promoter in atrophic myotubes, but not in non-atrophic myotubes, thus contributing to explain the lack of atrophy and atrogene upregulation in *Zeb1* (+/-) muscles under basal (non-immobilized) condition. Regulation of muscle differentiation by ZEB1 and other EMT factors (e.g. SNAI1/2) also occurs in a stage-dependent manner (Postigo & Dean, 1997; Soleimani et al., 2012; Siles et al., 2013). ZEB1 and SNAI1/2 share DNA-binding sites (E-box and E-box-like sequences) with MYOD1 in the promoters of muscle differentiation genes. During the myoblast stage, ZEB1 and SNAI1/2 occupy these promoters to repress their expression, but, as muscle differentiation proceeds, MYOD1 accumulates and displaces EMT factors from these genes, activating their expression (Postigo & Dean, 1997; Soleimani et al., 2012; Siles et al., 2013). During atrophy, we found a similarly reverse binding pattern in the binding of ZEB1 and MYOD1 to atrogenes. ZEB1 was excluded from the *Fbxo32* promoter in non-atrophic myotubes, where MYOD1 was instead occupying the promoter. MYOD1 has a higher affinity than ZEB1 for binding to E-boxes (Postigo & Dean, 1997) and, accordingly, overexpression of MYOD1 was able to displace ZEB1 from the *Fbxo32* promoter. Due to the high homology of DNA-binding sequences between ZEB1/2 and SNAI1/2 factors, it can be speculated that, as occurs for muscle differentiation genes (Soleimani et al., 2012), ZEB2 or SNAI1/2 could bind atrogene promoters, but in a different spatio-temporal pattern than ZEB1. Accordingly, during the EMT process induced by the TGFß pathway, SNAI1 is the first transcription factor transiently upregulated, while ZEB1 is upregulated at later stages, displacing SNAI1 from its target genes (Shirakihara et al., 2007).

The preferred binding of ZEB1 over MYOD1 to the *Fbxo32* promoter in atrophic myotubes is probably related not only to the slight upregulation of ZEB1 during atrophy (Figure 12A, B and Figure 18C), but also to the downregulation of *Myod1* mRNA during atrophy (data not shown) and the reported role of Atrogin-1 targeting MYOD1 protein for ubiquitin degradation (Tintignac et al., 2005; Lagirand-Cantaloube et al., 2009) (see model in Figure 49).

ZEB1 repressed the *Fbxo32* promoter through a mechanism that involved the recruitment of CtBP and the inhibition of FOXO3 transcriptional activity. Among all transcription factors that recruit it, CtBP has one of the highest affinity for ZEB1 (Shi et al., 2003). Still, *CtBP* knockdown upregulated *Fbxo32* and *Trim63* promoter's

transcription above the effect of *Zeb1* knockdown, suggesting that Atrogin-1 and MuRF1 expression are under negative regulation by CtBP-binding transcription factor(s) other than ZEB1. Notably, muscle atrophy-inducing conditions of very disparate origins—from immobilization or denervation to cancer cachexia, fasting or uremia—upregulate a highly overlapping set of atrogenes (Lecker et al., 2004; Sacheck et al., 2007; Milan et al., 2015). Therefore, it is possible that the role of ZEB1 inhibiting atrogene expression also takes place in other atrophy-inducing conditions.

It remains to be elucidated whether ZEB1 represses all atrogenes or only a subset. We found that, besides *Fbxo32* and *Trim63,* ZEB1 also represses other components of the ubiquitin–proteasome chain (*Psma1*), members of the autophagy-lysosomal system (*Ctsl, Gabarapl1*), as well as genes involved in protein synthesis (*4ebp1*) and oxidative stress (*Nrf2*). Although FOXO3 is required for muscle atrophy and a majority of atrogenes are induced by FOXO proteins, their dependence on FOXO is determined by the atrophy-inducing condition; thus, *Nrf2* is induced by FOXO proteins upon muscle denervation, but not in response to fasting (Milan et al., 2015). This draws a nuanced model of transcriptional regulation of atrogenes where other transcriptional activators beyond FOXO proteins may also induce atrogene expression. ZEB1 represses the activity of a wide range of transcriptional activators with its inhibitory effect and the mechanism involved that are determined by the promoter, the co-repressors it recruits and the activation/differentiation stage of cells (Postigo et al., 1997; Postigo & Dean, 1999b; Postigo et al., 2003,). Thus, it is also conceivable that ZEB1 represses the expression of atrogenes that are not activated by FOXO3.

ZEB1 can also function as a transcriptional activator; binding of ZEB1 to the histone acetyltransferase p300 acetylates the CID region of ZEB1, thus displacing CtBP (Postigo et al., 2003; Sánchez-Tilló et al., 2015). In that line, in B lymphocytes, ZEB1 synergizes with FOXO3, rather than repressing it, in the activation of cell cycle genes cyclin G2 (*Ccng2)* and p130 (*Rbl2*) (Chen et al., 2006). In muscle satellite cells, the muscle stem cells responsible for muscle regeneration, ZEB1 binds and activates the expression of *Foxo3* promoter, which is required for satellite cells self-

renewal capacity during regeneration (Siles et al., 2019), highlighting, once again, the promoter and cell-type specificity of the link between ZEB1 and FOXO3.

Skeletal muscles vary extremely in their fiber type composition, oxidative capacities, contractile properties and gene signatures (Spangenburg & Booth, 2003; Terry et al., 2018). Here we found that ZEB1 is important to sustain the slow-type I fibers formation, probably by regulating slow MHC *Myh7* gene and the myocyte enhancer factor-2, MEF2C. In *Zeb1*$^{skm\ -/-}$ mice, the slow-type I fiber percentage, and its respective slow MHC *Myh7* gene expression, are reduced compared to control mice. Moreover, *Zeb1*-deficient muscles show less oxidative stress markers and IMTG content. IMTG represent the predominant fuel of energy for the higher oxidative metabolism of slow-type I fibers and, accordingly, they accumulate preferentially in slow fibers (Badin et al., 2013). The lower oxidative stress intensity in *Zeb1*$^{skm-/-}$ muscles and the lower IMTG percentage probably reflect the different muscle fiber type composition rather than a higher fatty acid oxidation. In fact, a higher fatty acid metabolism should upregulate fatty acid oxidation enzymes expression, while *Zeb1*-deficient muscles present lower levels of *Atgl* than control counterparts.

The Myocyte Enhancer Factor 2 (MEF2) is a key transcriptional regulator of muscle biogenesis, sarcomeric gene expression and fiber type formation (Potthoff & Olson, 2007; Estrella et al., 2015). MEF2C is required for normal fiber type composition in skeletal muscle, and *Mef2c*$^{skm-/-}$ mice show lower body weight and lower slow-type I fiber percentage compared to age-matched control mice (Anderson et al., 2015). ZEB1 interacts with MEF2 factors in several tissues (Postigo et al., 2000; Su et al., 2016), including skeletal muscle, where it represses the myogenic factor MEF2C by blocking its transcriptional activity (Postigo et al., 1999). *Mef2c* mRNA levels are downregulated in *Zeb1*$^{skm-/-}$ muscles, which could contribute to explain their lower slow fiber type content. The co-factor PGC1α induces, in cooperation with MEF2C, the formation of type I fibers (Lin et al., 2002). *Pgc1α* is not downregulated in *Zeb1*-deficient muscles, suggesting that ZEB1 regulates fiber type composition through a PGC1α–independent mechanism. In contrast, we found that *Pgc1β* mRNA levels and the total muscle respiratory capacity were lower in *Zeb1*-

deficient muscles. This could be a consequence of the fewer slow-type I fiber content rather than a result of mitochondrial dysfunction. Accordingly, *Zeb1*$^{skm-/-}$ muscles do not exhibit higher oxidative stress, which is usually associated with mitochondrial dysfunction, nor a lower expression of nuclear encoded CIV subunits, like *Cox5a*, *Cox5b* and *Cox4i1*. PGC1*β* induces the formation of type IIx fibers, partially by co-activating the MEF2D factor (Larsson et al., 1991; Arany et al., 2007). Type IIx fibers are often oxidative and are important during the switch of type I and IIa fibers to II and IIb fibers, respectively, suggesting another potential mechanism by which ZEB1 regulates skeletal muscle fiber type composition in basal condition (Figure 50).

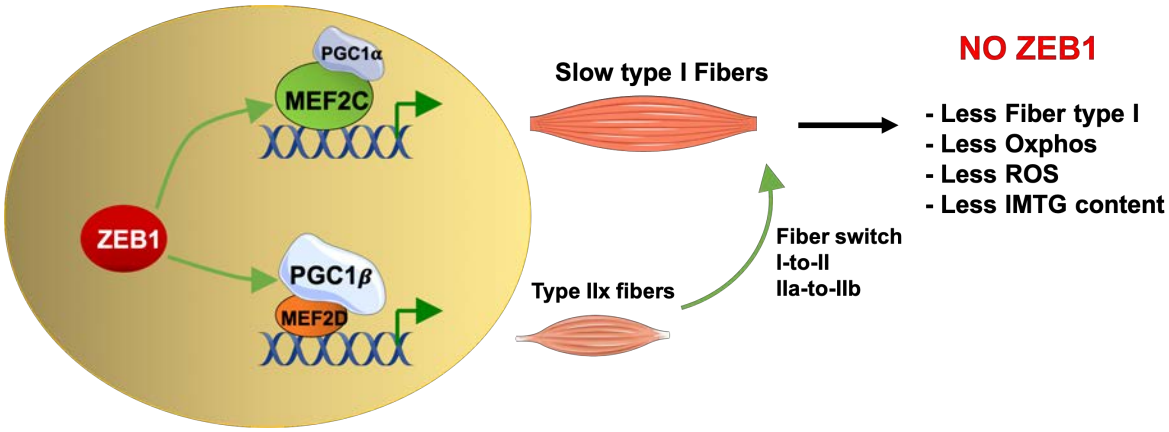

Figure 50: ZEB1's regulation of muscle fiber type composition. ZEB1 promotes the formation of slow-type I fibers through the transcriptional regulation of MEF2C and PGC1β. See the main text for details.

In addition to its role in immobilization-induced muscle atrophy, we found that ZEB1 protects against fasting-induced atrophy through the control of mitochondrial metabolism. *Zeb1*-deficient muscles showed a higher decrease in their total fiber cross-sectional area and a larger percentage of smaller fibers after fasting. The increased atrophy in *Zeb1*$^{skm-/-}$ muscles occurs especially in the more oxidative type I and IIa fibers than in glycolytic type IIb fibers, more sensitive to muscle atrophy (Mizushima et al., 2004), where ZEB1 seems to be dispensable. Like PGC1α, ZEB1 accumulates preferentially in slow fibers — e.g., soleus muscle, enriched in slow

fibers, expresses around double *Zeb1* mRNA levels compared to fast tibialis anterioris and mixed gastrocnemius muscle (Figure 29D). In addition, as occurs during hindlimb immobilization, Zeb1 increases during fasting (Figure 34B, C). This suggests that, as in immobilization-induced atrophy, ZEB1 also protects muscles from an otherwise excessive atrophy during nutrient deprivation, especially in oxidative fibers I and IIa.

During fasting, muscles change their fiber type composition to better adapt to atrophic stimuli (Scott et al., 2001). Here we found that after fasting, *Zeb1*-deficient muscles cannot efficiently shift their fibers from type I to II. This could be due to an ineffective transition through the MHCIIx fibers and/or to the aberrant regulations of *Myh* gene expression in *Zeb1*$^{skm-/-}$ muscles after fasting.

We also found that ZEB1 regulates the respiratory capacity of muscles as well as the expression of some genes involved in mitochondrial dynamics. After fasting, *Zeb1*-deficient gastrocnemius muscles showed higher *Mfn1* and *Mfn2* fusion gene expression compared to controls, and lower respiratory capacity and CIII enzymatic activity. Several nuclear encoded CIII and CIV gene transcripts were altered in *Zeb1*-deficient muscles, with a higher superoxide anion production and SDH intensity, probably associated with CIII dysfunction (Muller et al., 2004). Interestingly, we found that NRF1 and NRF2, two key mitochondrial and oxidative stress gene activators, were downregulated in *Zeb1* deficient muscles after fasting. The promoters of *Nrf1* and *Nrf2* contain several E-boxes and we found that ZEB1 directly binds the promoter of both *Nrf* genes in myoblasts, suggesting that ZEB1 activates the Oxphos genes through *Nrf1* and *Nrf2* regulation. Surprisingly, *Errα* mRNA levels were upregulated in *Zeb1*-deficient muscles after fasting. ERRα induces the transcription of several mitochondrial and oxidative genes, including *Mfn2* (Soriano et al., 2006). During fasting, mitochondria undergo an active fusion, by increasing *Mfn1* and *Mfn2* expression, to support energy production (Gomes et al., 2011; Rambold et al., 2011). Besides its role in mitochondrial fusion, MFN2 induces the transcription of oxidative genes and mitochondrial subunits of several complexes of the respiratory chain (Pich et al., 2005). Even though *Zeb1*-deficient muscles express higher levels of *Errα* and *Mfn2,* they show lower respiratory capacity, with significant lower CIII enzymatic

activity, and higher oxidative stress, suggesting that *Erra* upregulation during fasting is not sufficient to compensate *Nrf1* and *Nrf2* downregulation.

MYOD1 regulates several oxidative genes in the homeostatic muscle (Shintaku et al., 2016), including *Pgc1β* (but not *Pgc1α*) and NRF1. As noted above, MYOD1 and ZEB1 recognize the same DNA-binding sequences and, during atrophic conditions, MYOD1 is degraded by Atrogin1 (Tintignac et al., 2005; Lagirand-Cantaloube et al., 2009). This could explain why in homeostatic conditions the mRNA levels of NRF1 do not change between *Zeb1*$^{skm-/-}$ and control mice (data not shown), while during atrophy they are significantly lower induced in *Zeb1* deficient muscles. In contrast to immobilization-induced atrophy, in fasting condition ZEB1 acts as a transcriptional activator, instead as a repressor. Under homeostatic conditions, NRF2 is sequestered by Kelch like ECH associated protein1 (KEAP1) in the cytoplasm and targeted for proteasomal degradation (Itoh et al., 1999; Kobayashi et al., 2004). In response to stress, NRF2 detaches from KEAP1 and translocates to the nucleus, where it binds to the ARE sequences and activates the transcription of several antioxidant and mitochondrial genes (Bellezza et al., 2018). The *NRF2* promoter also contains ARE-like sequences and ChiP assays indicate that NRF2 binds and activates its own promoter in response to stressing stimuli (Kwak et al., 2002).

The binding site analyzed for ZEB1 in the *Nrf2* promoter (Figure 42) is located near the ARE-like sequence where NRF2 itself also binds (Kwak et al., 2002). The specificity of the DNA binding capacity of NRF2 is augmented by the acetylation of p300/CBP (Sun et al., 2009). At the same time, ZEB1 can switch from a transcriptional repressor to an activator by binding to p300/CBP suggesting another potential mechanism by which ZEB1 regulates NRF2 activity during fasting (Figure 51). In contrast, ZEB2 acts mainly as a transcriptional repressor, and it is tempting to speculate that ZEB2 may regulate NRF factors in an opposing manner than ZEB1.

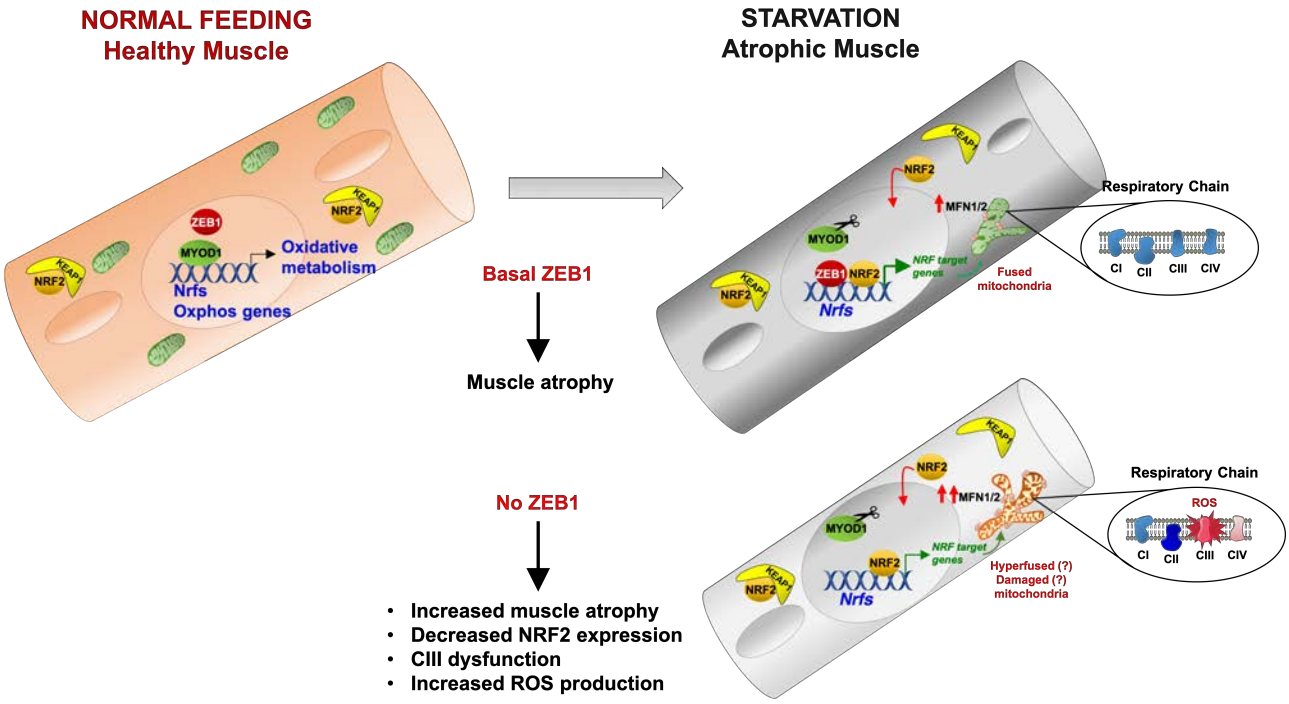

Figure 51: ZEB1's regulation of muscle atrophy during fasting. ZEB1 protects muscle from fasted-induced muscle atrophy through the regulation of *Nrf1* and *Nrf2* genes and muscle respiratory chain activity. See the main text for details.

Altogether, the results obtained in this dissertation unveiled unexpected roles for ZEB1 beyond its previously reported functions in cancer. The identification of ZEB1 as both an inhibitor of atrogene expression during immobilization-induced muscle atrophy and an activator of mitochondrial and oxidative NRFs genes during fasting-induced atrophy offers new approaches for therapies aimed at preventing or treating conditions accompanied by muscle loss.

CONCLUSIONS

CONCLUSIONS

From the results of this dissertation it can be concluded that:

1) ZEB1 inhibits muscle atrophy in a C2C12 cell-line based system and in a *Zeb1* +/- mouse model, through its direct binding to the *Fbxo32* and *Trim63* promoters and the CtBP-dependent transcriptional repression of FOXO3.

2) In homeostatic muscles, ZEB1 promotes and sustains the formation of slow-type I fibers in a conditional-muscle specific ZEB1 knockout mouse model. *Zeb1*$^{skm-/-}$ muscles exhibit lower levels of both *Mef2c*, which is required for type I fiber formation, and of *Pgc1β*, which promotes fiber type IIx formation. As a consequence of this fiber type dysregulation, *Zeb1* lacking fibers present less IMTG content, less Oxphos capacity and less ROS production.

3) ZEB1 protects muscles from atrophy in response to fasting by inducing the expression of NRF1 and NRF2. ZEB1 directly binds to and activates the promoters of both factors in myoblasts, thus preserving efficient mitochondrial respiratory chain activity and avoiding an excessive ROS production during atrophy.

BIBLIOGRAPHY

BIBLIOGRAPHY

Akundi, R. S., Huang, Z., Eason, J., Pandya, J. D., Zhi, L., Cass, W. A., … Büeler, H. (2011). Increased Mitochondrial Calcium Sensitivity and Abnormal Expression of Innate Immunity Genes Precede Dopaminergic Defects in Pink1-Deficient Mice. *PLoS ONE*, *6*(1), e16038.

Anderson, C. M., Hu, J., Barnes, R. M., Heidt, A. B., Cornelissen, I., & Black, B. L. (2015). Myocyte enhancer factor 2C function in skeletal muscle is required for normal growth and glucose metabolism in mice. *Skeletal Muscle*, *5*, 7.

Arany, Z., Lebrasseur, N., Morris, C., Smith, E., Yang, W., Ma, Y., … Spiegelman, B. M. (2007). The Transcriptional Coactivator PGC-1β Drives the Formation of Oxidative Type IIX Fibers in Skeletal Muscle. *Cell Metabolism*, *5*(1), 35–46.

Badin, P., Langin, D., & Moro, C. (2013). Dynamics of skeletal muscle lipid pools. *Trends in Endocrinology & Metabolism*, *24*(12), 607–615.

Banerjee, S., Xie, N., Cui, H., Tan, Z., Yang, S., Icyuz, M., … Liu, G. (2013). MicroRNA let-7c Regulates Macrophage Polarization. *The Journal of Immunology*, *190*(12), 6542–6549.

Barbieri, E., & Sestili, P. (2012). Reactive oxygen species in skeletal muscle signaling. *Journal of Signal Transduction*, *2012*, 982794.

Barja, G. (1999). Mitochondrial Oxygen Radical Generation and Leak: Sites of Production in States 4 and 3, Organ Specificity, and Relation to Aging and Longevity. *Journal of Bioenergetics and Biomembranes*, *31*(4), 347–366.

Behringer, R., Gertsenstein, M., Nagy, K., & Nagy, A. (2014). Manipulating the Mouse Embryo: A Laboratory Manual, Fourth Edition. *Cold Spring Harbor, New York: Cold Spring Harbor Laboratory Press;*, *Fourth Edition*, 814.

Bellezza, I., Giambanco, I., Minelli, A., & Donato, R. (2018). Nrf2-Keap1 signaling in oxidative and reductive stress. *Biochimica et Biophysica Acta (BBA) - Molecular Cell Research*, *1865*(5), 721–733.

Bentzinger, C. F., Wang, Y. X., & Rudnicki, M. A. (2012). Building Muscle: Molecular Regulation of Myogenesis. *Cold Spring Harbor Perspectives in Biology*, *4*(2), a008342.

Berkes, C. A., & Tapscott, S. J. (2005). MyoD and the transcriptional control of myogenesis. *Seminars in Cell & Developmental Biology*, *16*, 585–595.

Biswas, M., & Chan, J. Y. (2010). Role of Nrf1 in antioxidant response element-mediated gene expression and beyond. *Toxicology and Applied Pharmacology*, *244*(1), 16–20.

Blau, H. M., Chiu, C.-P., & Webster, C. (1983). Cytoplasmic activation of human nuclear genes in stable heterocaryons. *Cell*, *32*(4), 1171–1180.

Bloemberg, D., & Quadrilatero, J. (2012). Rapid Determination of Myosin Heavy Chain Expression in Rat, Mouse, and Human Skeletal Muscle Using Multicolor Immunofluorescence Analysis. *PLoS ONE*, *7*(4), 35273.

Bodine, S. C., & Baehr, L. M. (2014). Skeletal muscle atrophy and the E3 ubiquitin ligases MuRF1 and MAFbx/atrogin-1. *American Journal of Physiology. Endocrinology and Metabolism*, *307*(6), E469-84.

Bodine, S. C., Latres, E., Baumhueter, S., K-M Lai, V., Nunez, L., Clarke, B. A., …

Glass, D. J. (2001). Identification of Ubiquitin Ligases Required for Skeletal Muscle Atrophy. *Science*, *294*(23), 1704–1708.

Bonaldo, P., & Sandri, M. (2013). Cellular and molecular mechanism of muscle atrophy. *Disease Model & Mechanisms*, *6*, 25–39.

Bouman, L., Schlierf, A., Lutz, A. K., Shan, J., Deinlein, A., Kast, J., … Winklhofer, K. F. (2011). Parkin is transcriptionally regulated by ATF4: evidence for an interconnection between mitochondrial stress and ER stress. *Cell Death & Differentiation*, *18*(5), 769–782.

Braun, T., & Gautel, M. (2011). Transcriptional mechanisms regulating skeletal muscle differentiation, growth and homeostasis. *Nature Reviews. Molecular Cell Biology.*, *12*(6), 349–361.

Brocca, L., Toniolo, L., Reggiani, C., Bottinelli, R., Sandri, M., & Pellegrino, M. A. (2017). FoxO-dependent atrogenes vary among catabolic conditions and play a key role in muscle atrophy induced by hindlimb suspension. *The Journal of Physiology* , *595*, 1143–1158.

Brunet, A., Bonni, A., Zigmond, M. J., Lin, M. Z., Juo, P., Hu, L. S., … Greenberg, M. E. (1999). Akt promotes cell survival by phosphorylating and inhibiting a Forkhead transcription factor. *Cell*, *96*(6), 857–868.

Cai, D., Frantz, J. D., Tawa, N. E., Melendez, P. A., Oh, B.-C., Lidov, H. G. W., … Shoelson, S. E. (2004). IKKβ/NF-κB Activation Causes Severe Muscle Wasting in Mice. *Cell*, *119*(2), 285–298.

Cantó, C., Jiang, L. Q., Deshmukh, A. S., Mataki, C., Coste, A., Lagouge, M., … Auwerx, J. (2010). Interdependence of AMPK and SIRT1 for Metabolic Adaptation to Fasting and Exercise in Skeletal Muscle. *Cell Metabolism*, *11*(3), 213–219.

Caramel, J., Ligier, M., & Puisieux, A. (2018). Pleiotropic Roles for ZEB1 in Cancer. *Cancer Res*, *78*(1), 30–35.

Carrió, E., Magli, A., Muñoz, M., Peinado, M. A., Perlingeiro, R., & Suelves, M. (2016). Muscle cell identity requires Pax7-mediated lineage-specific DNA demethylation. *BMC Biology*, *14*(1).

Carrió, E., & Suelves, M. (2015). DNA methylation dynamics in muscle development and disease. *Frontiers in Aging Neuroscience*, Vol. 7.

Carter, W. O., Narayanan, P. K., & Robinson, J. P. (1994). Intracellular hydrogen peroxide and superoxide anion detection in endothelial cells. *Journal of Leukocyte Biology*, *55*(2), 253–258.

Castillero, E., Martín, A. I., López-Menduiña, M., Granado, M., Villanúa, M. Á., & López-Calderón, A. (2009). IGF-I system, atrogenes and myogenic regulatory factors in arthritis induced muscle wasting. *Molecular and Cellular Endocrinology*, *309*(1–2), 8–16.

Chakrabarti, P., & Kandror, K. V. (2009). FoxO1 controls insulin-dependent adipose triglyceride lipase (ATGL) expression and lipolysis in adipocytes. *The Journal of Biological Chemistry*, *284*(20), 13296–13300.

Chen, J., Yusuf, I., Andersen, H.-M., & Fruman, D. A. (2006). FOXO transcription factors cooperate with delta EF1 to activate growth suppressive genes in B lymphocytes. *Journal of Immunology*, *176*(5), 2711–2721.

Cheng, Z. (2019). The FoxO-Autophagy Axis in Health and Disease. *Trends in Endocrinology & Metabolism*, *30*(9), 658–671.

Cipolat, S., Martins de Brito, O., Dal Zilio, B., & Scorrano, L. (2004). OPA1 requires

mitofusin 1 to promote mitochondrial fusion. *Proceedings of the National Academy of Sciences of the United States of America*, *101*(45), 15927–15932.

Civiletto, G., Varanita, T., Cerutti, R., Gorletta, T., Barbaro, S., Marchet, S., … Zeviani, M. (2015). Opa1 overexpression ameliorates the phenotype of two mitochondrial disease mouse models. *Cell Metabolism*, *21*(6), 845–854.

Clayton, D. A. (1991). Replication and Transcription of Vertebrate Mitochondrial DNA. *Annual Review of Cell Biology*, *7*(1), 453–478.

Cohen, S., Brault, J. J., Gygi, S. P., Glass, D. J., Valenzuela, D. M., Gartner, C., … Goldberg, A. L. (2009). During muscle atrophy, thick, but not thin, filament components are degraded by MuRF1-dependent ubiquitylation. *The Journal of Cell Biology*, *185*(6), 1083–1095.

Cohen, S., Nathan, J. A., & Goldberg, A. L. (2015). Muscle wasting in disease: molecular mechanisms and promising therapies. *Nat Rev Drug Discov*, *14*(1), 58–74.

Collins, G. A., & Goldberg, A. L. (2017). The Logic of the 26S Proteasome. *Cell*, *169*(5), 792–806.

Cortés, M., Sanchez-Moral, L., de Barrios, O., Fernández-Aceñero, M. J., Martínez-Campanario, M. C., Esteve-Codina, A., … Postigo, A. (2017). Tumor-associated macrophages (TAMs) depend on ZEB1 for their cancer-promoting roles. *The EMBO Journal*, *36*(22), 3336–3355.

Crofts, A. R. (2004). THE CYTOCHROME BC 1 COMPLEX: Function in the Context of Structure. *Annu. Rev. Physiol*, *66*, 689–733.

Davis, R. L., Weintraub, H., & Lassar, A. B. (1987). Expression of a single transfected cDNA converts fibroblasts to myoblasts. *Cell*, *51*(6), 987–1000.

de Barrios, O., Győrffy, B., Fernández-Aceñero, M. J., Sánchez-Tilló, E., Sánchez-Moral, L., Siles, L., … Postigo, A. (2017). ZEB1-induced tumourigenesis requires senescence inhibition via activation of DKK1/mutant p53/Mdm2/CtBP and repression of macroH2A1. *Gut*, *66*(4), 666–682.

de Barrios, O., Sanchez-Moral, L., Cortés, M., Ninfali, C., Profitós-Pelejà, N., Martínez-Campanario, M., … Postigo, A. (2019). Inflammatory bowel disease ZEB1 promotes inflammation and progression towards inflammation-driven carcinoma through repression of the DNA repair glycosylase MPG in epithelial cells. *Gut*, *0*, 1–13.

Diebold, L., & Chandel, N. S. (2016). Mitochondrial ROS regulation of proliferating cells. *Free Radical Biology and Medicine*, *100*, 86–93.

Dobrowolny, G., Aucello, M., Rizzuto, E., Beccafico, S., Mammucari, C., Bonconpagni, S., … Musarò, A. (2008). Skeletal Muscle Is a Primary Target of SOD1G93A-Mediated Toxicity. *Cell Metabolism*, *8*(5), 425–436.

Dodd, S. L., Gagnon, B. J., Senf, S. M., Hain, B. A., & Judge, A. R. (2010). Ros-mediated activation of NF-kappaB and Foxo during muscle disuse. *Muscle & Nerve*, *41*(1), 110–113.

Dogra, C., Changotra, H., Mohan, S., & Kumar, A. (2006). Tumor necrosis factor-like weak inducer of apoptosis inhibits skeletal myogenesis through sustained activation of nuclear factor-kappaB and degradation of MyoD protein. *The Journal of Biological Chemistry*, *281*(15), 10327–10336.

Dongre, A., & Weinberg, R. A. (2019). New insights into the mechanisms of epithelial–mesenchymal transition and implications for cancer. *Nature Reviews-Molecular Cell Biology*, *20*, 69–84.

Estrella, N. L., Desjardins, C. A., Nocco, S. E., Clark, A. L., Maksimenko, Y., & Naya, F. J. (2015). MEF2 transcription factors regulate distinct gene programs in mammalian skeletal muscle differentiation. *The Journal of Biological Chemistry*, *290*(2), 1256–1268.

Evans, M. J., & Scarpulla, R. C. (1990). NRF-1: A trans-activator of nuclear-encoded respiratory genes in animal cells. *Genes and Development*, *4*(6), 1023–1034.

Evans, M. S., Chaurette, J. P., Adams, S. T., Reddy, G. R., Paley, M. A., Aronin, N., … Miller, S. C. (2014). A synthetic luciferin improves bioluminescence imaging in live mice. *Nature Methods*, *11*(4), 393–395.

Fischer, J., Lefèvre, C., Morava, E., Mussini, J.-M., Laforêt, P., Negre-Salvayre, A., … Salvayre, R. (2007). The gene encoding adipose triglyceride lipase (PNPLA2) is mutated in neutral lipid storage disease with myopathy. *Nature Genetics*, *39*(1), 28–30.

Fontemaggi, G., Gurtner, A., Damalas, A., Costanzo, A., Higashi, Y., Sacchi, A., … Blandino, G. (2005). δEF1 repressor controls selectively p53 family members during differentiation. *Oncogene*, *24*(49), 7273–7280.

Fontemaggi, G., Gurtner, A., Strano, S., Higashi, Y., Sacchi, A., Piaggio, G., & Blandino, G. (2001). The Transcriptional Repressor ZEB Regulates p73 Expression at the Crossroad between Proliferation and Differentiation. *Molecular and Cellular Biology*, *21*(24), 8461–8470.

Furusawa, T., Moribe, H., Kondoh, H., & Higashi, Y. (1999). Identification of CtBP1 and CtBP2 as corepressors of zinc finger-homeodomain factor deltaEF1. *Molecular and Cellular Biology*, *19*(12), 8581–8590.

García-Prat, L, Sousa-Victor, P., & Muñoz-Cánoves, P. (2017). Proteostatic and Metabolic Control of Stemness. *Cell Stem Cell*, *20*(5), 593–608.

García-Prat, Laura, Martínez-Vicente, M., Perdiguero, E., Ortet, L., Rodríguez-Ubreva, J., Rebollo, E., … Muñoz-Cánoves, P. (2016). Autophagy maintains stemness by preventing senescence. *Nature*, *529*(7584), 37–42.

Garesse, R., & Vallejo, C. G. (2001). Animal mitochondrial biogenesis and function: a regulatory cross-talk between two genomes. *Gene*, *263*, 1–16.

Genetta, T., Ruezinsky, D., & Kadesch, T. (1994). Displacement of an E-box-binding repressor by basic helix-loop-helix proteins: implications for B-cell specificity of the immunoglobulin heavy-chain enhancer. *Molecular and Cellular Biology*, *14*(9), 6153–6163.

Gheldof, A., Hulpiau, P., Van Roy, F., De Craene, B., & Berx, G. (2012). Evolutionary functional analysis and molecular regulation of the ZEB transcription factors. *Cell Mol Life Sci*, *69*(15), 2527–2541.

Gilliam, L. A. A., Moylan, J. S., Patterson, E. W., Smith, J. D., Wilson, A. S., Rabbani, Z., & Reid, M. B. (2012). Doxorubicin acts via mitochondrial ROS to stimulate catabolism in C2C12 myotubes. *American Journal of Physiology-Cell Physiology*, *302*(1), C195–C202.

Gleyzer, N., Vercauteren, K., & Scarpulla, R. C. (2005). Control of Mitochondrial Transcription Specificity Factors (TFB1M and TFB2M) by Nuclear Respiratory Factors (NRF-1 and NRF-2) and PGC-1 Family Coactivators. *Molecular and Cellular BiologyY*, *25*(4), 1354–1366.

Gomes, L. C., Benedetto, G. Di, & Scorrano, L. (2011). During autophagy mitochondria elongate, are spared from degradation and sustain cell viability. *Nature Cell Biology*, *13*(5), 589–598.

Gomes, M. D., Lecker, S. H., Thomas Jagoe, R., Navon, A., Goldberg, A. L., & Israel, B. (2001). Atrogin-1, a muscle-specific F-box protein highly expressed during muscle atrophy. *Proc. Natl. Acad. Sci. USA*, *98*, 14440–14445.

Gorza, L. (1990). Identification of a Novel Type 2 fibre population in mammalian skeletal muscle by compbined use of histochemical myosin ATPase and anti-myosin monoclonal antibodies. *The Journal of Histochemistry and Cytochemistry*, *38*(2), 257–265.

Guerci, A., Lahoute, C., Hé, S., Collard, L., Graindorge, D., Favier, M., … Sotiropoulos, A. (2012). Srf-Dependent Paracrine Signals Produced by Myofibers Control Satellite Cell-Mediated Skeletal Muscle Hypertrophy. *Cell Metabolism*, *15*, 25–37.

Handschin, C., & Spiegelman, B. M. (2006). Peroxisome Proliferator-Activated Receptor γ Coactivator 1 Coactivators, Energy Homeostasis, and Metabolism. *Endocrine Reviews*, *27*(7), 728–735. https://doi.org/10.1210/er.2006-0037

Hanna, R. A., Quinsay, M. N., Orogo, A. M., Giang, K., Rikka, S., & Gustafsson, Å. B. (2012). Microtubule-associated Protein 1 Light Chain 3 (LC3) Interacts with Bnip3 Protein to Selectively Remove Endoplasmic Reticulum and Mitochondria via Autophagy. *The Journal of Biological Chemistry*, *287*(2), 19094–19104.

Hardie, D. G. (2007). AMP-activated/SNF1 protein kinases: conserved guardians of cellular energy. *Nature Reviews Molecular Cell Biology*, *8*(10), 774–785.

Itoh, K., Wakabayashi, N., Katoh, Y., Ishii, T., Igarashi, K., Engel, J. D., & Yamamoto, M. (1999). Keap1 represses nuclear activation of antioxidant responsive elements by Nrf2 through binding to the amino-terminal Neh2 domain. *Genes & Development*, *13*(1), 76–86.

Jag, U. R., Zavadil, J., & Stanley, F. M. (2009). Insulin Acts through FOXO3a to Activate Transcription of Plasminogen Activator Inhibitor Type 1. *Molecular Endocrinology*, *23*(10), 1587–1602.

Jagoe, R. T., Lecker, S. H., Gomes, M., & Goldberg, A. L. (2002). Patterns of gene expression in atrophying skeletal muscles: response to food deprivation. In *FASEB J* (Vol. 16).

Janssen, I., Heymsfield, S. B., Baumgartner, R. N., & Ross, R. (2000). Estimation of skeletal muscle mass by bioelectrical impedance analysis. *Journal of Applied Physiology*, *89*(2), 465–471.

Jethanandani, P., & Kramer, R. H. (2005). Alpha7 integrin expression is negatively regulated by deltaEF1 during skeletal myogenesis. *The Journal of Biological Chemistry*, *280*(43), 36037–36046.

Jocken, J. W. E., Smit, E., Gijs, ·, Goossens, H., Essers, Y. P. G., Van Baak, M. A., … Blaak, E. E. (2008). Adipose triglyceride lipase (ATGL) expression in human skeletal muscle is type I (oxidative) Wber speciWc. *Histochem Cell Biol*, *129*, 535–538.

Kelley, D. E. (2005). Skeletal muscle fat oxidation: timing and flexibility are everything. *The Journal of Clinical Investigation*, *115*(7), 1699–1702.

Kelly, D. P., & Scarpulla, R. C. (2004). Transcriptional regulatory circuits controlling mitochondrial biogenesis and function. *Genes and Development*, *18*(314), 357–368.

Kobayashi, A., Kang, M.-I., Okawa, H., Ohtsuji, M., Zenke, Y., Chiba, T., … Yamamoto, M. (2004). Oxidative Stress Sensor Keap1 Functions as an Adaptor for Cul3-Based E3 Ligase To Regulate Proteasomal Degradation of Nrf2.

Molecular and cellular biology, *24*(16), 7130–7139.

Kraft, C. S., Lemoine, C. M. R., Lyons, C. N., Michaud, D., Mueller, C. R., & Moyes, C. D. (2006). Control of mitochondrial biogenesis during myogenesis. *Am J Physiol Cell Physiol*, *290*, 1119–1127.

Kwak, M.-K., Itoh, K., Yamamoto, M., & Kensler, T. W. (2002). Enhanced expression of the transcription factor Nrf2 by cancer chemopreventive agents: role of antioxidant response element-like sequences in the nrf2 promoter. *Molecular and Cellular Biology*, *22*(9), 2883–2892.

Lagirand-Cantaloube, J., Cornille, K., Csibi, A., Batonnet-Pichon, S., Leibovitch, M. P., & Leibovitch, S. A. (2009). Inhibition of Atrogin-1/MAFbx Mediated MyoD Proteolysis Prevents Skeletal Muscle Atrophy In Vivo. *PLoS ONE*, *4*(3), e4973.

Larsson, L., Edström, L., Lindegren, B., Gorza, L., & Schiaffino, S. (1991). MHC composition and enzyme-histochemical and physiological properties of a novel fast-twitch motor unit type. *The American Journal of Physiology*, *261*(1 Pt 1), C93-101.

Lecker, S. H., Ja-Goe, H., Gilbert, R. T., Gomes, A., Baracos, M., Bailey, V., … Goldberg, W. E. (2004). Multiple types of skeletal muscle atrophy involve a common program of changes in gene expression. *FASEB J*, *18*, 39–51.

Lee, H. J., Han, J., Jang, Y., Kim, S. J., Park, J. H., Seo, K. S., … Kweon, G. R. (2015). Docosahexaenoic acid prevents paraquat-induced reactive oxygen species production in dopaminergic neurons via enhancement of glutathione homeostasis. *Biochemical and Biophysical Research Communications*, *457*(1), 95–100.

Lee, J.-Y., Kapur, M., Li, M., Choi, M.-C., Choi, S., Kim, H.-J., … Yao, T.-P. (2014). MFN1 deacetylation activates adaptive mitochondrial fusion and protects metabolically challenged mitochondria. *Journal of Cell Science*, *127*, 4954–4963.

Lemercier, C., Verdel, A., Galloo, B., Curtet, S., Brocard, M. P., & Khochbin, S. (2000). mHDA1/HDAC5 histone deacetylase interacts with and represses MEF2A transcriptional activity. *The Journal of Biological Chemistry*, *275*(20), 15594–15599.

Lin, J., Puigserver, P., Donovan, J., Tarr, P., & Spiegelman, B. M. (2002). Peroxisome Proliferator-activated Receptor Coactivator 1 (PGC-1), A Novel PGC-1-related Transcription Coactivator Associated with Host Cell Factor*. *J Biol Chem*, *277*, 1645–1648.

Lin, J., Wu, H., Tarr, P. T., Zhang, C., & Wu, Z. (2002). Transcriptional co-activator PGC-1 a drives the formation of slow-twitch muscle fibres. *Nature*, *418*, 797–801.

Liu, Y., Lu, X., Huang, L., Wang, W., Jiang, G., Dean, K. C., … Dean, D. C. (2014). Different thresholds of ZEB1 are required for Ras-mediated tumour initiation and metastasis. *Nature Communications*, *5*(1), 5660.

Lluís, F., Perdiguero, E., Nebreda, A. R., & Muñoz-Cánoves, P. (2006, January). Regulation of skeletal muscle gene expression by p38 MAP kinases. *Trends in Cell Biology*, Vol. 16, pp. 36–44.

Madaro, L., Smeriglio, P., Molinaro, M., & Bouché, M. (2008). Unilateral immobilization: a simple model of limb atrophy in mice. *Basic Applied Myology*, *18*(5), 149–153.

Malenfant, P., Joanisse, D. R., Thériault, R., Goodpaster, B. H., Kelley, D. E., &

Simoneau, J. A. (2001). Fat content in individual muscle fibers of lean and obese subjects. *International Journal of Obesity and Related Metabolic Disorders*, *25*(9), 1316–1321.

Mammucari, C., Milan, G., Romanello, V., Masiero, E., Rudolf, R., Del Piccolo, P., … Sandri, M. (2007). FoxO3 Controls Autophagy in Skeletal Muscle In Vivo. *Cell Metabolism*, *6*(6), 458–471.

Masiero, E., Agatea, L., Mammucari, C., Blaauw, B., Loro, E., Komatsu, M., … Sandri, M. (2009). Autophagy Is Required to Maintain Muscle Mass. *Cell Metabolism*, *10*, 507–515.

Maurer, P., T'Sas, F., Coutte, L., Callens, N., Brenner, C., Van Lint, C., … Baert, J.-L. (2003). FEV acts as a transcriptional repressor through its DNA-binding ETS domain and alanine-rich domain. *Oncogene*, *22*(21), 3319–3329.

Mehlem, A., Hagberg, C. E., Muhl, L., Eriksson, U., & Falkevall, A. (2013). Imaging of neutral lipids by oil red O for analyzing the metabolic status in health and disease. *Nature Protocols*, *8*(6), 1149–1154.

Milan, G., Romanello, V., Pescatore, F., Armani, A., Paik, J.-H., Frasson, L., … Sandri, M. (2015). Regulation of autophagy and the ubiquitin-proteasome system by the FoxO transcriptional network during muscle atrophy. *Nature Communications*, *6*, 6670.

Mimaki, M., Wang, X., McKenzie, M., Thorburn, D. R., & Ryan, M. T. (2012). Understanding mitochondrial complex I assembly in health and disease. *Biochimica et Biophysica Acta (BBA) - Bioenergetics*, *1817*(6), 851–862.

Mishra, P., & Chan, D. C. (2014). Mitochondrial dynamics and inheritance during cell division, development and disease. *Nature Publishing Group*, *15*, 634–646.

Mizushima, N., Yamamoto, A., Matsui, M., Yoshimori, T., & Ohsumi, Y. (2004). In Vivo Analysis of Autophagy in Response to Nutrient Starvation Using Transgenic Mice Expressing a Fluorescent Autophagosome Marker. *Molecular Biology of the Cell*, *15*, 1101–1111.

Mortimore, G. E., & Poso, A. R. (1987). Intracellular Protein Catabolism and its Control During Nutrient Deprivation and Supply. *Annual Review of Nutrition*, *7*(1), 539–568.

Muller, F. (2000). The nature and mechanism of superoxide production by the electron transport chain: Its relevance to aging. *Journal of the American Aging Association*, *23*(4), 227–253.

Muller, F. L., Liu, Y., & Van Remmen, H. (2004). Complex III Releases Superoxide to Both Sides of the Inner Mitochondrial Membrane. *Journal of Biological Chemistry*, *279*(47), 49064–49073.

Nakae, J., Cao, Y., Hakuno, F., Takemori, H., Kawano, Y., Sekioka, R., … Itoh, H. (2012). Novel repressor regulates insulin sensitivity through interaction with Foxo1. *The EMBO Journal*, *31*(10), 2275–2295.

Nemeth, P., & Pette, D. (1981). Succinate dehydrogenase activity in fibres classified by myosin ATPase in three hind limb muscles of rat. *The Journal of Physiology*, *320*, 73–80. https://doi.org/10.1113/jphysiol.1981.sp013935

Nieto, A. M., Yun-Ju Huang, R., Jackson, R. A., & Paul Thiery, J. (2016). EMT: 2016. *Cell*, *166*(1), 21–45.

Ninfali, C., Siles, L., Darling, D. S., & Postigo, A. (2018). Regulation of muscle atrophy-related genes by the opposing transcriptional activities of ZEB1/CtBP and FOXO3. *Nucleic Acids Research*, *46*(20), 10697–10708.

Nowak, K., Killmer, K., Gessner, C., & Lutz, W. (2007). E2F-1 regulates expression of FOXO1 and FOXO3a. *Biochimica et Biophysica Acta (BBA) - Gene Structure and Expression*, *1769*(4), 244–252.

Pellegrino, M. A., Desaphy, J.-F., Brocca, L., Pierno, S., Camerino, D. C., & Bottinelli, R. (2011). Redox homeostasis, oxidative stress and disuse muscle atrophy. *The Journal of Physiology*, *589*(9), 2147–2160.

Pette, D., & Staron, R. S. (1997). *Mammalian Skeletal Muscle Fiber Type Transitions*. *170*, 143–223.

Pich, S., Bach, D., Briones, P., Liesa, M., Camps, M., Testar, X., … Zorzano, A. (2005). The Charcot-Marie-Tooth type 2A gene product, Mfn2, up-regulates fuel oxidation through expression of OXPHOS system. *Human Molecular Genetics*, *14*(11), 1405–1415.

Postigo, A. (2003). Opposing functions of ZEB proteins in the regulation of the TGFβ/BMP signaling pathway. *The EMBO Journal*, *22*(10), 2443–2452.

Postigo, A. A., & Dean, D. C. (1999a). Independent repressor domains in ZEB regulate muscle and T-cell differentiation. *Molecular and Cellular Biology*, *19*(12), 7961–7971.

Postigo, A. A., & Dean, D. C. (1999b). ZEB represses transcription through interaction with the corepressor CtBP. *Proc. Natrl. Acad. Sci. USA*, *96*, 6683–6688.

Postigo, A., & Dean, D. C. (1997). ZEB, a vertebrate homolog of Drosophila Zfh-1, is a negative regulator of muscle differentiation. *The EMBO Journal*, *16*(13), 3935–3943.

Postigo, A., Dean, D. C., & Kipnis, D. M. (2000). Differential expression and function of members of the zfh-1 family of zinc finger homeodomain repressors. *PNAS*, *97*(12), 6391–6396.

Postigo, A., Depp, J. L., Taylor, J. J., & Kroll, K. L. (2003). Regulation of Smad signaling through a differential recruitment of coactivators and corepressors by ZEB proteins. *The EMBO Journal*, *22*(10), 2453–2462.

Postigo, A., Sheppard, A. M., Mucenski, M. L., & Dean, D. C. (1997). c-Myb and Ets proteins synergize to overcome transcriptional repression by ZEB. *The EMBO Journal*, *16*(13), 3924–3934.

Postigo, A., Ward, E., Skeath, J. B., & Dean, D. C. (1999). zfh-1, the Drosophila homologue of ZEB, is a transcriptional repressor that regulates somatic myogenesis. *Molecular and Cellular Biology*, *19*(10), 7255–7263.

Potthoff, M. J., & Olson, E. N. (2007). MEF2: a central regulator of diverse developmental programs. *Development*, *134*(23), 4131–4140.

Potthoff, Matthew J, Olson, E. N., & Bassel-Duby, R. (2007). Skeletal muscle remodeling. *Current Opinion in Rheumatology*, *19*(6), 542–549.

Powers, S. K., Morton, A. B., Ahn, B., & Smuder, A. J. (2016). Redox control of skeletal muscle atrophy. *Free Radical Biology and Medicine*, *98*, 208–217.

Powers, S. K., Smuder, A. J., & Judge, A. R. (2012). Oxidative stress and disuse muscle atrophy: cause or consequence? *Current Opinion in Clinical Nutrition and Metabolic Care*, *15*(3), 240–245.

Raben, N., Hill, V., Shea, L., Takikita, S., Baum, R., Mizushima, N., … Plotz, P. (2008). Suppression of autophagy in skeletal muscle uncovers the accumulation of ubiquitinated proteins and their potential role in muscle damage in Pompe disease. *Human Molecular Genetics*, *17*(24), 3897–3908.

Rabinovitch, R. C., Samborska, B., Faubert, B., Ma, E. H., Gravel, S.-P., Andrzejewski, S., … Jones, R. G. (2017). AMPK Maintains Cellular Metabolic Homeostasis through Regulation of Mitochondrial Reactive Oxygen Species. *Cell Reports*, *21*(1), 1–9.

Ramamoorthy, T. G., Laverny, G., Schlagowski, A. I., Zoll, J., Messaddeq, N., Bornert, J. M., … Metzger, D. (2015). The transcriptional coregulator PGC-1β controls mitochondrial function and anti-oxidant defence in skeletal muscles. *Nature Communications*, *6*, 1–13.

Rambold, A. S., Kostelecky, B., Elia, N., & Lippincott-Schwartz, J. (2011). Tubular network formation protects mitochondria from autophagosomal degradation during nutrient starvation. *Proceedings of the National Academy of Sciences*, *108*(25), 10190–10195.

Rambold, Angelika S, & Pearce, E. L. (2018). Mitochondrial Dynamics at the Interface of Immune Cell Metabolism and Function. *Trends in Immunology*, *39*(1), 6–18.

Romanello, V., & Sandri, M. (2013). Mitochondrial biogenesis and fragmentation as regulators of protein degradation in striated muscles. *Journal of Molecular and Cellular Cardiology*, *55*, 64–72.

Romanello, V., & Sandri, M. (2016). Mitochondrial Quality Control and Muscle Mass Maintenance. *Frontiers in Physiology*, *6*, 422.

Rubattu, S., Pagliaro, B., Pierelli, G., Santolamazza, C., Di Castro, S., Mennuni, S., & Volpe, M. (2014). Pathogenesis of Target Organ Damage in Hypertension: Role of Mitochondrial Oxidative Stress. *International Journal of Molecular Sciences*, *16*(1), 823–839.

Sabourin, L. A., & Rudnicki, M. A. (2000). Developmental Biology: Frontiers for Clinical Genetics The molecular regulation of myogenesis. In *Clin Genet* (Vol. 57).

Sacchetti, M., Saltin, B., Olsen, D. B., & Van Hall, G. (2004). High triacylglycerol turnover rate in human skeletal muscle. *The Journal of Physiology*, *561*(3), 883–891.

Sacheck, J. M., Hyatt, J.-P. K., Raffaello, A., Jagoe, R. T., Roy, R. R., Reggie Edgerton, V., … Goldberg, A. L. (2007). Rapid disuse and denervation atrophy involve transcriptional changes similar to those of muscle wasting during systemic diseases. *The FASEB Journal*, *21*, 140–155.

Sánchez-Tilló, E, de Barrios, O., Valls, E., Darling, D. S., Castells, A., & Postigo, A. (2015). ZEB1 and TCF4 reciprocally modulate their transcriptional activities to regulate Wnt target gene expression. *Oncogene*, *34*(46), 5760–5770.

Sánchez-Tilló, Ester, De Barrios, O., Siles, L., Cuatrecasas, M., Castells, A., & Postigo, A. (2011). β-catenin/TCF4 complex induces the epithelial-to-mesenchymal transition (EMT)-activator ZEB1 to regulate tumor invasiveness. *PNAS*, *108*(48), 19204–19209.

Sánchez-Tilló, Ester, Liu, Y., De Barrios, O., Siles, L., Fanlo, L., Cuatrecasas, M., … Postigo, A. (2012). EMT-activating transcription factors in cancer: Beyond EMT and tumor invasiveness. *Cellular and Molecular Life Sciences*, *69*(20), 3429–3456.

Sánchez-Tilló, Ester, Siles, L., de Barrios, O., Cuatrecasas, M., Vaquero, E. C., Castells, A., & Postigo, A. (2011). Expanding roles of ZEB factors in tumorigenesis and tumor progression. *American Journal of Cancer Research*,

1(7), 897–912.
Sandri, M. (2008). Signaling in Muscle Atrophy and Hypertrophy. *Physiology*, *23*, 160–170.
Sandri, M. (2010). Autophagy in skeletal muscle. *FEBS Letters*, *584*(7), 1411–1416.
Sandri, M., Lin, J., Handschin, C., Yang, W., Arany, Z. P., Lecker, S. H., … Spiegelman, B. M. (2006). PGC-1 alpha protects skeletal muscle from atrophy by suppressing FoxO3 action and atrophy-specific gene transcription. *PNAS*, *13*(44), 16260–16265.
Sandri, M., Sandri, C., Gilbert, A., Skurk, C., Calabria, E., Picard, A., … Goldberg, A. L. (2004). Foxo transcription factors induce the atrophy-related ubiquitin ligase atrogin-1 and cause skeletal muscle atrophy. *Cell*, *117*(3), 399–412.
Schiaffino, S. (2010). Fibre types in skeletal muscle: A personal account. *Acta Physiologica*, *199*(4), 451–463.
Schiaffino, Stefano, Dyar, K. A., Ciciliot, S., Blaauw, B., & Sandri, M. (2013). Mechanisms regulating skeletal muscle growth and atrophy. *FEBS Journal*, *280*(17), 4294–4314.
Schiaffino, Stefano, Rossi, A. C., Smerdu, V., Leinwand, L. A., & Reggiani, C. (2015). Developmental myosins: expression patterns and functional significance. *Skeletal Muscle*, 5–22.
Schiaffino, Stefano, Sandri, M., & Murgia M. (2007). Activity-dependent signaling pathways controlling muscle diversity and plasticity. *Physiology*, *22*, 269–278.
Schreiber, S. N., Emter, R., Hock, M. B., Knutti, D., Cardenas, J., Podvinec, M., … Kralli, A. (2004). The estrogen-related receptor (ERR) functions in PPAR coactivator 1 (PGC-1)-induced mitochondrial biogenesis. *PNAS*, *101*(17), 6472–6477.
Schuler, M., Ali, F., Metzger, E., Chambon, P., & Metzger, D. (2005). Temporally Controlled Targeted Somatic Mutagenesis in Skeletal Muscles of the Mouse. *Genesis*, *41*, 165–170.
Schultz, B. E., & Chan, S. I. (2001). Structures and proton-pumping strategies of mitochondrial respiratory enzymes. *Annu Rev. Biophys. Biomol. Struct.*, *30*, 23–65.
Scott, W., Stevens, J., & Binder-Macleod, S. (2001). Human Skeletal Muscle Fiber Type Classifications. *Physical Therapy*, *81*(11), 1810–1816.
Sekido, R., Murai, K., Funahashi, J., Kamachi, Y., Fujisawa-Sehara, A., Nabeshima, Y., & Kondoh, H. (1994). The delta-crystallin enhancer-binding protein delta EF1 is a repressor of E2-box-mediated gene activation. *Molecular and Cellular Biology*, *14*(9), 5692–5700.
Shi, Y., Sawada, J., Sui, G., Affar, E. B., Whetstine, J. R., Lan, F., … Shi, Y. (2003). Coordinated histone modifications mediated by a CtBP co-repressor complex. *Nature*, *422*(6933), 735–738.
Shintaku, J., Peterson, J. M., Talbert, E. E., Wang, R., Sartorelli, V., & Guttridge, D. C. (2016). MyoD Regulates Skeletal Muscle Oxidative Metabolism Cooperatively with Alternative NF- k B. *CellReports*, *17*(2), 514–526.
Shirakihara, T., Saitoh, M., & Miyazono, K. (2007). Differential Regulation of Epithelial and Mesenchymal Markers by δEF1 Proteins in Epithelial–Mesenchymal Transition Induced by TGF-β. *Molecular Biology of the Cell*, *18*(9), 3533–3544.
Siles, L., Ninfali, C., Cortés, M., Darling, D. S., & Postigo, A. (2019). ZEB1 protects

skeletal muscle from damage and is required for its regeneration. *Nature Communications*, *10*(1), 1364.

Siles, L., Sánchez-Tilló, E., Lim, J.-W., Darling, D. S., Kroll, K. L., & Postigo, A. (2013). ZEB1 Imposes a Temporary Stage-Dependent Inhibition of Muscle Gene Expression and Differentiation via CtBP-Mediated Transcriptional Repression. *Molecular and Cellular Biology*, *33*(7), 1368–1382.

Smuder, A. J., Kavazis, A. N., Hudson, M. B., Nelson, W. B., & Powers, S. K. (2010). Oxidation enhances myofibrillar protein degradation via calpain and caspase-3. *Free Radical Biology and Medicine*, *49*(7), 1152–1160.

Soleimani, V. D., Yin, H., Jahani-Asl, A., Ming, H., Kockx, C. E. M., van Ijcken, W. F. J., … Rudnicki, M. A. (2012). Snail Regulates MyoD Binding-Site Occupancy to Direct Enhancer Switching and Differentiation-Specific Transcription in Myogenesis. *Molecular Cell*, *47*(3), 457–468.

Song, H., Liu, S., Li, C., Geng, Y., Wang, G., & Gu, Z. (2014). Pluronic L64-mediated stable hIF-1α expression in muscle for therapeutic angiogenesis in mouse hindlimb ischemia. *International Journal of Nanomedicine*, *9*, 3439–3452.

Soriano, F. X., Liesa, M., Bach, D., Chan, D. C., Palacín, M., & Zorzano, A. (2006). Evidence for a mitochondrial regulatory pathway defined by peroxisome proliferator-activated receptor-gamma coactivator-1 alpha, estrogen-related receptor-alpha, and mitofusin 2. *Diabetes*, *55*(6), 1783–1791.

Spangenburg, E. E., & Booth, F. W. (2003). Molecular regulation of individual skeletal muscle fibre types. *Acta Physiol Scand*, *178*, 413–424. Retrieved from

Stemmler, M. P., Eccles, R. L., Brabletz, S., & Brabletz, T. (2019). Non-redundant functions of EMT transcription factors. *Nature Cell Biology*, *21*(1), 102–112.

Su, L., Luo, Y., Yang, Z., Yang, J., Yao, C., Cheng, F., … Qian, C. (2016). MEF2D Transduces Microenvironment Stimuli to ZEB1 to Promote Epithelial-Mesenchymal Transition and Metastasis in Colorectal Cancer. *Cancer Research*, *76*(17), 5054–5067.

Sun, Z., Chin, Y. E., & Zhang, D. D. (2009). Acetylation of Nrf2 by p300/CBP Augments Promoter-Specific DNA Binding of Nrf2 during the Antioxidant Response. *Molecular and cellular biology*, *29*(10), 2658–2672.

Takagi, T., Moribe, H., Kondoh, H., & Higashi, Y. (1998). DeltaEF1, a zinc finger and homeodomain transcription factor, is required for skeleton patterning in multiple lineages. *Development*, *125*, 21–31.

Talbert, E. E., Smuder, A. J., Min, K., Kwon, O. S., Szeto, H. H., & Powers, S. K. (2013). Immobilization-induced activation of key proteolytic systems in skeletal muscles is prevented by a mitochondria-targeted antioxidant. *Journal of Applied Physiology*, *115*(4), 529–538.

Terry, E. E., Zhang, X., Hoffmann, C., Hughes, L. D., Lewis, S. A., Li, J., … Hughes, M. E. (2018). Transcriptional profiling reveals extraordinary diversity among skeletal muscle tissues. *ELife*, *7*.

Tintignac, L. A., Lagirand, J., Batonnet, S., Sirri, V., Leibovitch, M. P., & Leibovitch, S. A. (2005). Degradation of MyoD Mediated by the SCF (MAFbx) Ubiquitin Ligase. *Journal of Biological Chemistry*, *280*(4), 2847–2856.

Touvier, T., De Palma, C., Rigamonti, E., Scagliola, A., Incerti, E., Mazelin, L., … Brunelli, S. (2015). Muscle-specific Drp1 overexpression impairs skeletal muscle growth via translational attenuation. *Cell Death and Disease*, *6*, e1663.

Twig, G., Elorza, A., Molina, A. J., Mohamed, H., Wikstrom, J. D., Walzer, G., …

Shirihai, O. S. (2008). Fission and selective fusion govern mitochondrial segregation and elimination by autophagy. *The EMBO Journal*, *27*, 433–446.

van der Vos, K. E., Eliasson, P., Proikas-Cezanne, T., Vervoort, S. J., van Boxtel, R., Putker, M., … Coffer, P. J. (2012). Modulation of glutamine metabolism by the PI(3)K–PKB–FOXO network regulates autophagy. *Nature Cell Biology*, *14*(8), 829–837.

Vandewalle, C., Van Roy, F., & Berx, G. (2009). The role of the ZEB family of transcription factors in development and disease. *Cell Mol Life Sci*, *66*, 773–787.

Virbasius, J. V, & Scarpulla, R. C. (1994). Activation of the human mitochondrial transcription factor A gene by nuclear respiratory factors: A potential regulatory link between nuclear and mitochondrial gene expression in organelle biogenesis. In *Proc. Nati. Acad. Sci. USA* (Vol. 91).

Weintraub, H., Tapscott, S. J., Davis, R. L., Thayer, M. J., Adam, M. A., Lassar, A. B., & Miller, A. D. (1989). Activation of muscle-specific genes in pigment, nerve, fat, liver, and fibroblast cell lines by forced expression of MyoD. *Proceedings of the National Academy of Sciences of the United States of America*, *86*(14), 5434–5438.

Yoon, J. C., Ng, A., Kim, B. H., Bianco, A., Xavier, R. J., & Elledge, S. J. (2010). Wnt signaling regulates mitochondrial physiology and insulin sensitivity. *Genes & Development*, *24*(14), 1507–1518.

Zhao, J., Brault, J. J., Schild, A., Cao, P., Sandri, M., Schiaffino, S., … Goldberg, A. L. (2007). FoxO3 Coordinately Activates Protein Degradation by the Autophagic/Lysosomal and Proteasomal Pathways in Atrophying Muscle Cells. *Cell Metabolism*, *6*(6), 472–483.

Zickermann, V., Kerscher, S., Zwicker, K., Tocilescu, M. A., Radermacher, M., & Brandt, U. (2009). Architecture of complex I and its implications for electron transfer and proton pumping. *Biochimica et Biophysica Acta (BBA) - Bioenergetics*, *1787*(6), 574–583.

APPENDIX I

The data presented in Chapter I of this dissertation resulted in the publication of the following article:

- **Ninfali, C.,** Siles, L., Darling, D. S., & Postigo, A. (2018). Regulation of muscle atrophy-related genes by the opposing transcriptional activities of ZEB1/CtBP and FOXO3. *Nucleic Acids Research*, *46*(20), 10697–10708.

Published online 10 October 2018 *Nucleic Acids Research, 2018, Vol. 46, No. 20* ***10697–10708***
doi: 10.1093/nar/gky835

Regulation of muscle atrophy-related genes by the opposing transcriptional activities of ZEB1/CtBP and FOXO3

Chiara Ninfali[1], Laura Siles[1], Douglas S. Darling[2] and Antonio Postigo[1,3,4,*]

[1]Group of Transcriptional Regulation of Gene Expression, Department of Oncology and Hematology, IDIBAPS, Barcelona 08036, Spain, [2]Center for Genetics and Molecular Medicine and Department of Immunology and Infectious Diseases, University of Louisville, Louisville, KY 40202, USA, [3]Molecular Targets Program, James G. Brown Cancer Center, Louisville, KY 40202, USA and [4]ICREA, Barcelona 08010, Spain

Received May 31, 2018; Revised September 05, 2018; Editorial Decision September 06, 2018; Accepted October 09, 2018

ABSTRACT

Multiple physiopathological and clinical conditions trigger skeletal muscle atrophy through the induction of a group of proteins (atrogenes) that includes components of the ubiquitin–proteasome and autophagy-lysosomal systems. Atrogenes are induced by FOXO transcription factors, but their regulation is still not fully understood. Here, we showed that the transcription factor ZEB1, best known for promoting tumor progression, inhibits muscle atrophy and atrogene expression by antagonizing FOXO3-mediated induction of atrogenes. Compared to wild-type counterparts, hindlimb immobilization in *Zeb1*-deficient mice resulted in enhanced muscle atrophy and higher expression of a number of atrogenes, including Atrogin-1/*Fbxo32*, MuRF1/*Trim63*, *Ctsl, 4ebp1*, *Gabarapl1, Psma1* and *Nrf2.* Likewise, in the C2C12 myogenic cell model, ZEB1 knockdown augmented both myotube diameter reduction and atrogene upregulation in response to nutrient deprivation. Mechanistically, ZEB1 directly represses *in vitro* and *in vivo Fbxo32* and *Trim63* promoter transcription in a stage-dependent manner and in a reverse pattern with MYOD1. ZEB1 bound to the *Fbxo32* promoter in undifferentiated myoblasts and atrophic myotubes, but not in non-atrophic myotubes, where it is displaced by MYOD1. ZEB1 repressed both promoters through CtBP-mediated inhibition of FOXO3 transcriptional activity. These results set ZEB1 as a new target in therapeutic approaches to clinical conditions causing muscle mass loss.

INTRODUCTION

Under homeostatic conditions, skeletal muscle maintains a balance between protein synthesis and proteolysis by finely tuning hypertrophic and atrophic signals (reviewed in 1-3). Multiple physiopathological and clinical conditions (e.g. immobilization, aging, denervation) result in skeletal muscle atrophy, a reduction in muscle mass and in the cross-sectional area (CSA) of myofibers.

Ultimately, muscle atrophy is mediated by a number of genes collectively referred as 'atrogenes' and that includes members of the ubiquitin–proteasome and the autophagy-lysosomal systems (4–9). Most sarcomeric proteins are degraded by the ubiquitin–proteasome pathway; E3 ubiquitin ligases bind to their substrates and catalyze the transfer of ubiquitin from the E2 enzyme targeting proteins for subsequent degradation by the 26S proteasome (10,11). In turn, organelles, particularly mitochondria, are degraded by proteasomal degradation and autophagy (12,13). The two archetypal atrogene proteins whose expression increases the strongest during muscle atrophy are the E3 ubiquitin ligases Atrogin-1 (also known as MAFbx and encoded by the gene *Fbxo32*) and MuRF1 (encoded by *Trim63*) (4). *Fbxo32* (-/-) and *Trim63* (-/-) mice exhibit reduced muscle sparing in response to atrophy-inducing experimental protocols (4). Atrogin-1 and MuRF1 expression is directly activated by O-type forkhead transcription factors (FOXO), chiefly by FOXO3 (2,9,14). FOXO3 also activates atrogenes involved in the autophagy-dependent clearance of organelles (9,12,13). Nevertheless, the transcriptional mechanisms regulating the expression of Atrogin-1, MuRF1 and other atrogenes are not completely understood. Surprisingly, we found here that the transcription factor ZEB1 inhibits atrogene expression and muscle atrophy in a stage-dependent manner through repression of FOXO3 transcriptional activity.

Although ZEB1 is best known for promoting tumor progression by triggering an epithelial-to-mesenchymal tran-

*To whom correspondence should be addressed. Fax: +34 93 451 5272; Email: idib412@clinic.cat

© The Author(s) 2018. Published by Oxford University Press on behalf of Nucleic Acids Research.
This is an Open Access article distributed under the terms of the Creative Commons Attribution License (http://creativecommons.org/licenses/by/4.0/), which permits unrestricted reuse, distribution, and reproduction in any medium, provided the original work is properly cited.

10698 *Nucleic Acids Research, 2018, Vol. 46, No. 20*

sition (EMT) in cancer cells (15–17), it also plays important roles in embryogenesis—*Zeb1* (-/-) mice die before birth—and cell differentiation (18,19). ZEB1 is expressed in the primary myotome, where the first muscle progenitors arise (18), and imposes a stage-dependent inhibition of muscle differentiation, so *Zeb1* (-/-) and *Zeb1* (+/-) embryos display premature expression of adult muscle differentiation genes (20,21). Both mutation and overexpression of ZEB1's ortholog in *Drosophila* (zfh-1) disrupt somatic musculature (21,22). However, the expression and role of ZEB1 in muscle atrophy have not been explored. ZEB1 is induced by multiple signaling pathways whose activity and gene targets it modulates positively or negatively by recruitment of transcriptional co-activators (e.g. p300) or co-repressors (e.g. CtBP) (15,16,23–27).

Here, we showed that, compared to wild-type counterparts, hindlimb immobilization in *Zeb1* (+/-) mice resulted in enhanced muscle atrophy and higher expression of a number of atrogenes, including *Fbxo32*, *Trim63*, *Ctsl, 4ebp1*, *Gabarapl1, Psma1* and *Nrf2.* Likewise, in the C2C12 myogenic cell model, ZEB1 knockdown amplified both myotube diameter reduction and atrogene upregulation in response to nutrient deprivation. We identified ZEB1-binding sites in the regulatory regions of *Fbxo32* and *Trim63* and confirmed its direct binding and repression of these promoters in a stage-dependent manner and in a reverse pattern with MYOD1. ZEB1 bound to the *Fbxo32* promoter in undifferentiated myoblasts and atrophic myotubes, but not in non-atrophic myotubes where it is displaced by MYOD1. ZEB1-dependent repression of the *Fbxo32* promoter in atrophic muscles was also validated *in vivo* by bioluminescence imaging. Mechanistically, ZEB1 repressed atrogene expression through CtBP-dependent inhibition of the transcriptional activity of FOXO3.

The data presented here indicate that ZEB1 limits unrestrained muscle atrophy and atrogene overexpression in response to atrophic-inducing stimuli, thus offering a new target in therapeutic approaches to physiopathological and clinical conditions dealing with muscle mass loss.

MATERIALS AND METHODS

Mouse samples

The use of mouse models in this study was approved by Animal Experimentation Ethics Committee of the University of Barcelona under protocol number DAAM 8563. The source of mouse models used in the study, the hindlimb immobilization protocol and the *in vivo* analysis of atrogene promoter activity are detailed in Supplementary Data.

Cell lines and cell culture

C2C12 and 293T cell lines were obtained from the American Type Culture Collection (ATCC)-LGC Standards (Middlesex, England, UK). The culture conditions for myotube differentiation and starvation are detailed in Supplementary Data.

Antibodies, and DNA and RNA oligonucleotides

The antibodies used in western blot, and in the immunostaining of mouse muscle samples and C2C12 myotubes are detailed in Supplementary Data. DNA oligonucleotides used as primers in quantitative real-time polymerase chain reaction (qRT-PCR) are listed in the Supplementary Data. Lastly, RNA oligonucleotides used in RNA interference are described in the Supplementary Data.

Gene and protein expression

RNA extraction and subsequent analysis of gene expression by qRT-PCR, and transcriptional studies by luciferase reporter assays are described in Supplementary Data. Analysis of protein expression in mouse tissue samples and C2C12 myotubes as well as myofibers' CSA analysis of muscle sections are described in Supplementary Data.

Statistical analysis

Statistical analysis of data shown was performed using GraphPad Prism for Mac version 5.0a (GraphPad Software Inc., La Jolla, CA, USA). Normal distribution of the data was determined with Kolmogorov–Smirnov test. Statistical significance of the normally distributed data was assessed with a *t*-test and with a non-parametric Mann–Whitney *U* test for those with non-normal distribution. Error bars in histograms represent standard errors of means. Relevant comparisons were labeled as either significant at the $P \leq 0.001$ (***), $P \leq 0.01$ (**) or $P \leq 0.05$ (*) levels, or non-significant (ns) for values of $P > 0.05$.

RESULTS

ZEB1 protects skeletal muscle from sparing upon immobilization

To investigate a potential role of ZEB1 in muscle atrophy, we first examined whether its downregulation has an effect on muscle mass loss in response to immobilization. Two-to-three month-old wild-type and *Zeb1* (+/-) mice were subjected to unilateral hindlimb immobilization for up to 17 days and the weight of both gastrocnemius muscles, from the immobilized and non-immobilized hindlimbs, was assessed over time. As expected, and with respect to the control non-immobilized counterpart, gastrocnemius muscles in the immobilized hindlimb displayed a progressive weight loss (Figure 1A and B). Notably, muscle sparing by immobilization was larger in *Zeb1* (+/-) mice than in wild-type mice (Figure 1A and B). These data indicate that ZEB1 expression protects skeletal muscle from an otherwise excessive atrophy in response to immobilization.

Muscle weight loss during muscle atrophy is accompanied by an increase in the number of smaller size myofibers and a decrease of larger ones (4). Staining with hematoxylin/eosin, and immunofluorescence staining for the structural protein laminin revealed a smaller size in the myofibers of immobilized *Zeb1* (+/-) gastrocnemius muscles compared to wild-type counterparts (Figure 1C and D; Supplementary Figure S1A). Fiber CSA analysis confirmed that upon immobilization *Zeb1* (+/-) muscles contained a larger share of fibers $<800\ \mu m^2$ and a lower share of fibers of $800\ \mu m^2$ or more than wild-type muscles (Figure 1E and Supplementary Figure S1B-D).

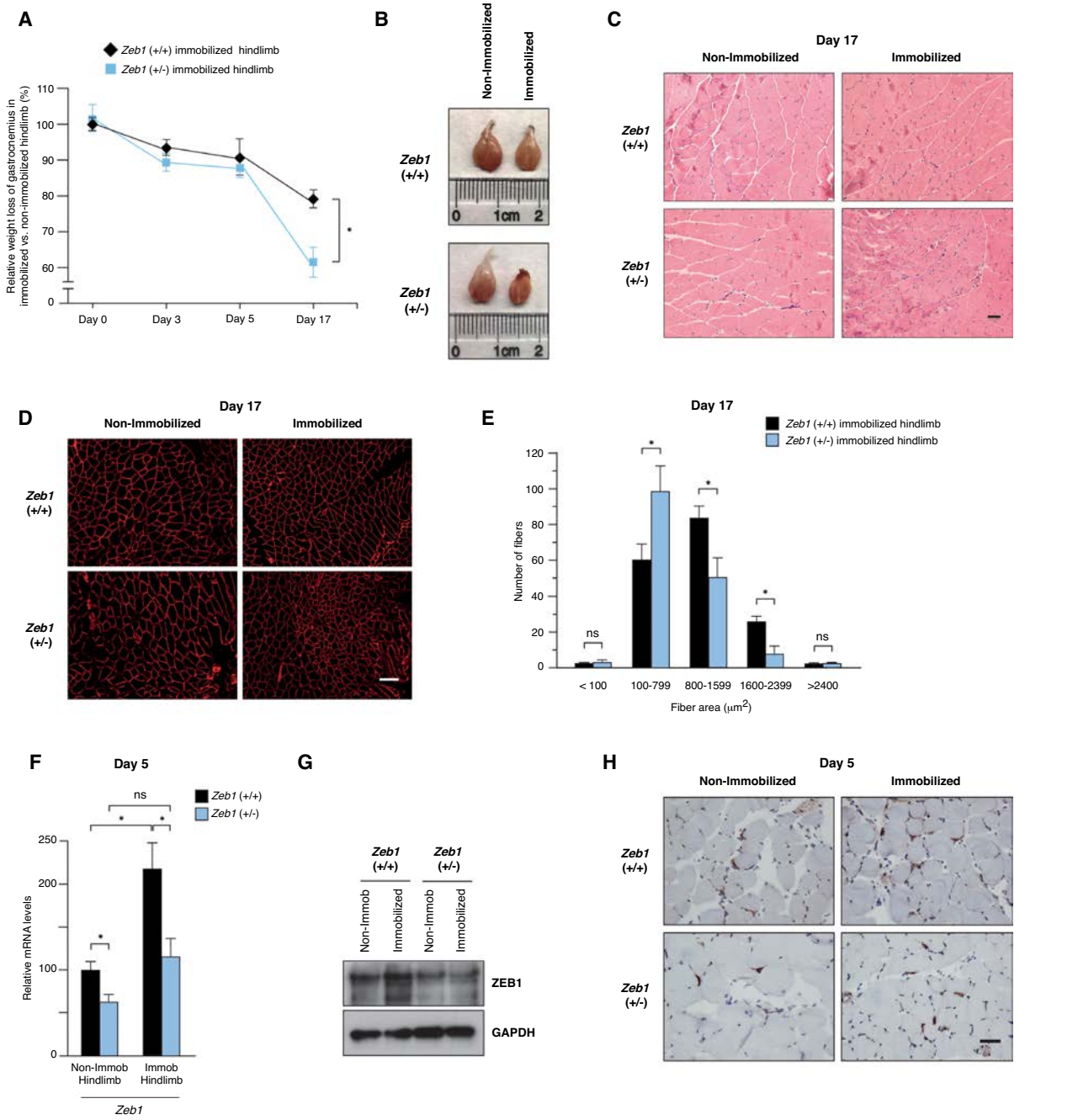

Figure 1. ZEB1 protects skeletal muscle from sparing upon immobilization. (**A**) Two-to-three-month old wild-type and *Zeb1* (+/-) mice were subjected to unilateral hindlimb immobilization for different periods as described in Supplementary Data. At each time point, mice were euthanized and the weight of their immobilized gastrocnemius muscles was assessed with respect to that in the contralateral non-immobilized hindlimb. The weight of the gastrocnemius in the immobilized hindlimb *vis-à-vis* that in the non-immobilized at the start of the protocol (day 0) was set arbitrarily to 100. At least five mice of each genotype were examined. (**B**) As in (A), representative images of non-immobilized and immobilized gastrocnemius muscles from wild-type and *Zeb1* (+/-) mice at day 17 of the immobilization protocol. (**C**) Wild-type and *Zeb1* (+/-) mice were subjected to unilateral hindlimb immobilization during 17 days as in (A), euthanized and their gastrocnemius muscles stained for hematoxylin/eosin. Scale bar: 50 μm. (**D**) As in (C), but sections were stained with an antibody against laminin (clone 48H-2). Scale bar: 100 μm. (**E**) Myofiber cross-sectional analysis in the immobilized gastrocnemius of wild-type and *Zeb1* (+/-) mice at day 17 of the immobilization protocol. Myofiber area was assessed as described in Supplementary Data. A total of 160 myofibers were measured from at least eight mice, half from each genotype. (**F**) *Zeb1* expression slightly increases upon immobilization. Wild-type and *Zeb1* (+/-) mice were subjected to unilateral hindlimb immobilization during 5 days. At that time, mice were euthanized and *Zeb1* messenger RNA (mRNA) levels were assessed in the immobilized and non-immobilized gastrocnemius by qRT-PCR using *Gapdh* as reference gene. The results are the mean with standard error of at least five mice for each genotype and condition. (**G**) As in (F), but ZEB1 expression was assessed at the protein level by Western blot. Gastrocnemius muscle lysates were blotted for ZEB1 (clone HPA027524) along with GAPDH (clone 14C10) as loading control. See Supplementary Figure S1E for full unedited blots. The blots shown are a representative of three independent experiments. (**H**) As in (F), but the ZEB1 expression was assessed by immunohistochemistry (clone H102) at day 5. Captures are representative of at least five mice for each genotype and condition. Scale bar: 40 μm.

10700 *Nucleic Acids Research, 2018, Vol. 46, No. 20*

Next, we examined whether ZEB1 expression is modulated during hindlimb immobilization. Immobilization resulted in a slight increase in ZEB1 messenger RNA (mRNA) and protein (Figure 1F and G; Supplementary Figure S1E). ZEB1 was expressed at the nuclei of some myofibers (Figure 1H and Supplementary Figure S1F) and the number of ZEB1$^+$ nuclei in gastrocnemius muscles from both genotypes was similar in the immobilized and non-immobilized hindlimbs (Supplementary Figure S1G).

ZEB1 inhibits the *in vivo* expression of atrogenes

We next investigated whether ZEB1 regulates the expression of atrogenes. Although muscle weight loss in response to immobilization progressively increases over time, expression of Atrogin-1 and MuRF1 peaks at around day 3 post-immobilization and declines afterward (4).

Wild-type and *Zeb1* (+/-) mice were subjected to unilateral hindlimb immobilization and their gastrocnemius muscles examined for Atrogin-1/*Fbxo32* mRNA and protein expression. Levels of Atrogin-1/*Fbxo32* expression were similar between the non-immobilized gastrocnemius muscles from both genotypes (Figure 2A and B). However, its induction upon immobilization was larger in *Zeb1* (+/-) muscles (Figure 2A and B; Supplementary Figure S2A). A similar pattern was observed for MuRF1/*Trim63*; non-immobilized gastrocnemius muscles from both genotypes expressed equivalent levels of this atrogene, but immobilization induced higher *Trim63* mRNA and MuRF1 protein levels in *Zeb1* (+/-) gastrocnemius muscles than in wild-type counterparts (Figure 2C and D; Supplementary Figure S2B). Altogether, these results indicate that ZEB1 inhibits Atrogin-1/*Fbxo32* and MuRF1/*Trim63* expression *in vivo.*

Atrogin-1 and MuRF1 are the archetypal atrogenes, but many other genes are induced during muscle atrophy (6–8). The set of atrogenes upregulated in response to different atrophy-inducing conditions is largely, although not completely, overlapping (7,8). We tested whether ZEB1 regulates some of these other atrogenes. The immobilized and non-immobilized gastrocnemius of wild-type and *Zeb1* (+/-) mice were examined for the expression of atrogenes involved in different cellular processes, namely, proteasome system [proteasome subunit, alpha type 1 (*Psma1*)], autophagy [Cathepsin L (*Ctsl*), GABA A-receptor associated protein-like 1 (*Gabarapl1*)], protein synthesis [eukaryotic translation initiation factor 4E binding protein 1 (*4ebp1*)] and oxidative stress [nuclear factor E2 related factor 2 (*Nrf2*)]. Although with different temporal patterns and at lower levels than in the case of *Fbxo32* and *Trim63*, expression of these atrogenes increased in immobilized wild-type gastrocnemius but, as for *Fbxo32* and *Trim63,* their induction was higher in *Zeb1* (+/-) muscles (Figure 2E). Altogether, these results indicate that atrogenes are under negative regulation by ZEB1 whose expression prevents unrestricted atrogene overexpression in response to immobilization.

ZEB1 inhibits atrogene expression and size reduction in starved C2C12 myotubes

We sought to confirm the role of ZEB1 in muscle atrophy using the C2C12 cell myogenic model, which has been widely employed to study gene expression during both muscle differentiation and atrophy (14,28,29). When grown in high serum (thereafter referred as growth medium), C2C12 cells maintain a proliferating myoblast-like phenotype (see scheme in Supplementary Figure S3A). Only when cells exit the cell cycle upon reaching confluence and are switched into a low-serum medium (differentiation medium) they fuse and form terminally differentiated multinucleated myotubes (28,29). When C2C12 myotubes are starved of serum, glucose and amino acids (atrophic medium), they undergo a rapid reduction in their mean myotube diameter (14).

At days 3 and 4 of their differentiation, C2C12 myotubes were transfected with either an siRNA control (siCtrl) or any of two siRNA sequences previously validated to specifically knock down *Zeb1* (si*Zeb1*-A, si*Zeb1*-B) (21) (Figure 3A and Supplementary Figure S3B). At day 5, the differentiation medium was replaced by atrophic medium for up to 8 h (Figure 3A). In line with our *in vivo* results above, the diameter reduction induced by the atrophic medium was larger in C2C12 myotubes that had been knocked down for *Zeb1* (Figure 3B and C). Likewise, *Zeb1* mRNA and protein expression slightly increased when C2C12 myotubes were cultured in atrophic medium (Figure 3D and E; Supplementary Figure S3C). Altogether, these data indicate that ZEB1 inhibits muscle atrophy both *in vivo* and in the C2C12 cell model.

The inhibition of atrogenes by ZEB1 was also examined in the C2C12 model. In line with the results above, and compared to C2C12 atrophic myotubes interfered with siCtrl, knockdown of *Zeb1* resulted in higher mRNA and protein levels of Atrogin-1/*Fbxo32* and MuRF1/*Trim63* (Figure 3F–H; Supplementary Figure S3D and E).

Stage-dependent binding and repression of the *Fbxo32* promoter by ZEB1

Expression of most atrogenes is activated by transcription factors of the *Forkhead box O* (Foxo) family (e.g. FOXO1, FOXO3 and FOXO4) (9,12–14). FOXO3 triggers muscle atrophy through protein degradation via activation of the ubiquitin–proteasome system as well as via autophagy-dependent clearance of organelles (1,2,12–14). The regulatory regions of many atrogenes contain multiple binding sites for FOXO proteins and, accordingly, progressively larger fragments of the *Fbxo32* promoter—that contain an increasing number of FOXO3-binding sites—displayed a parallel larger activation in response to FOXO3 overexpression (Supplementary Figure S4A).

ZEB1 regulates gene expression by binding to E-box and E-box-like sequences (CANNTG) in the regulatory regions of its target genes (30,31). Analysis of the *Fbxo32* and *Trim63* promoters revealed the existence of several consensus binding sites for ZEB1, particularly in the former where many FOXO3 consensus sites are located in close proximity to ZEB1's (Figure 4A). ZEB1 and MYOD1 partially overlap in their DNA sequence recognition (30–32), with ZEB1 repressing key muscle differentiation genes in a reverse temporal pattern *vis-à-vis* MYOD1 (20,21). Thus, during the myoblast stage, ZEB1 binds to E-boxes in the promoters of differentiation genes and represses their transcription, but,

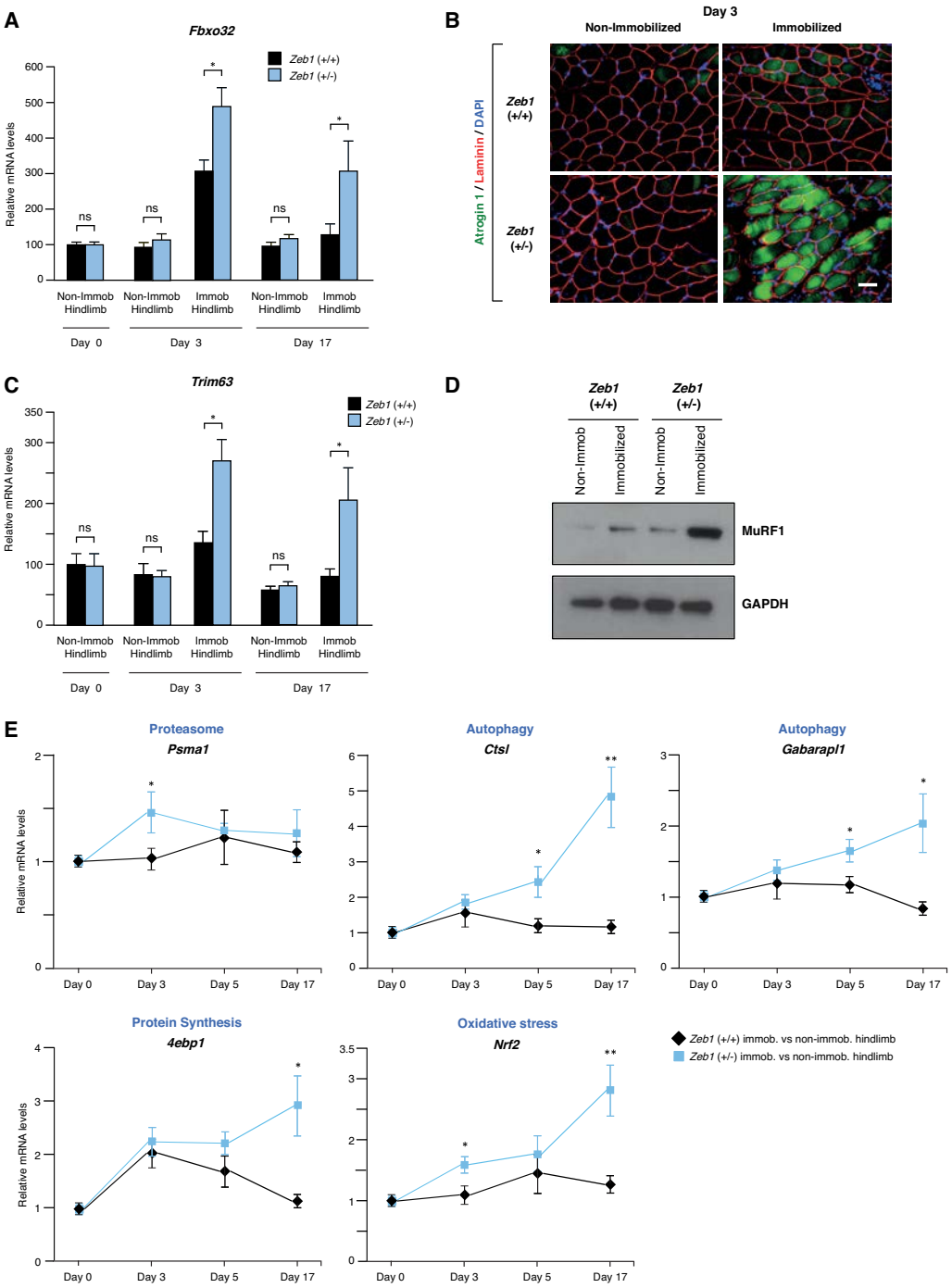

Figure 2. *Zeb1* inhibits the *in vivo* induction of atrogenes upon immobilization. (**A**) Wild-type and *Zeb1* (+/-) mice were subjected to unilateral hindlimb immobilization during 3 and 17 days and their immobilized and non-immobilized gastrocnemius were then examined for *Fbxo32* mRNA expression by qRT-PCR with respect to *Gapdh*. *Fbxo32* mRNA levels in the non-immobilized hindlimb at day 0 were arbitrarily set to 100 with all other data genotypes and conditions referred to them. Data represent the mean of at least five mice for each genotype and condition. (**B**) The gastrocnemius of mice from both genotypes after 3 days of the unilateral hindlimb immobilization protocol were stained with antibodies against Atrogin-1 (clone AP2041) and laminin (clone 48H-2), and counterstained for 4′,6-diamidino-2-phenylindole (DAPI) for nuclear staining. Captures for single immunostaining are shown in Supplementary Figure S2A. Scale bar: 50 μm. (**C**) As in (A), but for *Trim63*. (**D**) As in (B), but the lysates from gastrocnemius of mice from both genotypes after 3 days of the unilateral hindlimb immobilization protocol were blotted for MuRF1 (clone C11) along with GAPDH (clone 14C10) as loading control. See Supplementary Figure S2B for full unedited blots. The blots shown are representative of three independent experiments. (**E**) Wild-type and *Zeb1* (+/-) mice were subjected to the unilateral hindlimb immobilization protocol for 3, 5 and 17 days. At the end of each time point, they were euthanized and mRNA levels for *Psma1, Ctsl, Gabarapl1, 4ebp1* and *Nrf2* were assessed by qRT-PCR. For each gene, mRNA levels shown correspond to that in the gastrocnemius of the immobilized with respect to the contralateral non-immobilized hindlimb. The gene expression in the non-immobilized gastrocnemius at days 3, 5 and 17 was similar than that at day 0 shown. At least five mice from each genotype and day were analyzed.

10702 *Nucleic Acids Research, 2018, Vol. 46, No. 20*

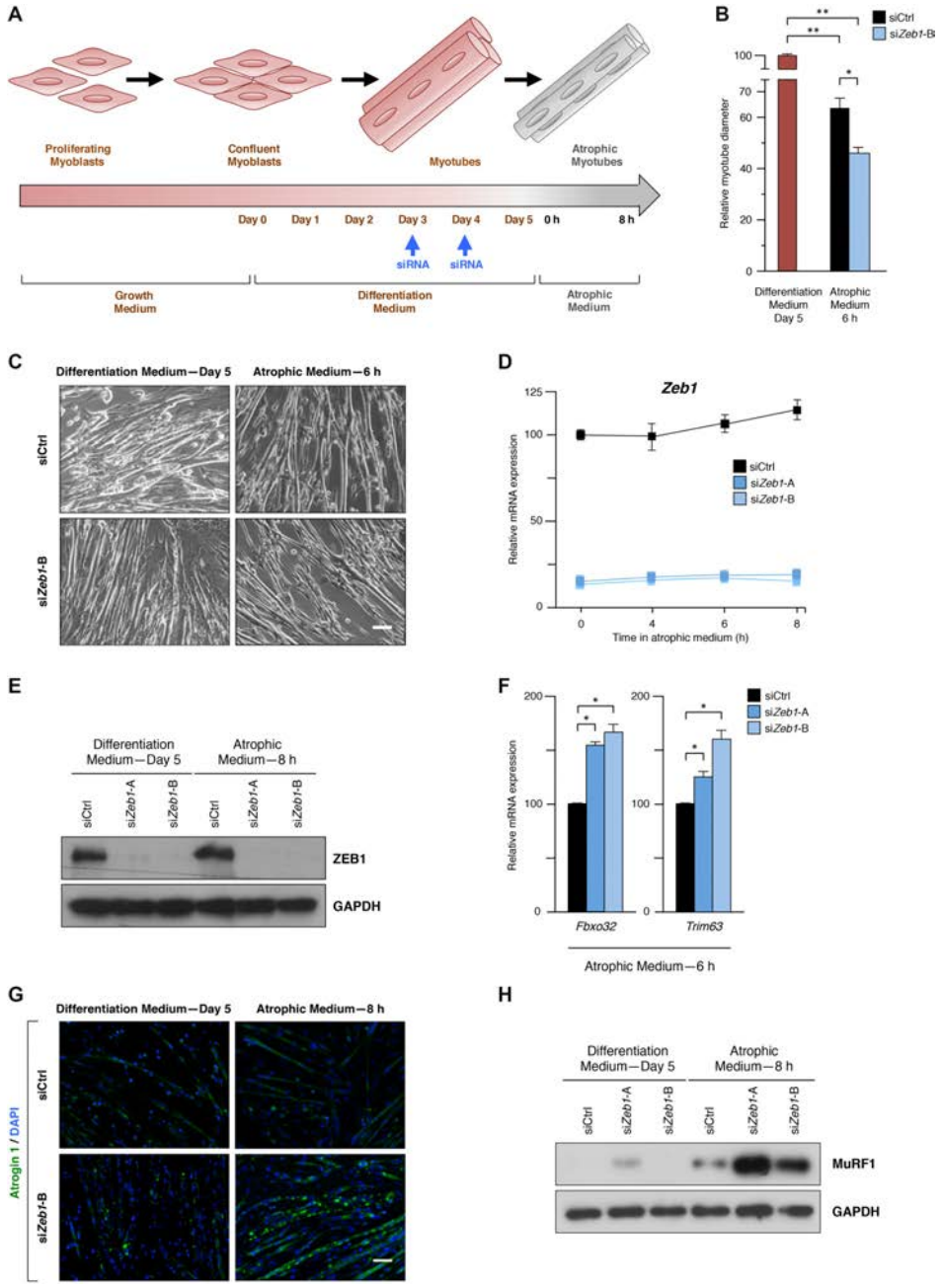

Figure 3. ZEB1 inhibits atrogene expression and size reduction in starved C2C12 myotubes. (**A**) Scheme of the starvation-induced atrophy protocol in C2C12 myotubes. C2C12 myotubes were transfected with siCtrl or any of two siRNA sequences previously validated to specifically knock down *Zeb1* (see Supplementary Figure S3B and C) and their differentiation medium was replaced by atrophic medium for up to 8 h. (**B**) The diameter of C2C12 myotubes subjected to the protocol in (A) was assessed as described in Supplementary Data. Myotube diameter in differentiation medium at day 5 was arbitrarily set at 100. Data represent the average of at least three experiments. (**C**) As in (B), representative captures of C2C12 myotubes transfected with siCtrl or si*Zeb1*-B following incubation in differentiation medium or atrophy medium. Scale bar: 50 μm. (**D**) *Zeb1* mRNA levels in C2C12 myotubes interfered with siCtrl, si*Zeb1*-A or si*Zeb1*-B and cultured in atrophic medium for the indicated periods were assessed by qRT-PCR with respect to *Gapdh*. *Zeb1* expression in cells interfered with siCtrl at 0 h of atrophic medium was arbitrarily set to 100. Data are representative of four independent experiments. (**E**) As in (C), lysates from C2C12 non-atrophic and atrophic myotubes were assessed by Western blot for ZEB1 expression (clone HPA027524) along with GAPDH (clone 14C10) as loading control. See Supplementary Figure S3C full unedited blots. The blots shown are a representative of four independent experiments. (**F**) As in (A), C2C12 myotubes were interfered with siCtrl, si*Zeb1*-A or si*Zeb1*-B and transferred to atrophy medium. Expression of *Fbxo32* and *Trim63* was assessed by qRT-PCR using *Gapdh* as reference gene. Data represent the average of at least three independent experiments. (**G**) As in (C), but C2C12 non-atrophic and atrophic myotubes were stained for Atrogin-1 (clone AP2041) along with DAPI for nuclear staining. See Supplementary Figure S3D for individual staining. Pictures shown are representative of three independent experiments. Scale bar: 50 μm. (**H**) As in (C), lysates from C2C12 non-atrophic and atrophic myotubes were assessed for MuRF1 expression (clone C11) along with GAPDH (clone 14C10) as loading control. See Supplementary Figure S3E for knockdown of ZEB1 (clone HPA027524) and full unedited blots of the three antibodies. The blots shown are representative of four independent experiments.

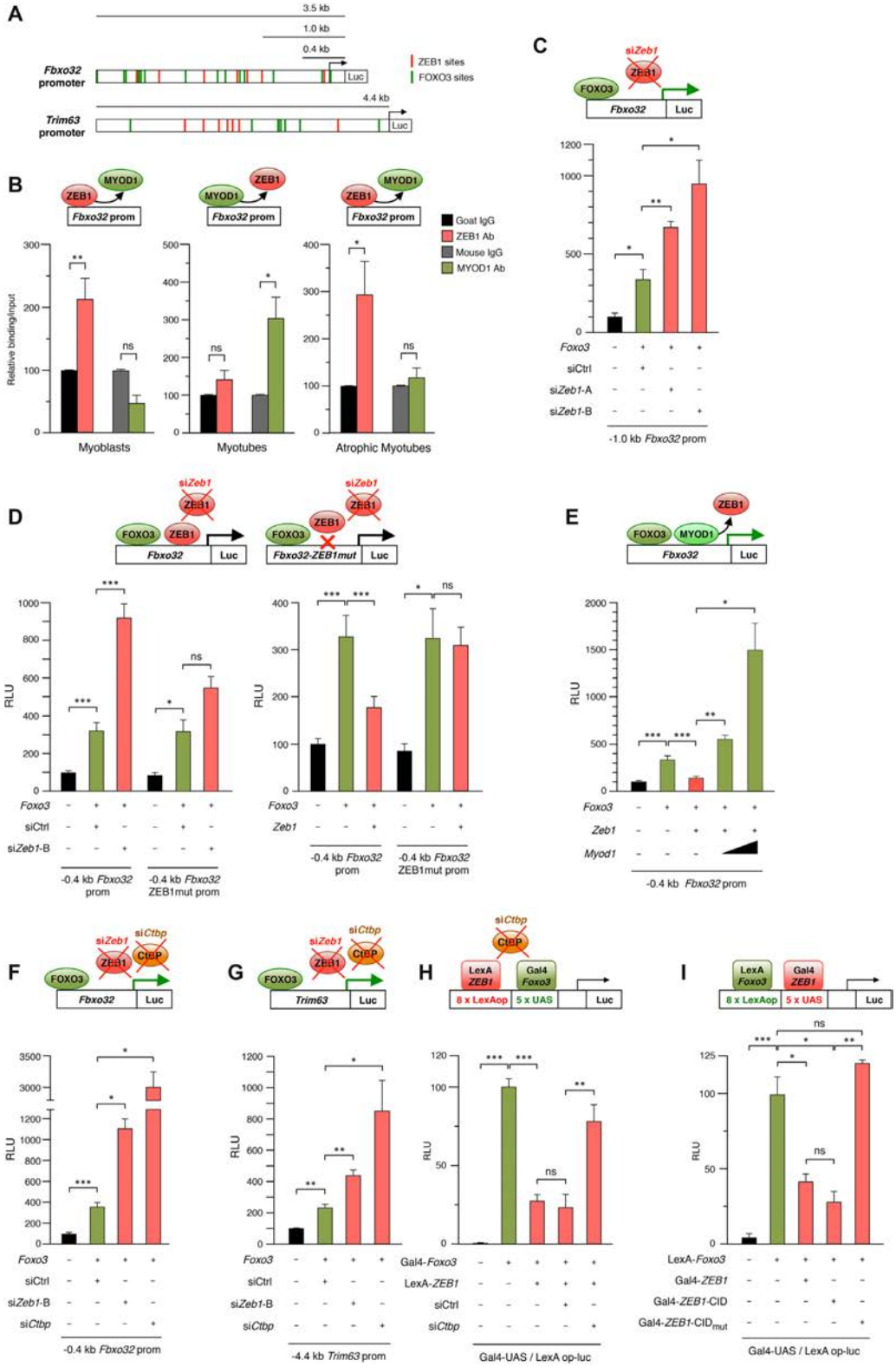

Figure 4. Stage-dependent inhibition of the *Fbxo32* and *Trim63* promoters by ZEB1 is mediated by CtBP-dependent repression of FOXO3 transcriptional activity. (**A**) Schematic representation of the consensus sites for ZEB1 (red boxes) and FOXO3 (green boxes) in the first 3.5 kb and 4.4 kb of the mouse *Fbxo32* and *Trim63* promoters, respectively. Consensus binding sequences for ZEB1 in the *Fbxo32* promoter were identified at –2899 bp, –2584 bp, –1894 bp, –1395 bp, –1254 bp, –1011 bp, and –85 bp. Consensus binding sites for ZEB1 in the Trim63 promoter were identified at –4488 bp, –4444 bp, –3078 bp, –2792 bp, –2566 bp, –2416 bp, –2358 bp, –2254 bp, and –777 bp. Consensus binding sites for FOXO3 in *Fbxo32* and *Trim63* promoters were

as differentiation proceeds, MYOD1 accumulates and displaces ZEB1 from these E-boxes (20,21).

To investigate whether ZEB1 regulation of *Fbxo32* involves direct binding to its promoter, we examined ZEB1's capacity to bind to a consensus binding site located at −85 bp of the *Fbxo32* promoter in myoblasts, myotubes and atrophic myotubes. Interestingly, we found that in myoblasts and atrophic myotubes, but not in non-atrophic myotubes, an anti-ZEB1 antibody—but not its specie-matched IgG control—immunoprecipitated a fragment of the *Fbxo32* promoter containing the −85 bp binding site (Figure 4B). This stage-specific binding of ZEB1 to the *Fbxo32* promoter was reversely mirrored by the pattern of binding of MYOD1; an anti-MYOD1 antibody—but not its respective IgG control—immunoprecipitated the *Fbxo32* promoter in myotubes, but not in atrophic myotubes or in myoblasts.

We next examined the transcriptional activity of the *Fbxo32* promoter following either the knockdown or overexpression of *Zeb1*. C2C12 cells were transfected with 0.4 and 1.0 kb fragments of *Fbxo32* promoter fused to luciferase along with an expression vector for FOXO3 to induce its transcription. As expected, FOXO3 activated both *Fbxo32* promoter reporters (Figure 4C and D). Compared to siCtrl, si*Zeb1*-A and si*Zeb1*-B further increased FOXO3-mediated induction of the *Fbxo32* promoter (Figure 4C and left panel of Figure 4D), indicating that the *Fbxo32* promoter is under negative transcriptional regulation by endogenous ZEB1. In turn, exogenous overexpression of *Zeb1* downregulated FOXO3-mediated induction of the *Fbxo32* promoter luciferase reporter (Figure 4D, right panel). When *Foxo3* was knocked down with a specific siRNA, overexpression of *Zeb1* had no significant effect on the transcriptional activity of the 0.4 kb *Fbxo32* promoter reporter (Supplementary Figure S4B and C). Mutation of the ZEB1-binding site at the −85 bp site in the context of the 0.4 kb *Fbxo32* luciferase reporter to a sequence known not to bind ZEB1 reduced the effect of both *Zeb1* knockdown and *Zeb1* overexpression on *Fbxo32* transcription (Figure 4D). ZEB1-mediated repression of the 0.4 kb *Fbxo32* promoter reporter was also reverted by overexpression of MYOD1 (Figure 4E).

ZEB1 inhibits *Fbxo32* and *Trim63* promoters through CtBP-dependent repression of FOXO3 transcriptional activity

ZEB1 represses transcription of its target genes by recruitment of non-DNA binding transcriptional co-repressors, chiefly of CtBP (21,25,27,33, and reviewed in 23). In that line, an siRNA against *Ctbp* increased *Fbxo32* promoter activity (Figure 4F). The large increase in *Fbxo32* transcription induced by si*Ctbp* suggests that *Fbxo32* is under negative regulation by other CtBP-binding factors besides ZEB1. ZEB1 repression of *Fbxo32* was also partially relieved by blocking of CtBP activity with 2-keto-4-methylthiobutyrate (MTOB), an intermediate in the methionine salvage pathway that binds and inactivates CtBP (33,34) (Supplementary Figure S4D).

Next, we examined the potential regulation of *Trim63* by ZEB1 at the transcriptional level. Knockdown of *Zeb1* and *Ctbp* upregulated FOXO3-induced transcription of the *Trim63* reporter (Figure 4G), indicating that, as for *Fbxo32*, MuRF1 expression is inhibited at the transcriptional level by endogenous ZEB1 and CtBP.

ZEB1 repression of several atrogenes (Figure 2) suggests that ZEB1 modulates the activity of a common activator of muscle atrophy. The results above also indicate that ZEB1 represses FOXO3-induced activation of the *Fbxo32* and *Trim63* promoters. We therefore investigated whether ZEB1 directly represses FOXO3-mediated transcriptional activity using a heterologous luciferase reporter (L8G5-luc) that contains binding sites for yeast Gal4 (Gal4-UAS)

previously identified in reference (14) or assessed as described in Supplementary Materials and Methods. (**B**) ZEB1 binds to the mouse *Fbxo32* promoter in myoblasts and atrophic myotubes but not in myotubes. DNA from C2C12 myoblasts, myotubes, or atrophic myotubes was immunoprecipitated with antibodies against ZEB1 (clone E-20X), MYOD1 (clone G-1) or their matched IgG controls (goat and mouse IgG, respectively). Immunoprecipitated DNA was then amplified by qRT-PCR in a region of the *Fbxo32* promoter containing a ZEB1 consensus binding site at –85 bp. The condition immunoprecipitated with the IgG control was set to 100. Data represent the average of at least three experiments. (**C**) Transcription of the *Fbxo32* promoter is under negative regulation by endogenous ZEB1. 0.48 μg of a luciferase reporter containing a 1.0 kb fragment of the mouse *Fbxo32* promoter (14) was co-transfected in C2C12 cells along with 0.82 μg of an expression vector for FOXO3 (or the corresponding molar amount of the empty expression vector) to induce *Fbxo32* transcription. Throughout this Figure, the effect of overexpressing the indicated genes (*Foxo3* in this panel) is shown with respect to their corresponding empty vectors. Where indicated, cells were also transfected with 50 nM of either siCtrl, si*Zeb1*-A or si*Zeb1*-B. Transfections and assessment of Relative luciferase units (RLU) were performed as described in Supplementary Information. The first condition was arbitrarily set to 100. Data represent the average of three independent experiments. (**D**) *Left panel:* As in (C) but cells were instead transfected with 0.43 μg of either a luciferase reporter containing a 0.4 kb fragment of the mouse *Fbxo32* promoter (14) or version of it where only the ZEB1 binding site at -85 bp has been mutated to a sequence known to not bind ZEB1 (see Supplementary Information for details). *Right panel:* As in the left panel, but 1.88 μg of an expression vector for *Zeb1* (or the corresponding molar amount of the empty expression vector) were also transfected. The first condition was arbitrarily set to 100. Data represent the average of three independent experiments. (**E**) Overexpression of MYOD1 displaces ZEB1 from its binding to the 0.4 kb *Fbxo32* luciferase reporter. As in the right panel of (D) but 0.04 μg or 0.13 μg of an expression vector for *Myod1* (or the corresponding molar amount of the empty expression vector) were transfected along with *Zeb1*. The first condition was arbitrarily set to 100. Data shown are the mean of three independent experiments. (**F**) Transcription of the *Fbxo32* promoter is under negative regulation by endogenous CtBP. As in (D) but cells were transfected with a siRNA against *Ctbp*. The first condition was arbitrarily set to 100. Data represent the average of three independent experiments. (**G**) As in (F) but cells were instead transfected with 0.77 μg of a luciferase reporter containing a 4.4 kb fragment of the mouse *Trim63* promoter. The first condition was arbitrarily set to 100. Data are the average of at least three independent experiments. (**H**) FOXO3 transcriptional activity is repressed by ZEB1 and CtBP. 293T cells were transfected with 0.50 μg of a reporter containing LexA operon and Gal-UAS sites (L8G5-luc) along with 1.04 μg Gal4-*Foxo3* and/or 1.15 μg LexA-*ZEB1* (or their corresponding empty vectors). Where indicated, cells were transfected with 10–20 nM of either siCtrl or si*Ctbp*. The condition overexpressing only Gal4-*Foxo3* was arbitrarily set to 100. Data represent the average of five independent experiments. (**I**) ZEB1 represses FOXO3 transcriptional activity through a CtBP-dependent mechanism. As in (H) but the Gal4 and LexA fusion proteins were swapped: *ZEB1*, *ZEB1*-CID and *ZEB1*-CID_{mut} were fused to Gal4 whereas *Foxo3* was fused to LexA. Cells were transfected with 0.50 μg of L8G5-luc, 0.70 μg of LexA-*Foxo3*, 1.50 μg Gal4-*ZEB1*, 0.79 μg of Gal4-*ZEB1*-CID and/or *ZEB1*-CID_{mut}. The condition overexpressing only LexA-*Foxo3* was arbitrarily set to 100. Data are the average of three independent experiments.

and bacterial LexA (LexAOp) proteins (scheme on top of Figure 4H). The cDNA of *Foxo3* fused to the DNA-binding domain of Gal4 (Gal4-*Foxo3*) activated the basal transcription of the L8G5-luc reporter (Figure 4H). In turn, the cDNA of *ZEB1* fused to the DNA-binding domain of LexA (LexA-*ZEB1*) repressed Gal4-*Foxo3*-induced transcriptional activation of the L8G5-luc reporter (Figure 4H). In line with the results above with the *Fbxo32* and *Trim63* promoters (Figure 4F and G), knockdown of *Ctbp* with an siRNA partially relieved the repression of Gal4-*Foxo3* by LexA-*ZEB1* (Figure 4H). A similar result was obtained when the cDNA of *Foxo3* was instead fused to the DNA-binding domain of LexA and that of ZEB1 to Gal4 (Figure 4I). *Foxo3*-mediated transcription in this heterologous system was also repressed by a ZEB1 fragment containing only its CtBP-interacting domain (CID) fused to Gal4 (Gal4-*ZEB1*-CID) (Figure 4I). However, mutation of the three CtBP sites within ZEB1's CID (Gal4-*ZEB1*-CID_{mut}) abrogated transcriptional repression of FOXO3 by *ZEB1*-CID. The conclusions from these results are twofold: first, ZEB1 inhibits *Foxo3*-mediated induction of atrogenes; and second, ZEB1 has the intrinsic capacity to repress *Foxo3* transcriptional activity through, at least in part, the recruitment of the CtBP co-repressor.

In vivo repression of the *Fbxo32* promoter by endogenous ZEB1

Lastly, we examined the *in vivo* regulation of the *Fbxo32* promoter by endogenous ZEB1 (see scheme in Figure 5A). Both hindlimbs of wild-type and *Zeb1* (+/-) mice were injected with the *Fbxo32* promoter fused to luciferase. After 3.5 days, the left hindlimb was immobilized during 3.5 additional days, while the right hindlimb remained non-immobilized. At day 7, luciferase signal emission was assessed by whole-body bioluminescence imaging. In line with the above results, the luminescence signal emitted by the *Fbxo32* promoter was higher in the immobilized hindlimb of *Zeb1* (+/-) mice than in that of wild-type counterparts. These results indicate that endogenous ZEB1 also inhibits the transcription of the *Fbxo32* promoter *in vivo* (Figure 5B and C).

DISCUSSION

The transcriptional regulation of muscle atrophy is still not completely understood. This study showed that ZEB1 inhibits muscle atrophy and atrogene expression (see summary model in Figure 6). Full levels of ZEB1 expression protected skeletal muscle from an otherwise unrestrained muscle atrophy and atrogene overexpression in response to immobilization as occurs when ZEB1 levels are reduced. In the C2C12 myogenic model, ZEB1 knockdown upregulated Atrogin-1 and MuRF1 expression and enhanced the reduction in myotube diameter triggered by growth factor starvation. At the mechanistic level, ZEB1 directly binds to the *Fbxo32* promoter in a stage-dependent manner and represses its transcription and that of *Trim63*—both in cell systems and/or *in vivo*—through CtBP-dependent inhibition of FOXO3 transcriptional activity.

The molecular mechanisms controlling fiber size under homeostasis and during atrophy are different (3), and we found here that under basal (non-immobilized) conditions, *Zeb1* (+/-) muscles display equivalent weight and expressed similarly low or non-existing levels of Atrogin-1 and MuRF1 as wild-type counterparts. This can be explained because in homeostatic (non-immobilized) conditions, ZEB1 does not bind to the *Fbxo32* promoter that it is instead occupied by MYOD1. Nevertheless, binding of MYOD1 does not seem to be sufficient to induce *Fbxo32* expression; transcriptional activation of atrogenes requires of FOXO3, which remains translocated to the cytoplasm in non-immobilized muscles (2,3,14).

In turn, a partial downregulation of *Zeb1*—to around half the levels with respect to that in wild-type mice—was sufficient to trigger enhanced muscle atrophy in response to immobilization in *Zeb1* (+/-) muscles. In addition, immobilization induced a moderate increase in ZEB1 mRNA and protein expression. This would suggest that the protecting role of ZEB1 against unrestrained muscle atrophy during immobilization depends on a fine threshold of its expression. Interestingly, an analogous expression threshold has been reported for ZEB1 tumor-promoting functions. Thus, a partial downregulation of *Zeb1* in either cancer cells or stromal cells of the tumor microenvironment is enough to completely block the malignant progression of lung, colon and ovarian carcinomas in *Zeb1* (+/-) mice (33,35,36). In addition, ZEB1 transcriptional activity is regulated by *cis* and *trans* mechanisms that determine its binding to target gene promoters and its recruitment of transcriptional co-activators and co-repressors (15). Muscles need to continuously and finely regulate their protein synthesis and proteolysis in response to atrophic and hypertrophic signals. In that regard, a multifunctional and tightly regulated protein like ZEB1 can play such role as a stage-dependent and discerning modulator of muscle loss.

ZEB1 inhibited muscle atrophy in a stage-dependent manner; ZEB1 bound to the *Fbxo32* promoter in atrophic myotubes, but not in non-atrophic myotubes, thus contributing to explain the lack of atrophy and atrogene upregulation in *Zeb1* (+/-) muscles under basal (non-immobilized) conditions. Regulation of muscle differentiation by ZEB1 and other EMT factors (e.g. SNAI1/2) also occurs in a stage-dependent manner (20,21,37). ZEB1 and SNAI1/2 share DNA-binding sites (E-box and E-box-like sequences) with MYOD1 in the promoters of muscle differentiation genes. During the myoblast stage, ZEB1 and SNAI1/2 occupy these promoters to repress their expression, but as muscle differentiation proceeds, MYOD1 accumulates and displaces EMT factors from these genes activating their expression (20,21,37). We found here a similar reverse binding pattern of ZEB1 and MYOD1 with respect to atrogenes. ZEB1 was excluded from the *Fbxo32* promoter in non-atrophic myotubes where MYOD1 was instead occupying the promoter. MYOD1 has higher affinity than ZEB1 for binding to E-boxes (20) and, accordingly, overexpression of MYOD1 was able to displace ZEB1 from the *Fbxo32* promoter. In that regard, the preferred binding of ZEB1 over MYOD1 to the *Fbxo32* promoter in atrophic myotubes is probably related not only to the slight upregulation of ZEB1 in atrophic muscles and myotubes (Figures 1F, G, and 3D), but also to the downregulation of *Myod1* mRNA during atrophy (Supplementary Figure S4E) and

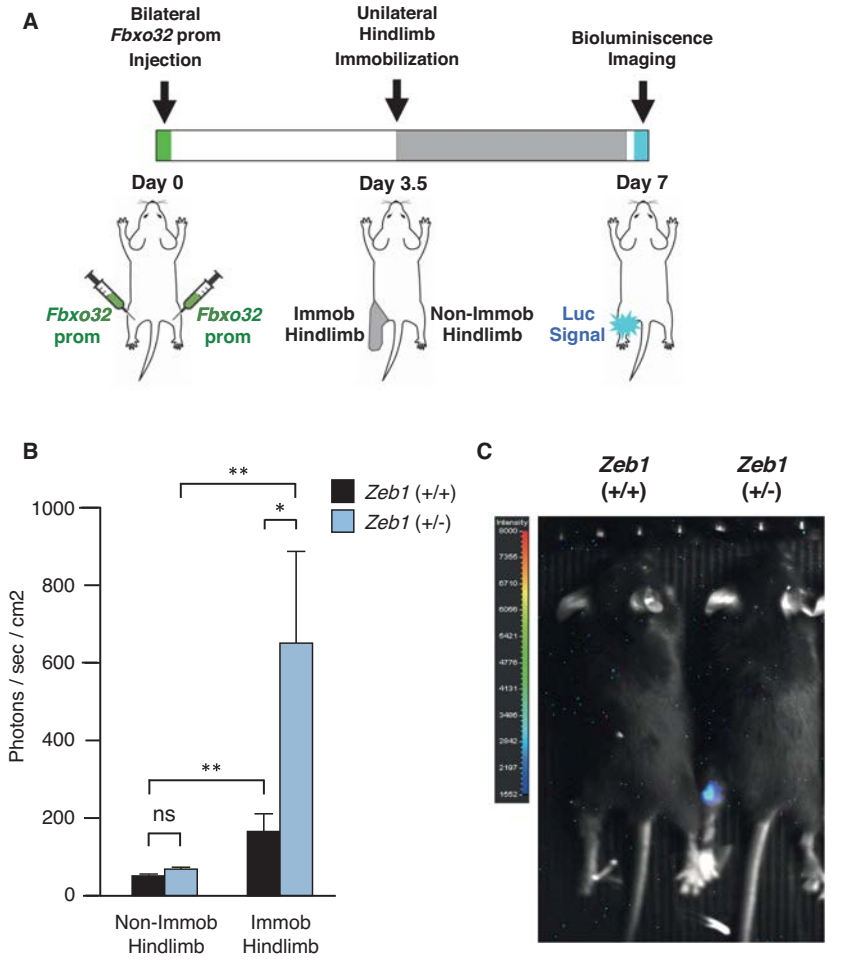

Figure 5. *In vivo* repression of the *Fbxo32* promoter by endogenous ZEB1. (**A**) Graphic representation of the protocol for the *in vivo* assessment of ZEB1 regulation of the *Fbxo32* promoter. Both hindlimbs of wild-type and *Zeb1* (+/-) mice were injected with a 3.5 kb fragment of the *Fbxo32* promoter fused to luciferase (14). After 3.5 days, mice were subjected to unilateral (left) hindlimb immobilization for 3.5 additional days. At day 7, *Fbxo32* promoter activity was assessed *in vivo* by whole-body bioluminescence imaging. See Supplementary Data for details. (**B**) ZEB1 inhibits the *Fbxo32* promoter *in vivo*. In both genotypes, the bioluminescence signal emitted by the *Fbxo32* promoter is higher in the immobilized hindlimb than in the non-immobilized hindlimb. However, immobilization induced greater bioluminescence signal in *Zeb1* (+/−) mice than in wild-type mice. Data represent the average of seven mice of each genotype. (**C**) Bioluminescence signal rendered by a representative mouse for each genotype at day 7.

the reported role of Atrogin-1 targeting MYOD1 protein for ubiquitin degradation (38,39) (see model in Figure 6).

ZEB1 repressed the *Fbxo32* promoter through a mechanism that involved recruitment of CtBP and inhibition of FOXO3 transcriptional activity. Despite that among all transcription factors CtBP has one of the highest affinity for ZEB1 (40), *CtBP* knockdown upregulated *Fbxo32* and *Trim63* promoters transcription above the effect of *Zeb1* knockdown, suggesting that Atrogin-1 and MuRF1 expression are under negative regulation by CtBP-binding transcription factor(s) other than ZEB1.

Notably, muscle atrophy-inducing conditions of very disparate origins—from immobilization or denervation to cancer cachexia, fasting or uremia—upregulate a highly overlapping set of atrogenes (7–9). It remains to be elucidated whether ZEB1 represses all atrogenes or only a subset. Nevertheless, data shown here indicate that, in addition to the E3 ubiquitin ligases *Fbxo32* and *Trim63,* ZEB1 also represses other components of the ubiquitin–proteasome chain (*Psma1*), members of the autophagy-lysosomal system (*Ctsl, Gabarapl1*), as well as genes involved in protein synthesis (*4ebp1*), and oxidative stress (*Nrf2*). Although FOXO3 is required for muscle atrophy and a majority of atrogenes are induced by FOXO proteins, their dependence on FOXO is determined by the atrophy-inducing condition; thus, *Nrf2* is induced by FOXO proteins upon muscle denervation, but not in response to fasting (9). This draws a nuance model of transcriptional regulation of atrogenes where other transcriptional activators, beyond FOXO proteins, may also induce atrogene expression. It is also possible that ZEB1 represses atrogenes that are independent of FOXO3. ZEB1 represses the activity of a wide range of transcriptional activators with its inhibitory effect and the mechanism involved determined by the promoter, the co-repressors it recruits and the activation/differentiation stage of cells (23,24,26,27,41). In addition, ZEB1 can also

Nucleic Acids Research, 2018, Vol. 46, No. 20 **10707**

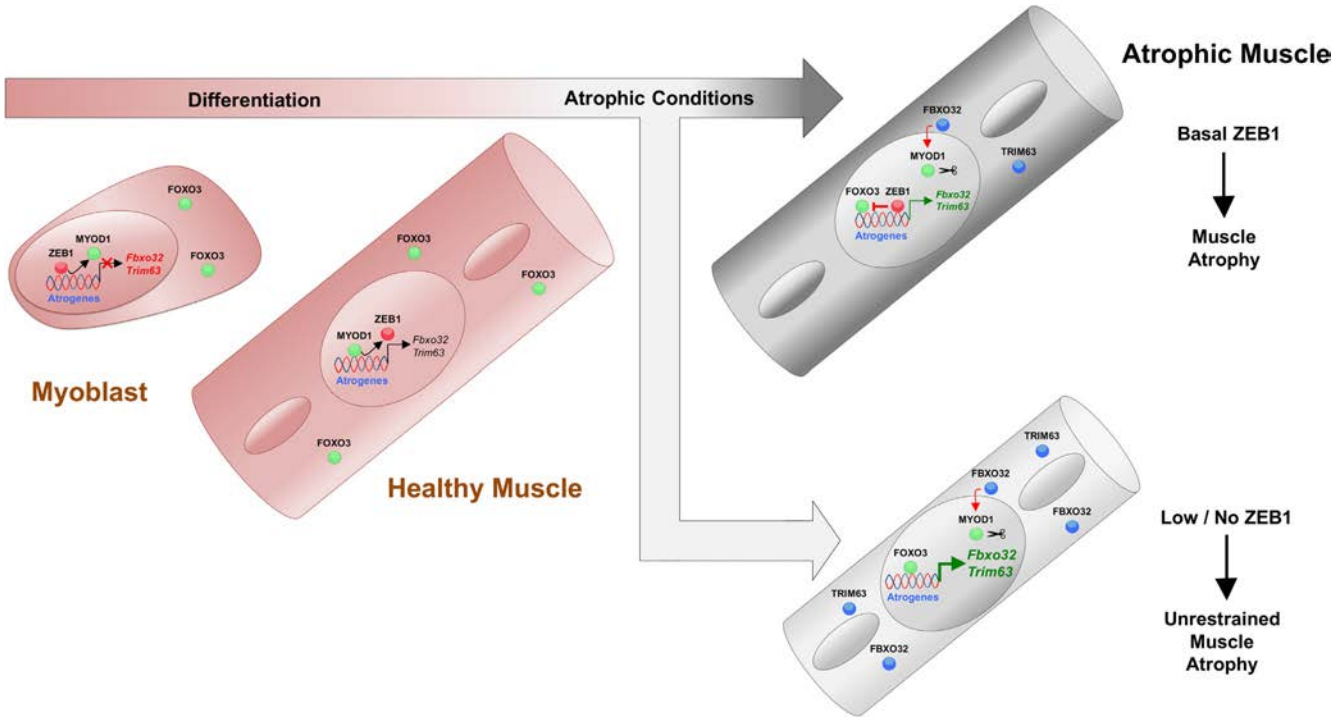

Figure 6. Summary model: ZEB1 inhibits muscle atrophy and atrogene expression in a stage-dependent manner through CtBP-mediated repression of FOXO3 transcriptional activity. See main text for details.

function as a transcriptional activator; binding of ZEB1 to the histone acetyltransferase p300 acetylates the CID region of ZEB1, thus displacing CtBP (27,42). In that line, in B lymphocytes, ZEB1 synergizes with FOXO3, rather than repressing it, in the activation of cell cycle genes cyclin G2 (*Ccng2*) and p130 (*Rbl2*) (43), highlighting once again the promoter and cell-type specificity of the link between ZEB1 and FOXO3.

This study unveiled an unexpected role for ZEB1 beyond cell differentiation and cancer. The identification here of ZEB1 as an inhibitor of atrogene expression offers new approaches for therapies aimed at preventing or treating muscle atrophy.

SUPPLEMENTARY DATA

Supplementary Data are available at NAR Online.

ACKNOWLEDGMENTS

We are indebted to all researchers that provided us with reagents and materials (see Supplementary Materials and Methods) and regret that some articles were only cited indirectly through reviews due to space limitations. We thank Sara Ninfali for her help with the drawing of Figure 5A.

FUNDING

The different parts of this study were independently funded by grants to A.P. from Duchenne Parent Project Spain [DPP-E 2018]; Catalan Agency for Management of University and Research Grants (AGAUR) [2014-SGR-475 and 2017-SGR-1174]; Ministry of Economy and Competitiveness [SAF2014-52874-R and SAF2017-84918-R], National Scientific and Technical Research and Innovation 2013-2016 and 2017-2020 Plans, which are co-financed by the European Regional Development Fund of the European Union Commission; [Avon Foundation SAU (AVFSAU)]. The IDIBAPS Institute is partly funded by the CERCA Program of Generalitat de Catalunya. CN was subsequently funded by a Unipharma Graduates-10 visiting scholarship by the Noopolis Foundation and Sapienza University of Rome (financed by European Union Program "Leonardo da Vinci") and a PhD scholarship from AGAUR [AGAUR-2015-FI_B-00121] and was later supported by [SAF2014-52874-R to AP]. LS was supported by grants [AVFSAU and SAF2014-52874-R to AP]. Funding for open access charge: Catalan Agency for Management of University and Research Grants (AGAUR) [2017-SGR-1174].
Conflict of interest statement. None declared.

REFERENCES

1. Cohen,S., Nathan,J.A. and Goldberg,A.L. (2015) Muscle wasting in disease: molecular mechanisms and promising therapies. *Nat. Rev. Drug Discov.*, **14**, 58–74.
2. Bonaldo,P. and Sandri,M. (2013) Cellular and molecular mechanisms of muscle atrophy. *Dis. Model Mech.*, **6**, 25–39.
3. Schiaffino,S., Dyar,K.A., Ciciliot,S., Blaauw,B. and Sandri,M. (2013) Mechanisms regulating skeletal muscle growth and atrophy. *FEBS J.*, **280**, 4294–4314.
4. Bodine,S.C., Latres,E., Baumhueter,S., Lai,V.K.M., Nunez,L., Clarke,B.A., Poueymirou,W.T., Panaro,F.J., Na,E., Dharmarajan,K. *et al.* (2001) Identification of ubiquitin ligases required for skeletal muscle atrophy. *Science*, **294**, 1704–1708.

5. Gomes,M.D., Lecker,S.H., Jagoe,R.T., Navon,A. and Goldberg,A.L. (2001) Atrogin-1, a muscle-specific F-box protein highly expressed during muscle atrophy. *Proc. Natl. Acad. Sci. U.S.A.*, **98**, 14440–14445.
6. Jagoe,R.T., Lecker,S.H., Gomes,M. and Goldberg,A.L. (2002) Patterns of gene expression in atrophying skeletal muscles: response to food deprivation. *FASEB J.*, **16**, 1697–1712.
7. Lecker,S.H., Jagoe,R.T., Gilbert,A., Gomes,M., Baracos,V., Bailey,J., Price,S.R., Mitch,W.E. and Goldberg,A.L. (2004) Multiple types of skeletal muscle atrophy involve a common program of changes in gene expression. *FASEB J.*, **18**, 39–51.
8. Sacheck,J.M., Hyatt,J.P., Raffaello,A., Jagoe,R.T., Roy,R.R., Edgerton,V.R., Lecker,S.H. and Goldberg,A.L. (2007) Rapid disuse and denervation atrophy involve transcriptional changes similar to those of muscle wasting during systemic diseases. *FASEB J.*, **21**, 140–155.
9. Milan,G., Romanello,V., Pescatore,F., Armani,A., Paik,J.H., Frasson,L., Seydel,A., Zhao,J., Abraham,R., Goldberg,A.L. *et al.* (2015) Regulation of autophagy and the ubiquitin-proteasome system by the FoxO transcriptional network during muscle atrophy. *Nat. Commun.*, **6**, 6670.
10. Bodine,S.C. and Baehr,L.M. (2014) Skeletal muscle atrophy and the E3 ubiquitin ligases MuRF1 and MAFbx/atrogin-1. *Am. J. Physiol. Endocrinol. Metab.*, **307**, E469–E484.
11. Collins,G.A. and Goldberg,A.L. (2017) The logic of the 26S proteasome. *Cell*, **169**, 792–806.
12. Mammucari,C., Milan,G., Romanello,V., Masiero,E., Rudolf,R., Del Piccolo,P., Burden,S.J., Di Lisi,R., Sandri,C., Zhao,J. *et al.* (2007) FoxO3 controls autophagy in skeletal muscle *in vivo*. *Cell Metab.*, **6**, 458–471.
13. Zhao,J., Brault,J.J., Schild,A., Cao,P., Sandri,M., Schiaffino,S., Lecker,S.H. and Goldberg,A.L. (2007) FoxO3 coordinately activates protein degradation by the autophagic/lysosomal and proteasomal pathways in atrophying muscle cells. *Cell Metab.*, **6**, 472–483.
14. Sandri,M., Sandri,C., Gilbert,A., Skurk,C., Calabria,E., Picard,A., Walsh,K., Schiaffino,S., Lecker,S.H. and Goldberg,A.L. (2004) Foxo transcription factors induce the atrophy-related ubiquitin ligase atrogin-1 and cause skeletal muscle atrophy. *Cell*, **117**, 399–412.
15. Sánchez-Tilló,E., Liu,Y., de Barrios,O., Siles,L., Fanlo,L., Cuatrecasas,M., Darling,D.S., Dean,D.C., Castells,A. and Postigo,A. (2012) EMT-activating transcription factors in cancer: beyond EMT and tumor invasiveness. *Cell. Mol. Life Sci.*, **69**, 3429–3456.
16. Hill,L., Browne,G. and Tulchinsky,E. (2013) ZEB/miR-200 feedback loop: at the crossroads of signal transduction in cancer. *Int. J. Cancer*, **132**, 745–754.
17. Nieto,M.A., Huang,R.Y.J., Jackson,R.A. and Thiery,J.P. (2016) EMT: 2016. *Cell*, **166**, 21–45.
18. Takagi,T., Moribe,H., Kondoh,H. and Higashi,Y. (1998) δEF1, a zinc finger and homeodomain transcription factor, is required for skeleton patterning in multiple lineages. *Development*, **125**, 21–31.
19. Vandewalle,C., Van Roy,F. and Berx,G. (2009) The role of the ZEB family of transcription factors in development and disease. *Cell. Mol. Life Sci.*, **66**, 773–787.
20. Postigo,A. and Dean,D.C. (1997) ZEB, a vertebrate homolog of Drosophila Zfh-1, is a negative regulator of muscle differentiation. *EMBO J.*, **16**, 3935–3943.
21. Siles,L., Sánchez-Tilló,E., Lim,J.W., Darling,D.S., Kroll,K.L. and Postigo,A. (2013) ZEB1 imposes a temporary stage-dependent inhibition of muscle gene expression and differentiation via CtBP-mediated transcriptional repression. *Mol. Cell. Biol.*, **33**, 1368–1382.
22. Postigo,A., Ward,E., Skeath,J.B. and Dean,D.C. (1999) zfh-1, the Drosophila homologue of ZEB, is a transcriptional repressor that regulates somatic myogenesis. *Mol. Cell. Biol.*, **19**, 7255–7263.
23. Sánchez-Tilló,E., Siles,L., de Barrios,O., Cuatrecasas,M., Vaquero,E.C., Castells,A. and Postigo,A. (2011) Expanding roles of ZEB factors in tumorigenesis and tumor progression. *Am. J. Cancer Res.*, **1**, 897–912.
24. Postigo,A., Sheppard,A.M., Mucenski,M.L. and Dean,D.C. (1997) c-Myb and Ets proteins synergize to overcome transcriptional repression by ZEB. *EMBO J.*, **16**, 3924–3934.
25. Postigo,A. and Dean,D.C. (1999) ZEB represses transcription through interaction with the corepressor CtBP. *Proc. Natl. Acad. Sci. U.S.A.*, **96**, 6683–6688.
26. Postigo,A. (2003) Opposing functions of ZEB proteins in the regulation of the TGFβ/BMP signaling pathway. *EMBO J.*, **22**, 2443–2452.
27. Postigo,A., Depp,J.L., Taylor,J.J. and Kroll,K.L. (2003) Regulation of Smad signaling through a differential recruitment of coactivators and corepressors by ZEB proteins. *EMBO J.*, **22**, 2453–2462.
28. Blau,H.M., Chiu,C.P. and Webster,C. (1983) Cytoplasmic activation of human nuclear genes in stable heterocaryons. *Cell*, **32**, 1171–1180.
29. Blais,A., Tsikitis,M., Acosta-Alvear,D., Sharan,R., Kluger,Y. and Dynlacht,B.D. (2005) An initial blueprint for myogenic differentiation. *Genes Dev.*, **19**, 553–569.
30. Genetta,T., Ruezinsky,D. and Kadesch,T. (1994) Displacement of an E-box-binding repressor by basic helix-loop-helix proteins: implications for B-cell specificity of the immunoglobulin heavy-chain enhancer. *Mol. Cell. Biol.*, **14**, 6153–6163.
31. Sekido,R., Murai,K., Funahashi,J.I., Kamachi,Y., Fujisawa-Sehara,A., Nabeshima,Y.L. and Kondoh,H. (1994) The δ-crystallin enhancer-binding protein δEF1 is a repressor of E2-box-mediated gene activation. *Mol. Cell. Biol.*, **14**, 5692–5700.
32. Cao,Y., Yao,Z., Sarkar,D., Lawrence,M., Sanchez,G.J., Parker,M.H., MacQuarrie,K.L., Davison,J., Morgan,M.T., Ruzzo,W.L. *et al.* (2010) Genome-wide MyoD binding in skeletal muscle cells: a potential for broad cellular reprogramming. *Dev. Cell*, **18**, 662–674.
33. de Barrios,O., Győrffy,B, Fernández-Aceñero,M.J., Sánchez-Tilló,E., Sánchez-Moral,L., Siles,L., Esteve-Arenys,A., Roué,G., Casal,J.I., Darling,D.S. *et al.* (2017) ZEB1-induced tumourigenesis requires senescence inhibition via activation of DKK1/mutant p53/Mdm2/CtBP and repression of macroH2A1. *Gut*, **66**, 563–564.
34. Di,L.J., Byun,J.S., Wong,M.M., Wakano,C., Taylor,T., Bilke,S., Baek,S., Hunter,K., Yang,H., Lee,M. *et al.* (2013) Genome-wide profiles of CtBP link metabolism with genome stability and epithelial reprogramming in breast cancer. *Nat. Commun.*, **4**, 1449.
35. Liu,Y., Lu,X., Huang,L., Wang,W., Jiang,G., Dean,K.C., Clem,B., Telang,S., Jenson,A.B., Cuatrecasas,M. *et al.* (2014) Different thresholds of ZEB1 are required for Ras-mediated tumour initiation and metastasis. *Nat. Commun.*, **5**, 5660.
36. Cortés,M., Sanchez-Moral,L., de Barrios,O., Fernández-Aceñero,M.J., Martínez-Campanario,M.C., Esteve-Codina,A., Darling,D.S., Győrffy,B., Lawrence,T., Dean,D.C. *et al.* (2017) Tumor-associated macrophages (TAMs) depend on ZEB1 for their cancer-promoting roles. *EMBO J.*, **36**, 3336–3355.
37. Soleimani,V.D., Yin,H., Jahani-Asl,A., Ming,H., Kockx,C.E., van Ijcken,W.F., Grosveld,F. and Rudnicki,M.A. (2012) Snail regulates MyoD binding-site occupancy to direct enhancer switching and differentiation-specific transcription in myogenesis. *Mol. Cell*, **47**, 457–468.
38. Tintignac,L.A., Lagirand,J., Batonnet,S., Sirri,V., Leibovitch,M.P. and Leibovitch,S.A. (2005) Degradation of MyoD mediated by the SCF (MAFbx) ubiquitin ligase. *J. Biol. Chem.*, **280**, 2847–2856.
39. Lagirand-Cantaloube,J., Cornille,K., Csibi,A., Batonnet-Pichon,S., Leibovitch,M.P. and Leibovitch,S.A. (2009) Inhibition of atrogin-1/MAFbx mediated MyoD proteolysis prevents skeletal muscle atrophy *in vivo*. *PLoS One*, **4**, e4973.
40. Shi,Y., Sawada,J.I., Sui,G., Affar,E.B., Whetstine,J.R., Lan,F., Ogawa,H., Luke,M.P., Nakatani,Y. and Shi,Y. (2003) Coordinated histone modifications mediated by a CtBP co-repressor complex. *Nature*, **422**, 735–778.
41. Postigo,A. and Dean,D.C. (1999) Independent repressor domains in ZEB regulate muscle and T-cell differentiation. *Mol. Cell. Biol.*, **19**, 7961–7971.
42. Sánchez-Tilló,E., De Barrios,O., Valls,E., Darling,D.S., Castells,A. and Postigo,A. (2015) ZEB1 and TCF4 reciprocally modulate their transcriptional activities to regulate Wnt target gene expression. *Oncogene*, **34**, 5760–5770.
43. Chen,J., Yusuf,I., Andersen,H.M. and Fruman,D.A. (2006) FOXO transcription factors cooperate with δEF1 to activate growth suppressive genes in B lymphocytes. *J. Immunol.*, **176**, 2711–2721.

APPENDIX II

I also participated in other two projects:

Siles, L., **Ninfali, C.**, Cortés, M., Darling, D. S., & Postigo, A. (2019). ZEB1 protects skeletal muscle from damage and is required for its regeneration. *Nature Communications*, *10*(1), 1364.

De Barrios, O., Sanchez-Moral, L., Cortés, M., **Ninfali, C.*,** Profitós-Pelejà, N.*, Martínez-Campanario, M.*, … Postigo, A. (2019). Inflammatory bowel disease ZEB1 promotes inflammation and progression towards inflammation-driven carcinoma through repression of the DNA repair glycosylase MPG in epithelial cells. *Gut*, *0*, 1–13.

*** These authors contributed equally as co-second authors to the work.**

ARTICLE

https://doi.org/10.1038/s41467-019-08983-8 OPEN

ZEB1 protects skeletal muscle from damage and is required for its regeneration

Laura Siles[1], Chiara Ninfali[1], Marlies Cortés[1], Douglas S. Darling[2] & Antonio Postigo[1,3,4]

Inflammatory bowel disease

ORIGINAL ARTICLE

ZEB1 promotes inflammation and progression towards inflammation-driven carcinoma through repression of the DNA repair glycosylase MPG in epithelial cells

Oriol de Barrios,[1] Lidia Sanchez-Moral,[1] Marlies Cortés,[1] Chiara Ninfali,[1] Nuria Profitós-Pelejà,[1] MC Martínez-Campanario,[1] Laura Siles,[1] Rosa del Campo,[2] María Jesús Fernández-Aceñero,[3] Douglas S Darling,[4] Antoni Castells,[5,6] Joan Maurel,[7] Azucena Salas,[5] Douglas C Dean,[8,9] Antonio Postigo[1,9,10]